REPORT NO.
UCB/SEMM-1999/05

STRUCTURAL ENGINEERING
MECHANICS AND MATERIALS

ON THE FORMULATION OF HIGH-FREQUENCY DISSIPATIVE TIME-STEPPING ALGORITHMS FOR NONLINEAR DYNAMICS

PART I: LOW-ORDER METHODS FOR TWO MODEL PROBLEMS AND NONLINEAR ELASTODYNAMICS

BY

F. ARMERO

AND

I. ROMERO

FEBRUARY 1999

DEPARTMENT OF CIVIL AND ENVIRONMENTAL ENGINEERING
UNIVERSITY OF CALIFORNIA
BERKELEY, CALIFORNIA

On the Formulation of High-Frequency Dissipative Time-Stepping Algorithms for Nonlinear Dynamics. Part I: Low Order Methods for Two Model Problems and Nonlinear Elastodynamics.

by

F. ARMERO* & I. ROMERO

Structural Engineering, Mechanics and Materials

Department of Civil and Environmental Engineering

University of California, Berkeley CA 94720, USA

Abstract

We present in this paper the development of a class of time-stepping algorithms for nonlinear elastodynamics that exhibits a controllable energy dissipation in the high-frequency range, thus allowing the elimination of the modeling/discretization errors that are known to accumulate in this range of frequencies. To motivate and illustrate better the developments in this general case, we present first the formulation and analysis of these methods for two simple model problems. Namely, we consider a nonlinear elastic spring/mass system and a simplified model of thin elastic beams. As it is discussed in detail in this paper, the conservation by the numerical algorithm of the momenta and corresponding relative equilibria of these characteristic Hamiltonian systems with symmetry is of the main importance. These conservation properties lead for a fixed and finite time step to a correct qualitative picture of the phase space where the discrete dynamics takes place, even in the presence of the desired and controlled numerical dissipation of the energy. This situation is contrasted with traditional "dissipative" numerical schemes, which are shown through rigorous analyses to not only loose their dissipative character in the general nonlinear range, but also the aforementioned conservation properties, thus leading to a qualitatively distorted approximation of the phase dynamics. The key for a successful algorithm in this context is the incorporation of the numerical dissipation in the internal modes of the motion while not affecting the group motions of the system. The algorithms presented in this work accomplish these goals. The focus in this first part is given to low order methods. Representative numerical simulations, ranging from applications in nonlinear structural dynamics to nonlinear continuum three-dimensional elastodynamics, are presented in the context of the finite element method to illustrate these ideas and results.

KEY WORDS: nonlinear elastodynamics; time-stepping algorithms; high-frequency dissipation; relative equilibria; finite element method.

* Corresponding author (armero@ce.berkeley.edu).

1. Introduction

Traditional time-stepping algorithms for the temporal integration of the equations of elastodynamics and structural dynamics were developed in the context of linear problems for the most part. Hence, it is not surprising to observe that algorithms that present excellent stability properties in the linear range lead to numerical instabilities in the general nonlinear range. These instabilities are usually manifested by an uncontrollable growth of the energy of the discrete system. This observation has motivated the development of the so-called conserving schemes, that is, time-stepping algorithms that conserve the energy and momentum for this general class of Hamiltonian systems with symmetry. Early examples of these methods can be found in LABUDDE & GREENSPAN [1976] and HUGHES et al [1978], consisting basically of projection strategies imposing these conservation laws. We can find in the more recent literature a strong interest in the development of time-stepping algorithms with these conservation laws built in. Representative examples are the works of SIMO & TARNOW [1992], CRISFIELD & SHI [1994] and GONZALEZ & SIMO [1995], among others. We also refer to KUHL & RAMM [1996] for a recent consideration of projection strategies. Applications to multi-body elastic systems, that is, with a focus on the conservative approximation of the contact interactions, can be found developed in ARMERO & PETOCZ [1996,97], and references therein.

Although the conservation of the physical energy is an interesting property for the numerical scheme to have, the need for the introduction of numerical dissipation in the resolution of the high-frequency range is commonly recognized. This need arises as a direct consequence of the error accumulated in this range of frequencies, because of the physical model (e.g., constrained systems modeled through a penalty formulation) or the spatial discretization in infinite-dimensional continuum systems. In this way, the formulation of numerical algorithms that exhibit this numerical dissipation in the high-frequency range can be found developed in detail for linear problems. A characteristic example of these methods is the so-called HHT α-method presented in HILBER et al [1977]; we refer to HUGHES [1987] for a complete account of these ideas for linear elastodynamics.

The lack of the dissipative character of these classical "dissipative" schemes in non-linear problems can be found documented in the literature; see e.g. ARMERO & PETOCZ [1996] and KUHL & CRISFIELD [1997], among others. The need for new time-stepping algorithms that exhibit these dissipative properties in the fully nonlinear range is therefore clear. Recent examples of algorithms developed to this purpose can be found in BAUCHAU & THERON [1996] and BOTASSO & BORRI [1998], where methods based on discontinuous Galerkin and Runge-Kutta approaches can be found applied to the integration of beam models. Even though high-order schemes have been proposed in these references, these approaches seem to apply to particular cases only, usually involving quadratic potentials and quadratic strain measures. Furthermore, schemes proposed in this framework do not allow a direct control of the amount of the numerical dissipation introduced in the simulations.

Motivated by the need of this fully controllable character of the numerical dissipation, we presented in ARMERO & PETOCZ [1996] a simple modification of conserving schemes for contact problems that leads to the introduction of numerical dissipation in the simulation of dynamic contact/impact of solids. These and additional ideas have been later explored in KUHL & CRISFIELD [1997] and CRISFIELD et al [1997] for general nonlinear elastodynamics and nonlinear beams. These schemes, however, do not show the added numerical dissipation in the high-frequency range when applied to the linearized problem. We present in this paper the formulation of time-stepping schemes that introduce rigorously the numerical dissipation in the high-frequency range for general nonlinear problems, while preserving the conservation of momentum and relative equilibria associated to the symmetries of the dynamical system.

A symmetry of a Hamiltonian system, defined by the action of a group that leaves invariant the Hamiltonian, is known to result in a conservation law (Noether's theorem) and the so-called relative equilibria. These equilibria consist of trajectories of the dynamical system generated by a fixed infinitesimal element of the group's algebra (its linearization). The resulting solutions of the system of equations are referred to as group motions. In this context, a general solution can then be roughly thought as possessing a component in a group motion and a component in the so-called reduced space of internal modes (the phase space modulo the momentum preserving group motions). Loosely speaking, for the problems of interest in this work where the main group of symmetries corresponds to rotations, the group motions are rigid rotations "locked" at an equilibrium deformation of the elastic solid, with the internal motions corresponding to internal variations of these equilibrium configurations. We refer to ABRAHAM & MARSDEN [1978] and MARSDEN [1992], among others, for complete details of these ideas. The need to conserve these relative equilibria and, in particular, the need for not introducing any numerical dissipation in the group motions is apparent. In fact, with the simple model problem of a rigid bar modeled with a stiff spring in a finite rotation around one of its ends, it can be clearly observed that the internal motions may even be an artifact of the modelization.

The analysis presented in this paper shows that traditional "dissipative" schemes loose these conservation properties. The analysis considers the simple model problem of a point mass connected to a central point with a nonlinear elastic spring and in free motion around it. This simple example has been also considered in numerous occasions in the past; see BATHE [1986], CRISFIELD & SHI [1994], GONZALEZ & SIMO [1996] and KUHL & CRISFIELD [1997], among others. Our goal in the present work is to consider the axial response of the spring as the "high frequency" component of the solution introduced in modeling the limit case of a rigid bar (note that the axial vibration is the only natural frequency introduced in the physical system). In this context, we analyze completely the properties of the traditional "dissipative" schemes (HHT, Newmark and particular cases of them). A characterization of the relative equilibria obtained with the midpoint rule and energy-momentum conserving schemes (two momentum conserving schemes) for this

model problem has been presented in GONZALEZ & SIMO [1996] through a complete parametrization of the reduced space. In contrast, the approach taken here explores the properties of the numerical approximation of the relative equilibria through the global characterization of these solutions as group motions (rigid rotations). This alternative approach does not need the conservation of the angular momentum by the numerical scheme, nor a complex parametrization of the reduced space. In addition, this approach allows also to characterize completely the relative equilibria in the general context of nonlinear continuum elastodynamics, as it is pursued herein.

The lack of a dissipative scheme in the high-frequency range that conserves at the same time the momentum and the relative equilibria of the exact dynamical system is concluded after these analyses. We then propose a simple modification of conserving schemes that accomplishes these properties in a fully controllable fashion. This control is illustrated with a closed-form relation between the dissipation numerical parameters and the spectral radius at infinity for an one-dimensional linear oscillator. We refer to the new method as the EDMC-1 scheme, which stands for "energy dissipative, momentum conserving" first order scheme. The proposed time-stepping algorithm is shown to introduce the numerical dissipation only in the internal motions, leading to the exact relative equilibria in the long-term. We focus in this first part of the series on the development and complete illustration of these ideas in several characteristic problems of nonlinear dynamics, including their treatment by traditional numerical schemes as indicated above. In this way, the methods considered herein are only first order accurate in time, degenerating to second order accurate conserving schemes along the trajectories of relative equilibria. First order methods are of practical interest, especially in problems where one is interested in the simulation of the relative equilibria. The forthcoming second part of this series addresses the extension of these ideas to the development of high-order methods exhibiting the same conservation/dissipation properties. The added complexity of the resulting schemes, as well as the need for complete analyses of their accuracy properties (including spectral analyses in the linear range), deserves this separate treatment.

The new dissipative schemes consist of a modified stress formula together with a modified dynamic equation relating displacements and velocities. To illustrate the flexibility of these ideas, and before considering the general system of continuum nonlinear elastodynamics, we develop dissipative schemes for a simplified model of thin beams, the second model problem. For the sake of simplicity, we consider a system of masses subjected to a system of internal forces arising from axial and bending contributions of nonlinear hyperelastic springs connecting them. In this very simple setting, we can illustrate the introduction of the numerical dissipation through the axial part of the problem, while maintaining conservative the approximation of the bending contributions. This strategy is shown to be very effective in arriving to robust numerical schemes, avoiding the high frequency response associated to the sudden changes of the axial response in typical systems of nonlinear structural dynamics, as it has been observed to lead to difficulties in

non-dissipative schemes (see, e.g., CARDONA & GERARDIN [1988]). These ideas extrapolate to the more general case of geometrically exact theories of rods and shells with the added rotational updates. We plan to address these cases in forthcoming publications.

An outline of the rest of the paper is as follows. Section 2 describes in detail the first model problem considered in this work, consisting of the aforementioned nonlinear elastic spring/mass system. In particular, we include details of the variational characterization of the relative equilibria in this simple mechanical Hamiltonian system, as it is of the interest in the following numerical analysis. This analysis is undertaken in Section 3. More specifically, Section 3.1 considers some existing time-stepping algorithms and summarizes their conservation/dissipation properties in the general setting presented in the previous sections. Details of these analyses can be found in Appendix I. The formulation and analysis of the new dissipative EDMC-1 scheme is presented in Section 3.2. Representative numerical simulations illustrating these different results are presented in Section 3.3 for this first model problem. Next, Section 4 develops these ideas for the aforementioned simplified model of thin beams, including complete details of the formulation of the newly proposed schemes and representative numerical simulations in Section 4.3. Finally, Section 5 illustrates the formulation and analyses of these methods in the general setting of nonlinear continuum elastodynamics. Concluding remarks can be found in Section 6.

2. Model Problem I: a Nonlinear Elastic Spring/Mass System

We consider in this section the model problem of a nonlinear elastic spring fixed at one end with a mass at the opposite end in a force free motion. For large values of the stiffness of the spring, this system can be understood as a penalty regularization of a rigid bar rotating around its end. In this simple context, the high-frequency introduced by the numerical approximation becomes clear. In addition, this simple setting allows to characterize many of the numerical properties of the time-stepping algorithms of interest in this work.

We describe in this section in relatively high level of detail the different properties of the dynamics of the problem under consideration. Our main motivation is the complete definition of the different concepts and tools of analysis employed in the numerical analyses presented in the forthcoming sections. To this purpose, Section 2.1 defines the governing equation of this model problem, with a complete summary of the conservation properties of the resulting Hamiltonian system described in Section 2.2. The material presented in this section is a straightforward application of the general theoretical results that can be found in many textbook on geometric mechanics and symmetry; we refer to ABRAHAM & MARSDEN [1978], MARSDEN [1992] and MARSDEN & RATIU [1994] for complete details and further developments and proofs of many of the statements presented herein.

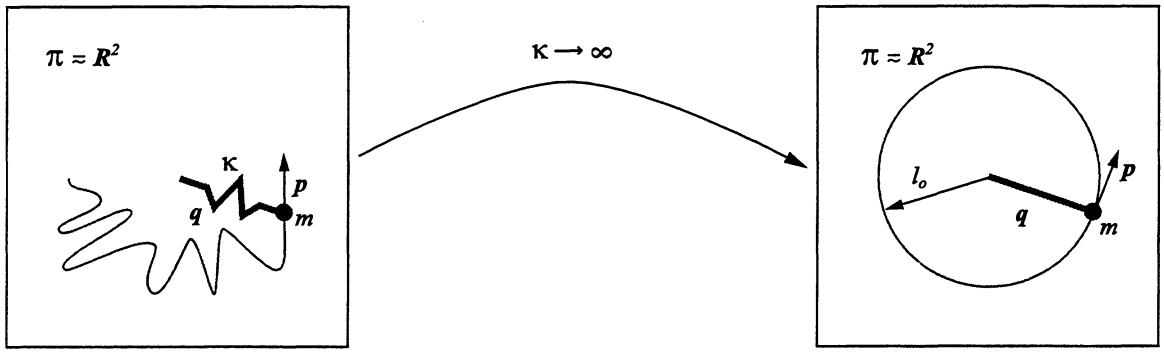

FIGURE 2.1. Model problem: nonlinear elastic spring/mass system. Planar definition of the problem under investigation. The case of a rigid bar $\|\boldsymbol{q}(t)\| = l_o \ \forall t$ is recovered in the limit $\kappa \to \infty$.

2.1. Problem definition

Figure 2.1 depicts the problem defined by a nonlinear spring fixed at the end O with a mass $m > 0$ concentrated at the opposite end. For the force-free motion considered herein, the nonlinear oscillation and finite rotation (around O) of the mass takes place in a plane $\Pi \simeq \mathbb{R}^2$. The state of the system can then be by the phase space $P = \mathbb{R}^2/\mathbf{0} \times \mathbb{R}^2$, consisting of the pairs $(\boldsymbol{q}, \boldsymbol{p}) \in P$ with the position vector $\boldsymbol{q} \in Q := \mathbb{R}^2/\mathbf{0}$ of the mass m with respect to O and its linear momentum $\boldsymbol{p} \in T^*_{\boldsymbol{q}}Q = \mathbb{R}^2$.

With this notation at hand, the motion of the mass m (that is, the functions $(\boldsymbol{q}(t), \boldsymbol{p}(t)) \in P$ of the time $t \in \mathbb{R}^+$) is defined by the simple mechanical Hamiltonian system

$$\left.\begin{aligned} \dot{\boldsymbol{q}} &= \frac{\partial H}{\partial \boldsymbol{p}} = m^{-1}\, \boldsymbol{p}\,, \\ \dot{\boldsymbol{p}} &= -\frac{\partial H}{\partial \boldsymbol{q}} = -V'(l)\, \frac{\boldsymbol{q}}{\|\boldsymbol{q}\|}\,, \end{aligned}\right\} \tag{2.1}$$

with the time derivatives $\dot{(\cdot)}$ and the length of the spring $l := \|\boldsymbol{q}\| = \sqrt{\boldsymbol{q} \cdot \boldsymbol{q}}$ for the standard Euclidean inner product and corresponding norm in $\mathbb{R}^2$. Equation (2.1) considers the Hamiltonian

$$H(\boldsymbol{q}, \boldsymbol{p}) = \underbrace{\tfrac{1}{2} m^{-1}\, \pi^2}_{K(\pi)} + V(l)\,, \tag{2.2}$$

for the kinetic energy $K(\pi)$ depending on $\pi := \|\boldsymbol{p}\|$, and the potential $V(l)$ (with derivative denoted by V') modeling the hyperelastic response of the spring (resulting in the internal force $\boldsymbol{f}_\kappa := V'(l)\, \boldsymbol{q}/\|\boldsymbol{q}\|$ in the spring, as it appears in $(2.1)_2$). The numerical simulations presented in Section 3.3 consider the particular case given by

$$V(l) = \tfrac{1}{2}\, \kappa\, (l - l_o)^2\,, \tag{2.3}$$

for a spring stiffness parameter κ. Note that $\boldsymbol{l}$ does not define a quadratic function of the unknown vector $\boldsymbol{q}$. No additional external forces are assumed in (2.1). The nonlinear first order system of ordinary equations (2.1) is supplemented by the initial conditions at $t = 0$

$$\boldsymbol{q}(0) = \boldsymbol{q}_o \qquad \text{and} \qquad \boldsymbol{p}(0) = \boldsymbol{p}_o \,. \tag{2.4}$$

The velocity $\boldsymbol{v}$ of the mass m is recovered as $\boldsymbol{v} = m^{-1}\boldsymbol{p}$.

We observe that the nonlinearity of the dynamical problem under consideration stems from the nonlinear relation of the internal force vector in terms of the unknown vector $\boldsymbol{q}$ (material nonlinearity) and the finite rotation of the mass m around the center O (geometric nonlinearity). In this way, this model problem exhibits the basic nonlinearities characteristic of the nonlinear elastodynamic problem of interest in this work and considered in Section 5. In fact, the characteristic error introduced in the high-frequency spectrum in this infinite dimensional context by typical spatial discretizations can be modeled in the simple model example presented in this section by the consideration of the limit case of a rigid bar given by the DAE system

$$\left.\begin{aligned} \dot{\boldsymbol{q}} &= m^{-1}\,\boldsymbol{p}\,, \\ \dot{\boldsymbol{p}} &= -f_{bar}\,\frac{\boldsymbol{q}}{\|\boldsymbol{q}\|}\,, \\ g(\boldsymbol{q}) &:= \|\boldsymbol{q}\| - l_o = 0\,, \end{aligned}\right\} \tag{2.5}$$

for the unknown internal force magnitude f_{bar} in the bar, the Lagrange multiplier imposing the holonomic constraint $(2.5)_3$ of constant length of the spring to its initial value $l_o = \|\boldsymbol{q}_o\|$.

Introducing the structure matrix $\widehat{\mathbb{J}}$ in $\mathbb{R}^2$, given by

$$\widehat{\mathbb{J}} := \begin{bmatrix} 0 & -1 \\ 1 & 0 \end{bmatrix}\,, \tag{2.6}$$

in a Cartesian basis $\{\boldsymbol{e}_1, \boldsymbol{e}_2\}$ of $\Pi \simeq \mathbb{R}^2$, the exact solution of the system of equations (2.5) is expressed as

$$\boldsymbol{q}(t) = \exp(t\;\Omega_o\;\widehat{\mathbb{J}})\;\boldsymbol{q}_o \qquad \text{and} \qquad \boldsymbol{p}(t) = m\;\Omega_o\;\widehat{\mathbb{J}}\;\boldsymbol{q}(t) = \exp(t\;\Omega_o\;\widehat{\mathbb{J}})\;\boldsymbol{p}_o\,, \tag{2.7}$$

for the angular velocity Ω_o given by

$$\Omega_o = \mathcal{I}_o^{-1}\;\mu_o \qquad \text{for} \quad \mathcal{I}_o := m\;l_o^2 > 0 \quad \text{and} \quad \mu_o := \boldsymbol{p}_o \cdot \widehat{\mathbb{J}}\;\boldsymbol{q}_o\,, \tag{2.8}$$

the inertia $\mathcal{I}_o$ and angular momentum μ_o, respectively. The magnitude of the internal force in the bar is given

$$f_{bar} = m\;l_o\;\Omega_o^2 = \frac{\mu_o^2}{m\;l_o^3} = \frac{\mu_o^2}{\mathcal{I}_o\;l_o}\,, \tag{2.9}$$

as a straightforward calculation shows. We note the skew-symmetry of $\widehat{\mathbb{J}}$, that is,

$$\boldsymbol{d} \cdot \widehat{\mathbb{J}} \boldsymbol{d} = 0 \qquad \forall \boldsymbol{d} \in \mathbb{R}^2 \,, \tag{2.10}$$

for later use.

The system of equations (2.1) for a $0 < \kappa < \infty$ can be understood as a *penalty regularization* of the constrained system (2.5), imposing the constraint $(2.5)_3$ in the limit $\kappa \to \infty$ (see e.g. ARNOLD et al [1988], and references therein). The physically motivated case of a convex potential $V(\cdot)$ is assumed in the developments that follow, that is, we have the relation

$$\vartheta \, V(l_1) + (1-\vartheta) \, V(l_2) - V(\vartheta \, l_1 + (1-\vartheta) \, l_2) \geq 0 \qquad \text{for} \quad \vartheta \in [0,1] \,, \tag{2.11}$$

or, equivalently $V'' \geq 0$ for the case of a smooth function $V(\cdot)$, as considered herein. We observe that the potential (2.3) satisfies this relation. The solution of the penalized system (2.1) involves the rigid rotation similar to (2.7) together with the "high-frequency" oscillation of the spring, the group and internal motions, respectively.

2.2. Symmetries: energy and momentum conservation, relative equilibria

The system of equations (2.1) is a characteristic example of a Hamiltonian system with symmetry, leading to several conservation laws. In particular, and motivated by the numerical analysis presented in Section 3, we have the following properties:

i. *Conservation of energy.* Given the autonomous character of the Hamiltonian (2.2), we have the classical law of conservation of energy, namely,

$$\begin{aligned} \frac{dH}{dt} &= \frac{\partial H}{\partial \boldsymbol{q}} \cdot \dot{\boldsymbol{q}} + \frac{\partial H}{\partial \boldsymbol{p}} \cdot \dot{\boldsymbol{p}} \\ &= \frac{\partial H}{\partial \boldsymbol{q}} \cdot \frac{\partial H}{\partial \boldsymbol{p}} - \frac{\partial H}{\partial \boldsymbol{p}} \cdot \frac{\partial H}{\partial \boldsymbol{q}} = 0 \qquad \Longrightarrow \qquad \boxed{H = \text{constant}} \end{aligned} \tag{2.12}$$

along the solutions $(\boldsymbol{q}(t), \boldsymbol{p}(t)) \in P$ of (2.1).

ii. *Rotational symmetry and conservation of angular momentum.* The action of the group of rotations $G := SO(2)$ on $Q = \mathbb{R}^2/\mathbf{0}$ leads to the action on the phase space P (the so-called cotangent lifted action) given by

$$(\boldsymbol{q}, \boldsymbol{p}) \quad \longmapsto \quad (\boldsymbol{\Lambda q}, \boldsymbol{\Lambda p}) \qquad \forall \boldsymbol{\Lambda} \in SO(2) \quad \text{and} \quad (\boldsymbol{q}, \boldsymbol{p}) \in P \,. \tag{2.13}$$

The invariance of the Hamiltonian (2.2) under this action, that is,

$$H(\boldsymbol{\Lambda q}, \boldsymbol{\Lambda p}) = H(\boldsymbol{q}, \boldsymbol{p}) \qquad \forall \boldsymbol{\Lambda} \in SO(2) \,, \tag{2.14}$$

follows from the invariance of the Euclidean norm under the action of the group of rotations. The dual Lie algebra of G (denoted by $\mathcal{G}^*$) corresponds to the linear space of skew-symmetric matrices $\mathcal{G}^* = so(2)$ in $\mathbb{R}^2$. The consideration of the canonical isomorphism $\widehat{\ } : so(2) \to \mathbb{R}$ given by the relation

$$\mu \in \mathbb{R} \quad \longmapsto \quad \widehat{\boldsymbol{\mu}} = \mu\, \widehat{\mathbb{J}} = \begin{bmatrix} 0 & -\mu \\ \mu & 0 \end{bmatrix} \in so(2)\,, \tag{2.15}$$

leads to the identification $so(2) \simeq \mathbb{R}$. In this context, the momentum map $\boldsymbol{J} : P \to \mathcal{G}^*$ corresponding to the action (2.13) is given by

$$(\boldsymbol{q}, \boldsymbol{p}) \in P \quad \longmapsto \quad \boldsymbol{J}(\boldsymbol{q}, \boldsymbol{p}) = \boldsymbol{p} \cdot \widehat{\mathbb{J}}\boldsymbol{q} \in \mathbb{R}\,. \tag{2.16}$$

A simple calculation shows that along the solutions of (2.1)

$$\dot{\boldsymbol{J}}(\boldsymbol{q}, \boldsymbol{p}) = \boldsymbol{p} \cdot \widehat{\mathbb{J}}\dot{\boldsymbol{q}} + \dot{\boldsymbol{p}} \cdot \widehat{\mathbb{J}}\boldsymbol{q} = m^{-1}\, \boldsymbol{p} \cdot \widehat{\mathbb{J}}\boldsymbol{p} - \frac{V'}{\|\boldsymbol{q}\|}\, \boldsymbol{q} \cdot \widehat{\mathbb{J}}\boldsymbol{q} = 0 \tag{2.17}$$

given the skew-symmetry property (2.10). Equation (2.17) translates in the conservation of the angular momentum

$$\boxed{\boldsymbol{J}(\boldsymbol{q}, \boldsymbol{p}) = \text{constant}\,,} \tag{2.18}$$

for the mechanical system under consideration.

Remark 2.1. The above developments have considered from the start the formulation of the governing equations of the mechanical system of interest in $\Pi \simeq \mathbb{R}^2$. Alternatively, we may consider the dynamics in the general three-dimensional space through the embedding $\Pi \subset \mathbb{R}^3$. Denoting the canonically embedded value $\tilde{\boldsymbol{q}} := (\boldsymbol{q}, 0) \in \mathbb{R}^2 \times \mathbb{R} \simeq \mathbb{R}^3$, we have

$$\boldsymbol{J}(\boldsymbol{q}, \boldsymbol{p}) = \tilde{\boldsymbol{q}} \times \tilde{\boldsymbol{p}} = \boldsymbol{p} \cdot \widehat{\mathbb{J}}\boldsymbol{q}\ \tilde{\boldsymbol{e}}_\perp\,, \tag{2.19}$$

for the standard vector product $\times$ in $\mathbb{R}^3$ and the unit vector $\tilde{\boldsymbol{e}}_\perp$ perpendicular to Π in $\mathbb{R}^3$ (i.e., $\tilde{\boldsymbol{q}} \cdot \tilde{\boldsymbol{e}}_\perp = 0\ \forall \tilde{\boldsymbol{q}} \in \Pi$) with the orthonormal triad $\{\tilde{\boldsymbol{e}}_1, \tilde{\boldsymbol{e}}_2, \tilde{\boldsymbol{e}}_\perp\}$ defining the positive orientation of $\mathbb{R}^3$ through the standard right-hand rule. □

iii. *Relative equilibria.* Trajectories of the dynamical system (2.1) consisting of group motions correspond to the so-called *relative equilibria,* that is, solutions of the form

$$\boldsymbol{q}(t) = \exp(t\Omega_e \widehat{\mathbb{J}})\ \boldsymbol{q}_e\,, \qquad \boldsymbol{p}(t) = \exp(t\Omega_e \widehat{\mathbb{J}})\ \boldsymbol{p}_e \tag{2.20}$$

for fixed $\boldsymbol{z}_e := (\boldsymbol{q}_e, \boldsymbol{p}_e) \in P$ and a fixed $\Omega_e \in \mathcal{G}$ (the Lie algebra of $\boldsymbol{G}$) generating the group motion. Note that we have the trivial identification $\mathcal{G} \simeq \mathcal{G}^* \simeq \mathbb{R}$, with the duality relation given simply by the scalar product in $\mathbb{R}$. We introduce the notation

$$G_\mu = \left\{ \boldsymbol{\Lambda} \in G \quad | \quad \boldsymbol{J}(\boldsymbol{\Lambda}\boldsymbol{q}, \boldsymbol{\Lambda}\boldsymbol{p}) = \boldsymbol{J}(\boldsymbol{q}, \boldsymbol{p}) \quad \text{for} \quad (\boldsymbol{q}, \boldsymbol{p}) \in \boldsymbol{J}^{-1}(\mu) \right\}, \tag{2.21}$$

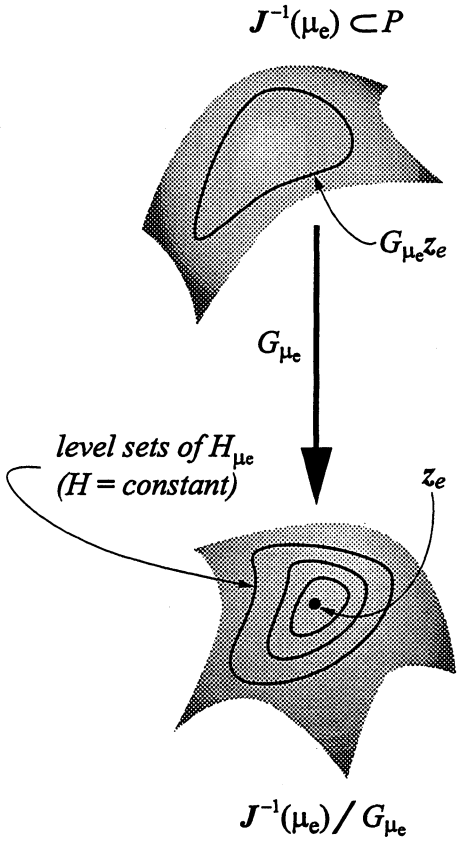

FIGURE 2.2. Sketch of the reduction implied by the symmetry defined by the action of G. The relative equilibria $\boldsymbol{z}_e = (\boldsymbol{q}_e, \boldsymbol{p}_e) \in P$ can be characterized as the stationary points of the Hamiltonian H in the reduce manifold $\boldsymbol{J}^{-1}(\mu_e)/G_{\mu_e}$ for the angular momentum μ_e at the equilibrium.

that is, the subgroup of rotations preserving the angular momentum μ. For the mechanical system under study in this section, we trivially have $G_\mu \equiv G$ due to the commutative character of G; this situation does not hold in the more general setting of nonlinear elastodynamics considered in Section 5. With this notation at hand, relative equilibria are characterized for a given angular momentum μ_e by the angular velocity $\Omega_e \in \mathbb{R}$ and $\boldsymbol{z}_e \in \boldsymbol{J}^{-1}(\mu_e)/G_{\mu_e}$, that is, in the subset $\boldsymbol{J}^{-1}(\mu_e) \subset P$ of states having the equilibrium angular momentum μ_e, up to rotations preserving μ_e. See Figure 2.2 for an illustration.

The introduction of the expressions (2.20) in the governing equations leads to the relations

$$\mu_e = \mathcal{I}_e \, \Omega_e \,, \qquad \boldsymbol{p}_e = m \, \Omega_e \, \widehat{\mathbb{J}} \, \boldsymbol{q}_e \,, \quad \text{and} \quad \underbrace{V'(l_e) - \frac{\mu_e^2}{m \, l_e^3}}_{V'_{\mu_e}} = 0 \,, \tag{2.22}$$

where we have introduced the notation $l_e := \|\boldsymbol{q}_e\|$, the *locked inertia* $\mathcal{I}_e := m \, l_e^2 > 0$ at the

equilibrium, and

$$V_\mu(l) := V(l) + \frac{1}{2}\,\frac{\mu^2}{m\,l^2}\,, \tag{2.23}$$

the *Smale's amended potential.* Condition $(2.22)_3$ corresponds to the equilibrium of the internal force in the spring and the centrifugal force (μ_e^2/ml_e^3). The analogy of the relations (2.22) with the limit rigid solution (2.7)-(2.9) is to be noted: the dynamical system is said to be *"locked"* at the relative equilibrium, since it corresponds to a rigid rotation at the fixed stretching l_e given by the roots of (2.22).

Equations (2.22) can be obtained as the stationary conditions of the augmented Hamiltonian

$$\begin{aligned} H_{\mu_e}(\boldsymbol{q},\boldsymbol{p},\Omega) &= H(\boldsymbol{q},\boldsymbol{p}) + \Omega\left(\boldsymbol{p}\cdot\widehat{\mathbb{J}}\boldsymbol{q} - \mu_e\right) \\ &= \underbrace{\tfrac{1}{2}\|\boldsymbol{p}-\boldsymbol{p}_{\mu_e}(\boldsymbol{q})\|^2}_{K_{\mu_e}} + V_{\mu_e}(l) \end{aligned} \tag{2.24}$$

where

$$\boldsymbol{p}_{\mu_e} := m\,\mathcal{I}_q^{-1}\mu_e\,\widehat{\mathbb{J}}\boldsymbol{q} = \frac{\mu_e}{l^2}\,\widehat{\mathbb{J}}\boldsymbol{q}\,, \tag{2.25}$$

for the locked inertia $\mathcal{I}_q = m\,l^2$ at $\boldsymbol{q}$ (with $l = \|\boldsymbol{q}\|$), as a simple calculation shows. Relative equilibria can then be characterized as stationary points of the Hamiltonian $H(\boldsymbol{q},\boldsymbol{p})$ in $\boldsymbol{J}^{-1}(\mu_e)/G_{\mu_e}$. Note that

$$H_{\mu_e}(\boldsymbol{q},\boldsymbol{p}) = H(\boldsymbol{q},\boldsymbol{p}) \qquad \text{in} \quad \boldsymbol{J}^{-1}(\mu_e)\,. \tag{2.26}$$

These ideas are illustrated in Figure 2.2. The dynamics in the phase space P reduce to the dynamics in $\boldsymbol{J}^{-1}(\mu_e)/G_{\mu_e}$, which can be shown to be canonically Hamiltonian by the classical *reduction theorem* (see ABRAHAM & MARSDEN [1978] or MARSDEN [1992]). The conservation of the Hamiltonian in the reduced dynamics (that is, following the level sets of H depicted in Figure 2.2) can be shown to lead to the *formal stability* of the relative equilibria $\boldsymbol{z}_e$ (in the Liapunov sense) if the Hamiltonian has a definite second variation at $\boldsymbol{z}_e$. Given the positive definite character of K_{μ_e} in (2.24), one arrives at the classical stability condition

$$V''_{\mu_e}\Big|_{l_e} > 0\,, \tag{2.27}$$

that is, the convexity of the amended potential V_{μ_e} at the equilibrium. We refer to MARSDEN [1992] (page (106) and SIMO et al [1991] for complete details of these considerations, where the so-called *reduced energy-momentum method* is developed for the characterization of the stability of simple Hamiltonian systems of the form (2.1). We also refer to ARNOLD et al [1988] (page 102) for an alternative derivation.

Remark 2.2. The reduced dynamics in $\boldsymbol{J}^{-1}(\mu_e)/G_{\mu_e}$ can be constructed explicitly. This requires, however, the construction of an appropriate coordinate system in this manifold. For the case of interest, this involves the (Hamiltonian) evolution of the axial stretch

$l = \|\boldsymbol{q}\|$ of the spring, the so-called *internal motions* in contrast with the *group motions* given by the action of G. This is precisely the methodology considered in GONZALEZ & SIMO [1996] for the analysis of the stability properties of the midpoint rule and an energy-momentum conserving time-stepping algorithms applied to the system of equations (2.1). As it can be seen in this reference, the resulting expressions must be constructed for each considered numerical algorithm and become algebraically highly complicated even in this simple model problem. Since the final interest in the current work is the characterization of the conservation/dissipation properties in the general and more complex setting of nonlinear elastodynamics, we consider the more qualitative description presented above. □

3. Time-Stepping Algorithms for Model Problem I

We describe in this section the numerical analysis of the evolution equations (2.1) in the qualitative picture depicted in the previous section for the continuum problem. In particular, Section 3.1 presents the analysis of some classical schemes which motivates the newly proposed dissipative methods presented in Section 3.2.

3.1. Existing time-stepping integration schemes

Consider a partition $\cup_{n=0}^{N-1}[t_n, t_{n+1}]$ of a time interval $t_0 = 0$ and $t_N = T$, with a typical time increment $\Delta t = t_{n+1} - t_n$ (not necessarily constant). We denote by $\boldsymbol{q}_n \approx \boldsymbol{q}(t_n)$ and $\boldsymbol{p}_n \approx \boldsymbol{p}(t_n)$ the discrete approximations of its continuum counterparts at t_n. With this notation at hand, we consider the following time stepping algorithms.

i. *The generalized α-method.* This three-parameter family of methods generalizes the HHT $\alpha-$method of HILBER et al [1977] in a way that includes the general Newmark's methods as particular cases. For the evolution equations (2.1) under investigation, we write

$$\boxed{\begin{aligned} \boldsymbol{0} &= m\boldsymbol{a}_{n+1} + V'(\|\boldsymbol{q}_{n+\alpha}\|)\frac{\boldsymbol{q}_{n+\alpha}}{\|\boldsymbol{q}_{n+\alpha}\|} \\ \boldsymbol{q}_{n+1} &= \boldsymbol{q}_n + \Delta t m^{-1}\boldsymbol{p}_n + \frac{\Delta t^2}{2}\Big[(1-2\beta)\boldsymbol{a}_n + 2\beta\boldsymbol{a}_{n+1}\Big] \\ \boldsymbol{p}_{n+1} &= \boldsymbol{p}_n + m\Delta t\Big[(1-\gamma)\boldsymbol{a}_n + \gamma\boldsymbol{a}_{n+1}\Big] \end{aligned}} \tag{3.1}$$

where $\boldsymbol{a}_n \approx \ddot{\boldsymbol{q}}(t_n)$ is the algorithmic approximation to the acceleration of the mass m at time t_n, and

$$\boldsymbol{q}_{n+\alpha} = (1-\alpha)\boldsymbol{q}_n + \alpha\boldsymbol{q}_{n+1}\,. \tag{3.2}$$

The following methods are recovered as particular cases:

Algo.1. *The α-method.* The widely used HHT α-methods of HILBER et al [1977] are obtained from (3.2) with the parameters

$$(\alpha,\beta,\gamma) = \Big(\alpha, \Big(1-\frac{\alpha}{2}\Big)^2, \Big(\frac{3}{2}-\alpha\Big)\Big)\,, \quad 0.7 \le \alpha \le 1 \tag{3.3}$$

The resulting schemes define a second order accurate approximation exhibiting high-frequency dissipation proven rigorously for the case linear elastodynamics only.

Algo.2. *A "dissipative" Newmark scheme.* Newmark's method is recovered by setting $\alpha = 1$ for $0 \le \beta, \gamma \le 1$. The particular one-parameter family of methods given by

$$\tfrac{1}{2} < \gamma \le 1,\ \beta = (\gamma + \tfrac{1}{2})^2/4 \tag{3.4}$$

defines first order accurate methods, exhibiting optimal unconditionally stability and numerical dissipation in the high frequencies; see HUGHES [1987].

Algo.3. *The trapezoidal rule.* The member of Newmark's methods defined by $(\alpha,\beta,\gamma) = (1, \frac{1}{2}, \frac{1}{4})$ corresponds to the so-called trapezoidal rule, defining a second order method that conserves energy in the context of linear elastodynamics.

Algo.4. *The midpoint rule.* The combination $(\alpha,\beta,\gamma) = (\frac{1}{2}, \frac{1}{2}, 1)$ defines a second order method that conserves angular momentum in the general nonlinear problem, and energy for the case of linear elastodynamics.

ii. *A discrete energy-momentum scheme* (**Algo.5.**) A conserving approximation of the internal force term can be accomplished with the scheme

$$\boxed{\begin{aligned} \frac{\boldsymbol{q}_{n+1}-\boldsymbol{q}_n}{\Delta t} &= m^{-1}\,\boldsymbol{p}_{n+\frac{1}{2}}\,, \\ \frac{\boldsymbol{p}_{n+1}-\boldsymbol{p}_n}{\Delta t} &= -\frac{V(l_{n+1})-V(l_n)}{l_{n+1}-l_n}\frac{\boldsymbol{q}_{n+1}+\boldsymbol{q}_n}{l_{n+1}+l_n}\,, \end{aligned}} \tag{3.5}$$

where $l_{n+1} := \|\boldsymbol{q}_{n+1}\|$ and $l_n := \|\boldsymbol{q}_n\|$. The scheme (3.5) goes back to LABUDDE & GREENSPAN [1976] for the canonical Hamiltonian system of interest herein. The limit case of $l_{n+1} \to l_n$ in equation (3.5) is well-defined, and leads to the relation

$$\frac{V(l_{n+1})-V(l_n)}{l_{n+1}-l_n} \longrightarrow V'\Big(\frac{l_{n+1}+l_n}{2}\Big) \qquad \text{as} \quad l_{n+1} \longrightarrow l_n\,. \tag{3.6}$$

The resulting method defines a second order approximation of the dynamics inheriting the laws of conservation of energy (2.12) and angular momentum (2.18).

3.1.1. Numerical analysis: summary of the results

Complete analyses of the discrete energy-momentum scheme (**Algo.5.**) and the midpoint rule (**Algo.4.**) can be found in GONZALEZ & SIMO [1996]. These authors showed through an explicit construction of the discrete reduced dynamical equations (see Remark 2.2.2 above) that **Algo.5.** inherits the same relative equilibria of the continuum problem (defined by equations (2.22)), whereas **Algo.4.** was shown to possess Δt-dependent relative equilibria and, thus, different from its continuum counterpart. We note that both schemes conserve the angular momentum (2.18). The unconditional spectral stability of the relative equilibria for the discrete energy-momentum scheme **Algo.5.** was also concluded in this reference, upon linearization of the discrete reduced equations.

Extending these results, we have included in Appendix I complete analyses of all the numerical schemes (**Algo.1.–5.**) without the need of the construction of the reduced dynamics. The conclusions of this analysis can be summarized as follows:

1. The only relative equilibria that the α-method **Algo.1.** exhibits is given by the trivial *static equilibrium* $\boldsymbol{p}_e = 0$. For sufficiently small time steps Δt, the discrete solution dissipates totally to the static equilibrium: the mass stops. The numerical simulations presented in Section 3.3 show that the unconditional dissipative character of the method is lost, and energy growth may appear for large time steps Δt in the general nonlinear range.

2. The Newmark schemes **Algo.2.** show the same numerical properties as discussed in the previous item for the α-method. The lost of the unconditional dissipative character in linear problems and the absence of non-static trivial relative equilibria is, therefore, concluded

3. The trapezoidal rule **Algo.3.** does possess the same relative equilibria as the continuum problem. Along these relative equilibria (that is, when the initial conditions correspond to a relative equilibria), the scheme does conserve energy and angular momentum. These conservation properties do not hold, however, when starting in a general state of the system. In this case, uncontrollable growth of energy may be observed for large time-steps Δt.

4. The midpoint rule **Algo.4.** exhibits relative equilibria different that their continuum counterparts (that is, Δt-dependent), thus confirming the analysis of GONZALEZ & SIMO [1996] discussed above. Angular momentum is conserved but not the energy in the general nonlinear setting, which may lead to uncontrollable growth of energy for large time-steps Δt.

5. The discrete energy-momentum **Algo.5.** conserved energy and angular momentum for the general nonlinear dynamic system, preserving the relative equilibria of the continuum problem.

3.2. A nonlinear energy decaying scheme

The results summarized in the previous section identified the absence of a scheme exhibiting energy dissipation in the fully nonlinear range for a general potential and, more specifically, showing the dissipation in the high frequency range. In the context discussed in Section 2 for the model problem of interest, we consider the variations of the exact solution (2.7) of the limit rigid case as an artifact of the approximation defined by a finite value of the stiffness parameter κ. The goal is to eliminate this high-frequency of the solution, while maintaining the different features of (2.7). To this purpose, we develop a modification of the discrete energy-conserving scheme **Algo.5.** exhibiting this high-frequency energy dissipation by construction. We emphasize again that the current problem is to be motivated only by analog situations in the more interesting infinite dimensional case of nonlinear elastodynamics as studied in Section 5 below.

3.2.1. Formulation of the method

A class of time-stepping algorithms that rigorously show energy decaying in the full nonlinear case can be obtained by the following modification of the original conservative scheme (3.5). First, we consider the generalized approximation of the derivative of the potential

$$\begin{aligned} V'(l) &\approx \frac{(1+\frac{1}{2}\chi_1)V(l_{n+1}) - (1-\frac{1}{2}\chi_1)V(l_n) - \chi_1\ V(\frac{l_{n+1}+l_n}{2})}{l_{n+1}-l_n} \\ &= \frac{V(l_{n+1}) - V(l_n) + \mathcal{D}_V}{l_{n+1}-l_n}\ , \end{aligned} \tag{3.7}$$

for a scalar parameter χ_1, while maintaining the direction of the force to $(\boldsymbol{q}_{n+1}+\boldsymbol{q}_n)/(l_{n+1}+l_n)$ as in (3.5). The last equality in (3.7) follows from straightforward algebraic manipulations for

$$\mathcal{D}_V = \chi_1 \left(\tfrac{1}{2}\Big[V(l_{n+1}) + V(l_n)\Big] - V\Big(\frac{l_{n+1}+l_n}{2}\Big)\right)\ . \tag{3.8}$$

The residual character of this last expression is to be noted. Expression $(3.7)_2$ corresponds then to a dissipative modification of the original momentum conserving approximation for

$$\mathcal{D}_V \geq 0\ , \tag{3.9}$$

see Section 3.2.2 below for details. Property (3.9) applies to the case of interest for $\chi_1 \geq 0$ given the assumed convexity (2.11) of $V(\cdot)$; see Remark 3.1.2 below otherwise. For the particular potential (2.3), expression (3.7) reduces to

$$V'(l) \approx \kappa \left[\vartheta\ l_{n+1} + (1-\vartheta)\ l_n - l_o\right] \qquad \text{for} \quad \vartheta := \tfrac{1}{2}\ (1+\frac{1}{4}\chi_1)\ , \tag{3.10}$$

reminiscent of the so-called ϑ-method for linear problems; see e.g. WOOD [1990]. Expression (3.10) can be found proposed originally in ARMERO & PETOCZ [1996] in the context

of frictionless dynamic contact problems, with the quadratic potential $V(\cdot)$ corresponding to a penalty regularization of the contact constraint in terms of the normal gap. This expression was then employed by KUHL & CRISFIELD [1997] and CRISFIELD et al [1997] in general continuum and beam problems. As shown in the next section, the expression proposed in (3.14) preserves the dissipative properties of the scheme when applied to general potentials.

A spectral analysis of the resulting time-stepping scheme applied to a 1D linear oscillator (i.e., the linearized counterpart of (2.1) at $\boldsymbol{q} = 0$ and $\boldsymbol{p} = 0$) shows that the above dissipative approximation is not enough to introduce energy dissipation in the high-frequency range; see Remark 3.2 below. To accomplish this goal (and guided by the aforementioned spectral analysis) we consider the similar modification of the dynamical update equation $(3.5)_1$

$$\begin{aligned} K'(\pi) &\approx \frac{(1+\frac{1}{2}\chi_2)K(\pi_{n+1}) - (1-\frac{1}{2}\chi_2)K(\pi_n) - \chi_2\ K(\frac{\pi_{n+1}+\pi_n}{2})}{\pi_{n+1}-\pi_n} \\ &= \frac{K(\pi_{n+1}) - K(\pi_n) + \mathcal{D}_K}{\pi_{n+1}-\pi_n}\ , \end{aligned} \tag{3.11}$$

for a scalar parameter χ_2. Equation (3.11) makes use of the notation $\pi_{n+1} := \|\boldsymbol{p}_{n+1}\|$, $\pi_n := \|\boldsymbol{p}_n\|$, and

$$\mathcal{D}_K = \chi_2 \left(\tfrac{1}{2}\Big[K(\pi_{n+1}) + K(\pi_n)\Big] - K\Big(\frac{\pi_{n+1}+\pi_n}{2}\Big)\right)\ , \tag{3.12}$$

which is non-negative (i.e. $\mathcal{D}_K \geq 0$) for $\chi_2 \geq 0$ and convex kinetic energy $K(\cdot)$. For the typical quadratic kinetic energy (2.2), the dynamic equation resulting of the dissipative property (3.11) reads

$$\frac{\boldsymbol{q}_{n+1}-\boldsymbol{q}_n}{\Delta t} = m^{-1}\left(1+\frac{1}{4}\,\chi_2\,\frac{\pi_{n+1}-\pi_n}{\pi_{n+1}+\pi_n}\right)\boldsymbol{p}_{n+\frac{1}{2}}\ , \tag{3.13}$$

as a straightforward algebraic calculation shows.

The final time-stepping scheme can then be written in general form as

$$\boxed{\begin{aligned} \frac{\boldsymbol{q}_{n+1}-\boldsymbol{q}_n}{\Delta t} &= m^{-1}\,\boldsymbol{p}_{n+\frac{1}{2}} + \frac{\mathcal{D}_K}{\pi_{n+1}-\pi_n}\,\frac{\boldsymbol{p}_{n+1}+\boldsymbol{p}_n}{\pi_{n+1}+\pi_n}\ , \\ \frac{\boldsymbol{p}_{n+1}-\boldsymbol{p}_n}{\Delta t} &= -\frac{V(l_{n+1})-V(l_n)+\mathcal{D}_V}{l_{n+1}-l_n}\,\frac{\boldsymbol{q}_{n+1}+\boldsymbol{q}_n}{l_{n+1}+l_n}\ , \end{aligned}} \tag{3.14}$$

for two dissipation functions $\mathcal{D}_K = \widehat{\mathcal{D}_K}(\pi_n, \pi_{n+1})$ and $\mathcal{D}_V = \widehat{\mathcal{D}_V}(l_n, l_{n+1})$, satisfying the relations

$$\frac{\widehat{\mathcal{D}_K}(\pi_n, \pi_{n+1})}{\pi_{n+1}-\pi_n} \longrightarrow 0 \qquad \text{as} \quad \pi_{n+1} \longrightarrow \pi_n \tag{3.15}$$

and

$$\frac{\widehat{\mathcal{D}_V}(l_n, l_{n+1})}{l_{n+1} - l_n} \longrightarrow 0 \qquad \text{as} \quad l_{n+1} \longrightarrow l_n \tag{3.16}$$

to assure the numerical consistency of the approximation (3.14). We show in Section 3.2.2 below that the general relation (3.14) exhibits energy dissipation and conservation of momentum, under certain conditions of the different parameters. For this reason, we refer to this algorithm as the first order *energy dissipative–momentum conserving scheme* or EDMC-1 for short. The energy-momentum conserving scheme (3.5) is recovered by simply setting $\chi_2 = \chi_1 = 0$.

Remarks 3.1.

1. We note that alternative expressions for the dissipation functions $\mathcal{D}_K$ and $\mathcal{D}_V$ can be used. For example, an alternative definition of $\mathcal{D}_V$ in (3.8) for a smooth potential $V(\cdot)$ is given by

$$\mathcal{D}_V = \frac{\chi_1}{8} \left(V'(l_{n+1}) - V'(l_n)\right)(l_{n+1} - l_n) \geq 0 \,, \tag{3.17}$$

or by

$$\mathcal{D}_V = \frac{\chi_1}{8} V''(l_t)\,(l_{n+1} - l_n)^2 \geq 0 \,, \tag{3.18}$$

for the stretch l_t at some time t. Both expressions (3.17) and (3.18) are non-negative for $\chi_1 \geq 0$ and a convex potential $V(\cdot)$ (i.e., satisfying (2.11)). The factors used in (3.17) and (3.18) are such that for a quadratic potential these expressions coincide with (3.8). The consistency condition (3.15) can be easily verified for (3.17) and (3.18).

2. As a matter of fact, the dissipation functions $\mathcal{D}_V$ and $\mathcal{D}_K$ may not be necessarily based on the real energy functions $K(\cdot)$ and $V(\cdot)$, respectively; see, in this respect, the discussion in Section for the model problem of thin beams incorporating the numerical dissipation through only of the potential contributions to the final response of the dynamical system. In particular for the case of a non-convex potential $V(\cdot)$ on the strain measure l, the use of the (lower) convex envelope of $V(\cdot)$ (see e.g. DACOROGNA [1989], page 35) defined by

$$CV = \sup\{\, g \leq V \;\; | \;\; g \;\; \text{convex}\} \,, \tag{3.19}$$

in the expression of the dissipation (3.8) assures the dissipative property (3.9).

3. For χ_2 and χ_1 constant, the above approximation is only first order accurate in time. Second order approximations (in the sense that the truncation error is quadratic in Δt as $\Delta t \to 0$) can be easily obtained by considering $\chi_2 = \chi_1 = \mathcal{O}(\omega \Delta t)$ for $\omega = \sqrt{\kappa/m}$. In this case, however, the numerical properties of the scheme for a fixed and finite

Δt are the same of the first order method with corresponding parameters χ_2 and χ_1. More complex alternative definitions of these numerical parameters is therefore required. This issue is the focus of the second part of this series. □

3.2.2. Discrete conservation/dissipation properties

The numerical properties of the time-stepping algorithm (3.14) are summarized in the following Proposition.

Proposition 3.1 *The numerical scheme (3.14) possesses the following conservation/ dissipation properties:*

1. *The angular momentum is conserved, that is,*

$$\boldsymbol{J}_{n+1} = \boldsymbol{J}_n \ . \tag{3.20}$$

2. *The total energy H satisfies the relation decreases for any Δt*

$$H_{n+1} - H_n = -\left[\mathcal{D}_K + \mathcal{D}_V\right] \ , \tag{3.21}$$

Hence the scheme is unconditionally dissipative (i.e., the energy decays or is conserved for any time step Δt) $\mathcal{D}_K \geq 0$ and $\mathcal{D}_V \geq 0$. In particular, these last two conditions are satisfied by the definitions (3.12) and (3.8) for convex functions $K(\cdot)$ and $V(\cdot)$, and $\chi_2 \geq 0$ and $\chi_1 \geq 0$.

3. *The discrete dynamical exhibits the solutions*

$$\boldsymbol{q}_{e_n} = \boldsymbol{\Lambda}_n \boldsymbol{q}_e \ , \qquad \boldsymbol{p}_{e_n} = \boldsymbol{\Lambda}_n \boldsymbol{p}_e \ , \tag{3.22}$$

for $\{\boldsymbol{q}_e, \boldsymbol{p}_e\}$ satisfying the exact equilibrium relations (2.22) and

$$\boldsymbol{\Lambda}_{n+1} = \boldsymbol{\Lambda}_n \underbrace{\left[1 + \frac{\Delta t}{2}\Omega_e \, \widehat{\mathbb{J}}\right]\left[1 - \frac{\Delta t}{2}\Omega_e \, \widehat{\mathbb{J}}\right]^{-1}}_{cay\left(\Delta t \Omega_e \widehat{\mathbb{J}}\right)} \in SO(2) \ , \tag{3.23}$$

for the arbitrary rotation $\boldsymbol{\Lambda}_o$.

Proof: The proof of these discrete properties follows closely the counterpart proofs of the continuum system. We have briefly:

i. *Conservation of angular momentum.* Multiplying equation $(3.14)_1$ by $\widehat{\mathbb{J}}\boldsymbol{p}_{n+\frac{1}{2}}$, we obtain

$$(\boldsymbol{q}_{n+1} - \boldsymbol{q}_n) \cdot \widehat{\mathbb{J}}\boldsymbol{p}_{n+\frac{1}{2}} = 0 \,, \tag{3.24}$$

after noting that the right-hand-side vanishes due to skew-symmetry property $\boldsymbol{p}_{n+\frac{1}{2}} \cdot \widehat{\mathbb{J}}\boldsymbol{p}_{n+\frac{1}{2}} = 0$. Similarly, multiplying $(3.14)_2$ by $\widehat{\mathbb{J}}\boldsymbol{q}_{n+\frac{1}{2}}$, we have

$$(\boldsymbol{p}_{n+1} - \boldsymbol{p}_n) \cdot \widehat{\mathbb{J}}\boldsymbol{q}_{n+\frac{1}{2}} = 0 \,. \tag{3.25}$$

Finally, combining (3.24) and (3.25), we obtain

$$\begin{aligned} \boldsymbol{J}_{n+1} - \boldsymbol{J}_n &= \boldsymbol{p}_{n+1} \cdot \widehat{\mathbb{J}}\boldsymbol{q}_{n+1} - \boldsymbol{p}_n \cdot \widehat{\mathbb{J}}\boldsymbol{q}_n \\ &= (\boldsymbol{p}_{n+1} - \boldsymbol{p}_n) \cdot \widehat{\mathbb{J}}\boldsymbol{q}_{n+\frac{1}{2}} + \boldsymbol{p}_{n+\frac{1}{2}} \cdot \widehat{\mathbb{J}}\,(\boldsymbol{q}_{n+1} - \boldsymbol{q}_n) = 0 \,, \end{aligned} \tag{3.26}$$

after some straightforward algebraic manipulations and the use once more of the skew-symmetry property (2.10). The conservation of the angular momentum (3.20) follows.

ii. *Energy dissipation.* Multiplying equation $(3.14)_1$ by $(\boldsymbol{p}_{n+1} - \boldsymbol{p}_n)$, $(3.14)_2$ by $(\boldsymbol{q}_{n+1} - \boldsymbol{q}_n)$ and subtracting the resulting expressions, we obtain after some simple algebraic manipulations the relation

$$\underbrace{K_{n+1} + V_{n+1}}_{H_{n+1}} - \underbrace{K_n + V_n}_{H_n} = -\left[\mathcal{D}_K + \mathcal{D}_V\right] \tag{3.27}$$

The decay of the energy

$$H_{n+1} \leq H_n \,, \tag{3.28}$$

follows for $\mathcal{D}_K \geq 0$ and $\mathcal{D}_V \geq 0$. As noted in the previous section, these last two relations follow from the convexity of the (quadratic) kinetic energy and from the assumption of a convex potential function $V(\cdot)$, respectively, with $\chi_2 \geq 0$ and $\chi_1 \geq 0$. The case of a non-convex potential is discussed in Remark 3.1.2. The unconditional dissipative character of the proposed scheme follows.

iii. *Conservation of the relative equilibria.* We first note that $\mathcal{D}_K = \mathcal{D}_V = 0$ for an incremental rotation between $\{\boldsymbol{q}_{n+1}, \boldsymbol{p}_{n+1}\}$ and $\{\boldsymbol{q}_n, \boldsymbol{p}_n\}$ like (3.22). Note that $\pi_n = \pi_{n+1} = \pi_e$ and $l_n = l_{n+1} = l_e$, with the limit expression (3.6) applying in this case. A direct calculation shows that the sequence (I.2) satisfies the discrete governing equations (3.14), after noting the algebraic relation for the Cayley transform (3.23) with $\Omega_e \in \mathbb{R}$

$$\boldsymbol{\Lambda}_{n+1} - \boldsymbol{\Lambda}_n = \frac{\Omega_e \Delta t}{2}\, [\boldsymbol{\Lambda}_{n+1} + \boldsymbol{\Lambda}_n]\widehat{\mathbb{J}} \,, \tag{3.29}$$

if the conditions

$$\boldsymbol{p}_e = \Omega_e \widehat{\mathbb{J}} \boldsymbol{q}_e \,, \qquad \text{and} \qquad V'(l_e) = \frac{\mu_e^2}{m\, l_e^3} \qquad \text{for} \qquad \mu_e = \underbrace{m\, l_e^2}_{\mathcal{I}_e}\, \Omega_e \,, \tag{3.30}$$

are satisfied. We conclude again that $l_e = \|\boldsymbol{q}_e\|$ and Ω_e satisfying exactly the relations (2.22) as in the continuum problem. The only approximation involved in the numerical approximation reduces then to the consideration of the Cayley transform (3.23) instead of the exponential mapping (2.20) in the symmetry group $G = SO(2)$. As noted in Remark I.2 of Appendix I, the resulting equations in this case coincide with the corresponding equations of the trapezoidal rule and energy-momentum conserving scheme. The relative equilibria characterized by (3.22), (3.23) and (3.30) correspond also then to these cases. □

Proposition 3.1 identifies the unconditional stability of the proposed scheme under the assumptions stated in it. Namely, we observe that the Hamiltonian $H(\cdot)$ of the exact problem defines a Liapunov function of the discrete dynamical system

$$(\boldsymbol{q}_o, \boldsymbol{p}_o) \quad \longmapsto \quad (\boldsymbol{q}_n, \boldsymbol{p}_n) \qquad n = 0, 1, 2, \dots \,, \tag{3.31}$$

assumed to exist (maybe imposing a restriction on Δt for the equations (3.14) to define $(\boldsymbol{q}_{n+1}, \boldsymbol{p}_{n+1})$ continuously in terms of $(\boldsymbol{q}_n, \boldsymbol{p}_n)$). That is, the exact Hamiltonian $H(\cdot)$ defines a decreasing function along the flow and, as indicated in Section 2.2 for the exact problem (independently of the actual algorithm used), $H(\cdot)$ exhibits a stationary point at $\boldsymbol{z}_e = (\boldsymbol{q}_e, \boldsymbol{p}_e)$ in $\boldsymbol{J}^{-1}(\mu_e)/G_{\mu_e}$. Since by Proposition 3.1 the algorithm also preserves the angular momentum $\boldsymbol{J}(\boldsymbol{q}, \boldsymbol{p}) = \mu$, the dynamical system (3.31) does take place in $\boldsymbol{J}^{-1}(\mu_e)$, that is,

$$(\boldsymbol{q}_n, \boldsymbol{p}_n) \in \boldsymbol{J}^{-1}(\mu_e) \qquad n = 0, 1, 2, \dots \tag{3.32}$$

with simply $\mu_e = \boldsymbol{J}(\boldsymbol{q}_o, \boldsymbol{p}_o)$ for the initial conditions. The stability of the relative equilibria $\boldsymbol{z}_e = (\boldsymbol{q}_e, \boldsymbol{p}_e)$ for the discrete dynamical system (3.31) in $\boldsymbol{J}^{-1}(\mu_e)/G_{\mu_e}$ follows then by Liapunov theorem (see e.g. HIRSCH & SMALE [1974], page 193) when $H|_{\boldsymbol{J}^{-1}(\mu_e)/G_{\mu_e}} = H_{\mu_e}$ exhibits a minimum at $\boldsymbol{z}_e$. This is the same condition as for the exact continuum system and imposes the convexity of the amended potential (2.27).

We note that for the particular case (2.3), we have

$$\mathcal{D}_V = \widehat{\mathcal{D}_V}(l_n, l_{n+1}) < 0 \qquad \text{for} \quad l_{n+1} \neq l_n \,, \tag{3.33}$$

and similarly for $\mathcal{D}_K$ in terms of the quadratic kinetic energy. We also note that if $\|\boldsymbol{q}_n\| = \|\boldsymbol{q}_{n+1}\|$, then $\boldsymbol{q}_n$ and $\boldsymbol{q}_{n+1}$ define the same element of $\boldsymbol{J}^{-1}(\mu_e)/G_{\mu_e}$ (that is, there is a rotation relating both). Therefore, the qualitative picture in $\boldsymbol{J}^{-1}(\mu_e)/G_{\mu_e}$ with a stable relative equilibria $\boldsymbol{z}_e$ attracting asymptotically the trajectories of the discrete dynamical system (3.31) becomes clear. See Figure 3.1 for an illustration. Following a similar

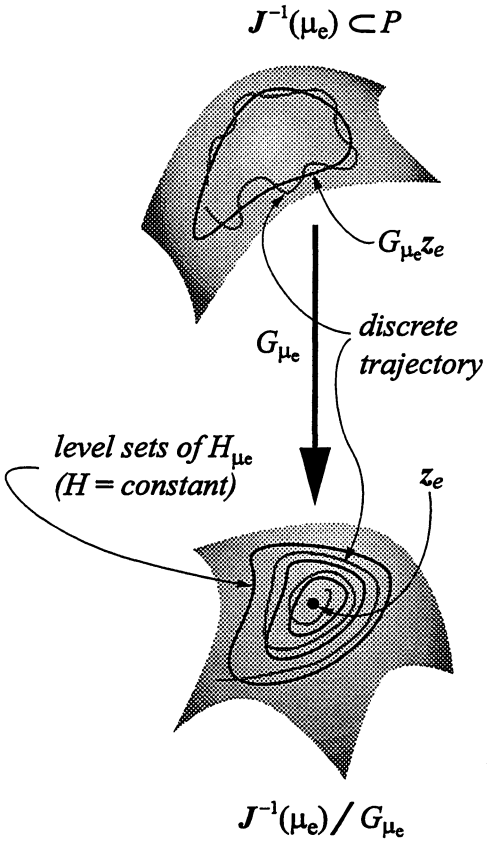

FIGURE 3.1. Sketch of the discrete dynamics induced by the numerical scheme. High-frequency energy dissipation is introduced in the internal motions, while maintaining a second order approximation of the group motions of the relative equilibria.

argument, we also observe that for the case that the exact continuum system exhibits an unstable relative equilibria at z_e, with $H|_{J^{-1}(\mu_e)/G_{\mu_e}}$ not exhibiting a minimum at z_e, the discrete dynamical system will exhibit the same properties for the relative equilibria.

Proposition 3.1 characterizes completely the stability properties of the resulting discrete dynamical system in the fully nonlinear range. In fact, the final response is fully depicted in Figure 3.1, where the dissipation of the internal modes in the reduced space $J^{-1}(\mu_e)/G_{\mu_e}$ is shown. The group motions are not dissipated and only approximated by the Cayley transform (3.23) instead of the exact exponential map of (2.20). The long-term solution of the discrete dynamical system corresponds then to a second order approximation, energy and momentum conserving approximation of the relative equilibria of the exact problem. This situation is to be contrasted with the existing "dissipative" schemes considered in Section 3.1, leading only at best to the static equilibrium position asymptotically in the long-term. As noted in the introductory Section 1, the introduction of numerical dissipation only in the internal motions of the problem as fundamental for a

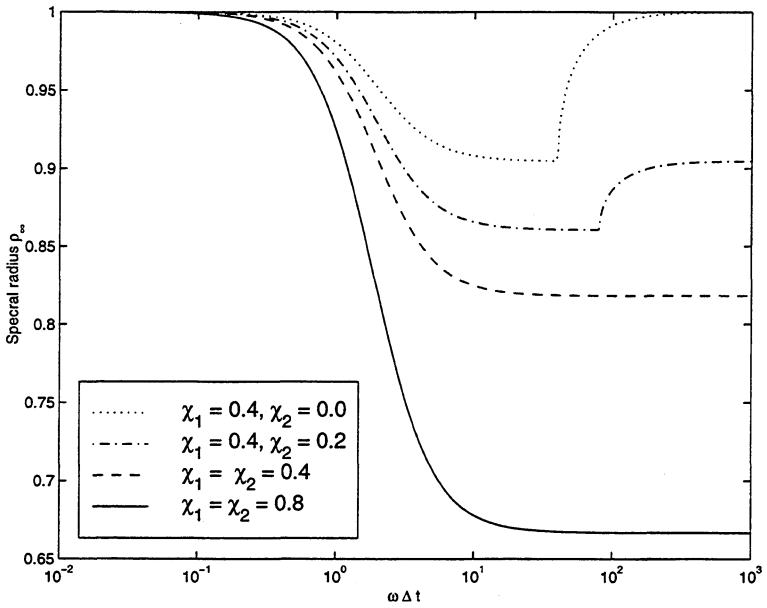

FIGURE 3.2. Spectral radius versus non-dimensional frequency $\Omega = \omega\Delta t$ for a linear 1D oscillator and different algorithmic parameters. The presence of high-frequency dissipation $\rho_\infty < 1$ for $\chi_1, \chi_2 > 0$ can be observed.

good integrator in the fully nonlinear range.

Remark 3.2. As also noted in the introduction, it is crucial to assure the presence of the energy dissipation in the high-frequency range. We evaluate this (linear) property by performing a spectral analysis of the discrete equations for a 1D linear oscillator with a natural frequency ω $(= \sqrt{\kappa/m})$. We refer to Part II of this series for additional details in conjunction with high order methods. These calculations reveal the spectral radius distribution in terms of the non-dimensional frequency $\Omega := \omega\Delta t$ depicted in Figure 3.2 for different values of the numerical parameters χ_1 and χ_2. The spectral radius at infinity ρ_∞ is given by the expression

$$\boxed{\rho_\infty = \max\left(\frac{|1 - \frac{1}{4}\chi_1|}{1 + \frac{1}{4}\chi_1}, \frac{|1 - \frac{1}{4}\chi_2|}{1 + \frac{1}{4}\chi_2}\right)} \tag{3.34}$$

showing the full symmetry of the actual analysis in the parameters χ_1 and χ_2. For $\chi_1 \neq \chi_2$ a bifurcation in the high-frequency range can be observed, making optimal the consideration of equal parameters $\chi_1 = \chi_2$. In particular, the consideration of $\chi_2 = 0$ leads to $\rho_\infty = 1$, thus precluding the presence in the high-frequency range. □

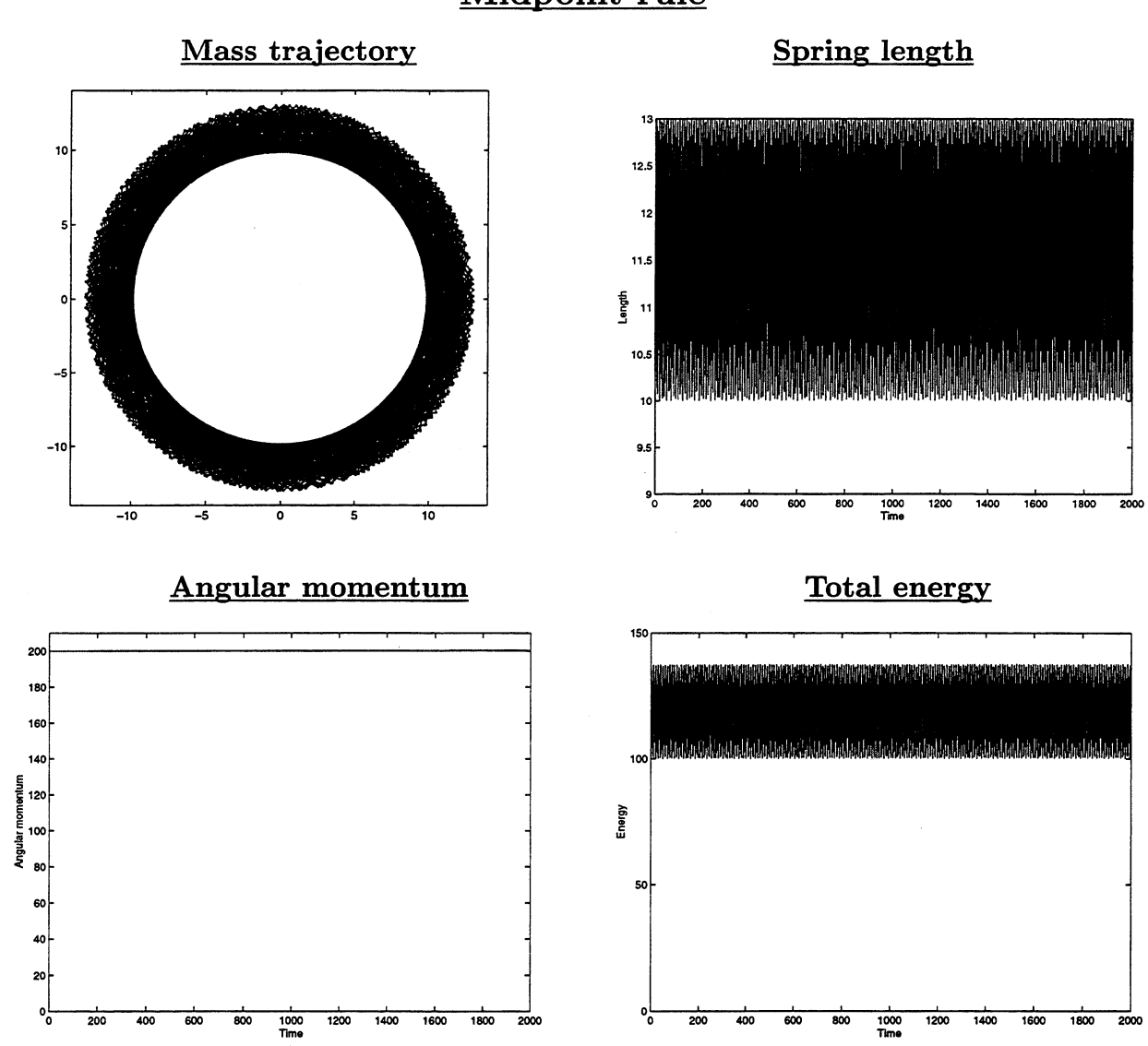

FIGURE 3.3. Nonlinear mass-spring system. Solution obtained with the midpoint rule.

3.3. Representative numerical simulations

To illustrate the analytical results presented in the previous sections we present next the numerical results obtained with the different time-stepping under investigation for a particular case. We consider a spring characterized by the potential (2.3) with parameters $l_o = 10$ and $\kappa = 15$. The value of the mass mass is $m = 2$. The assumed initial conditions are

$$\boldsymbol{q}_o = [0 \quad 10]^T \qquad \text{and} \qquad \boldsymbol{p}_o = [-20 \quad 0]^T \,, \tag{3.35}$$

leading to an initial angular momentum of $\mu_o = \boldsymbol{p}_o \cdot \widehat{\mathbb{J}}\boldsymbol{q}_o = 200$ and initial energy of $H_o = 100$. The relative equilibrium length corresponding to the angular momentum μ_o,

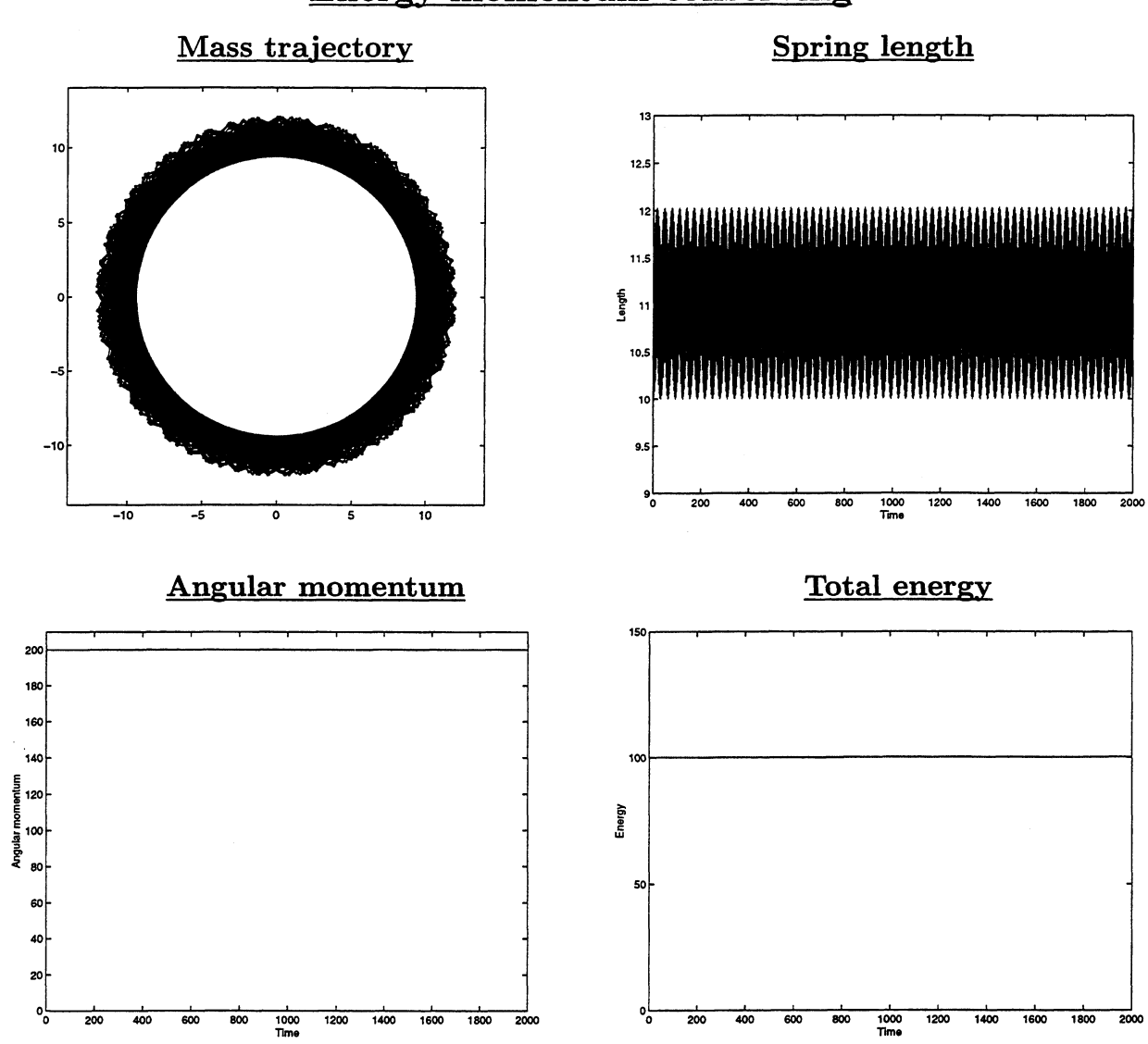

FIGURE 3.4. Nonlinear mass-spring system. Solution obtained with the energy-momentum conserving scheme.

given by (2.22), is $l_e = 11.001377$.

We run the simulations using the previously considered time-stepping algorithms with a constant time step of $\Delta t = 1$ for $2,000$ time steps total. Figures 3.3 to 3.7 show the results for the midpoint rule, energy-momentum conserving scheme, "dissipative" Newmark ($\gamma = 0.611$), HHT ($\alpha = 0.889$) and dissipative EDMC-1 ($\chi_1 = \chi_2 = 0.44$) schemes. The spectral radius at infinity of $\rho_\infty = 0.8$ has been set for the last three schemes. In all cases, we plot the trajectory of the mass, the spring's length, angular momentum and total energy.

Figure 3.3 shows the results for the midpoint rule. We observe the well-known non-conservation of energy and conservation of angular momentum in this nonlinear range.

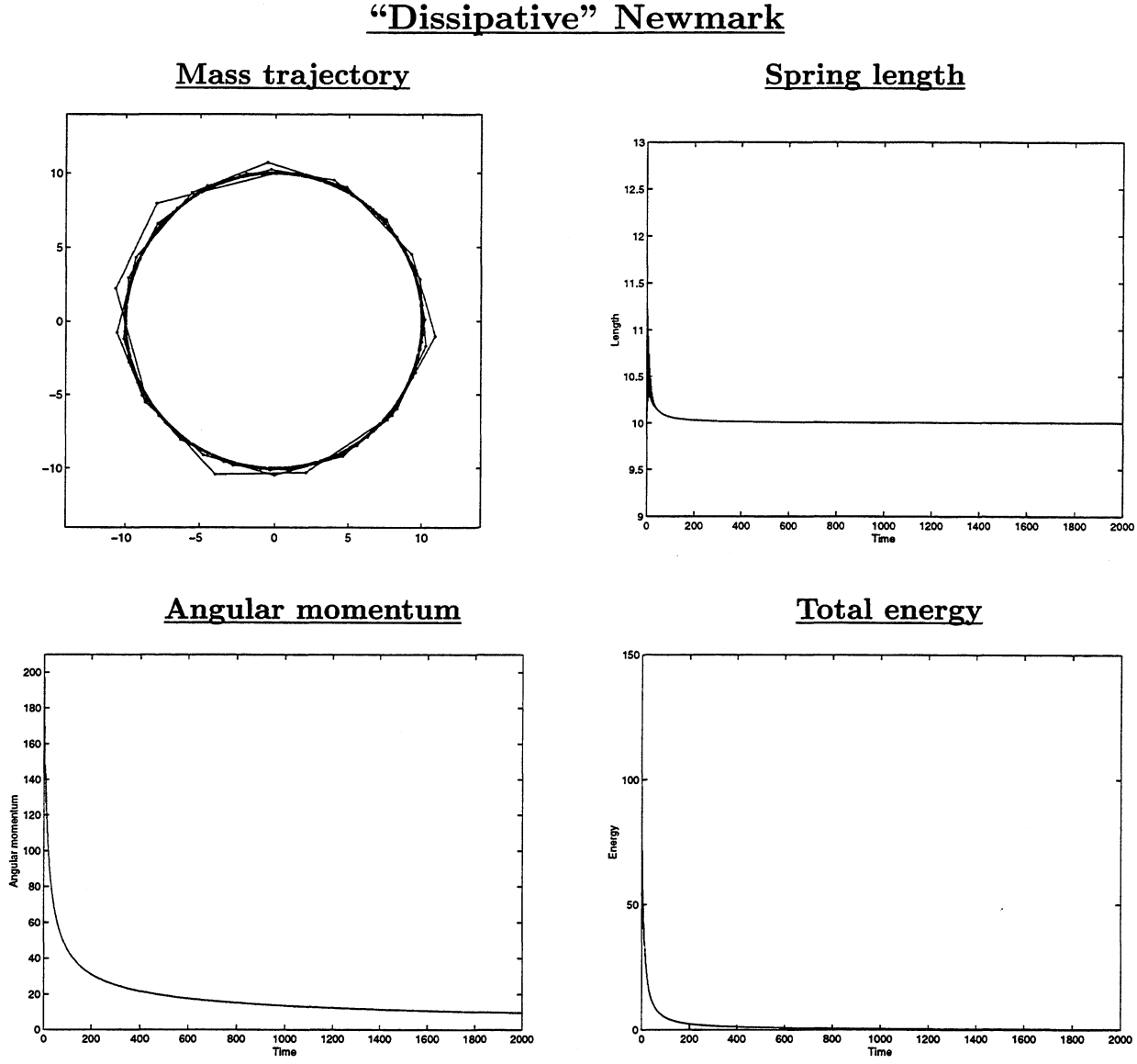

FIGURE 3.5. Nonlinear mass-spring system. Solution obtained with the"dissipative" Newmark scheme.

The oscillation of the spring's length is also apparent. An increase of the time step leads eventually to an unstable response characterized by an uncontrollable growth in the energy (see GONZALEZ & SIMO [1996]). The results obtained with the energy-momentum conserving scheme are shown in Figure 3.4. We observe the improved energy response given by the conservation of the total energy. However, we can still observe the presence of "high-frequency" response in the solution as illustrated by the oscillation of the spring's length.

To eliminate this oscillation in the spring's and, thus, to obtain a better approximation of the limit rigid case, we consider two "dissipative" schemes. Figures 3.5 and 3.6 show

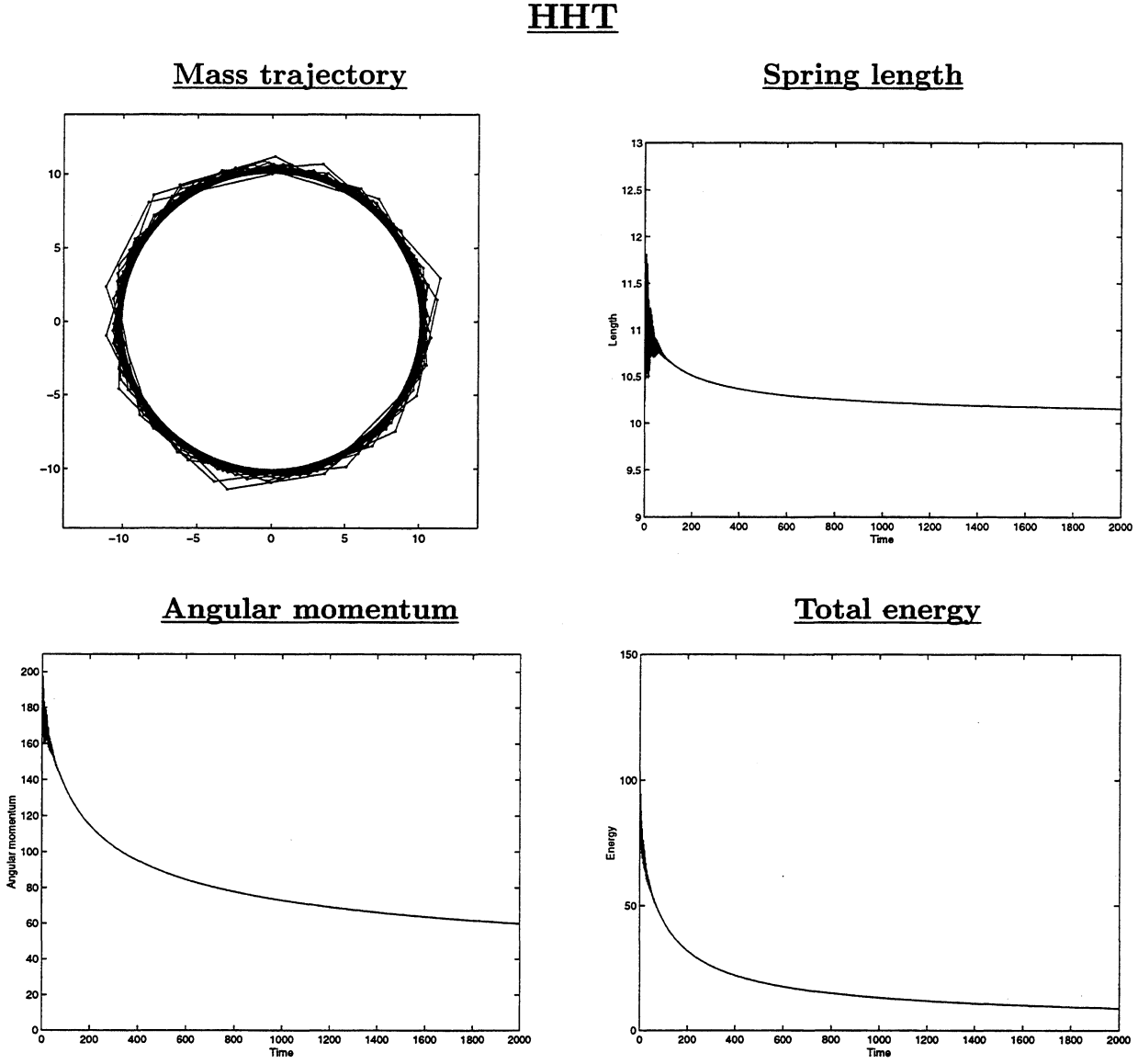

FIGURE 3.6. Nonlinear mass-spring system. Solution obtained with the HHT scheme.

the results for the "dissipative" Newmark and HHT schemes, both with $\rho_\infty = 0.8$. In both cases, we observe the elimination of the oscillation in the spring's length after an initial period. As shown in the analyses presented in Section 3.1.1, this dissipation comes also with a complete dissipation of both the angular and total energy in the system. The system tends *asymptotically* to the static relative equilibrium of a mass at rest. We observe a much more rapid dissipation in the Newmark scheme, a feature that can be traced back to the first order accuracy of this scheme in contrast of the second order HHT scheme. In any case, the computed solutions are unacceptable when compared with the exact rigid limit solution (2.7).

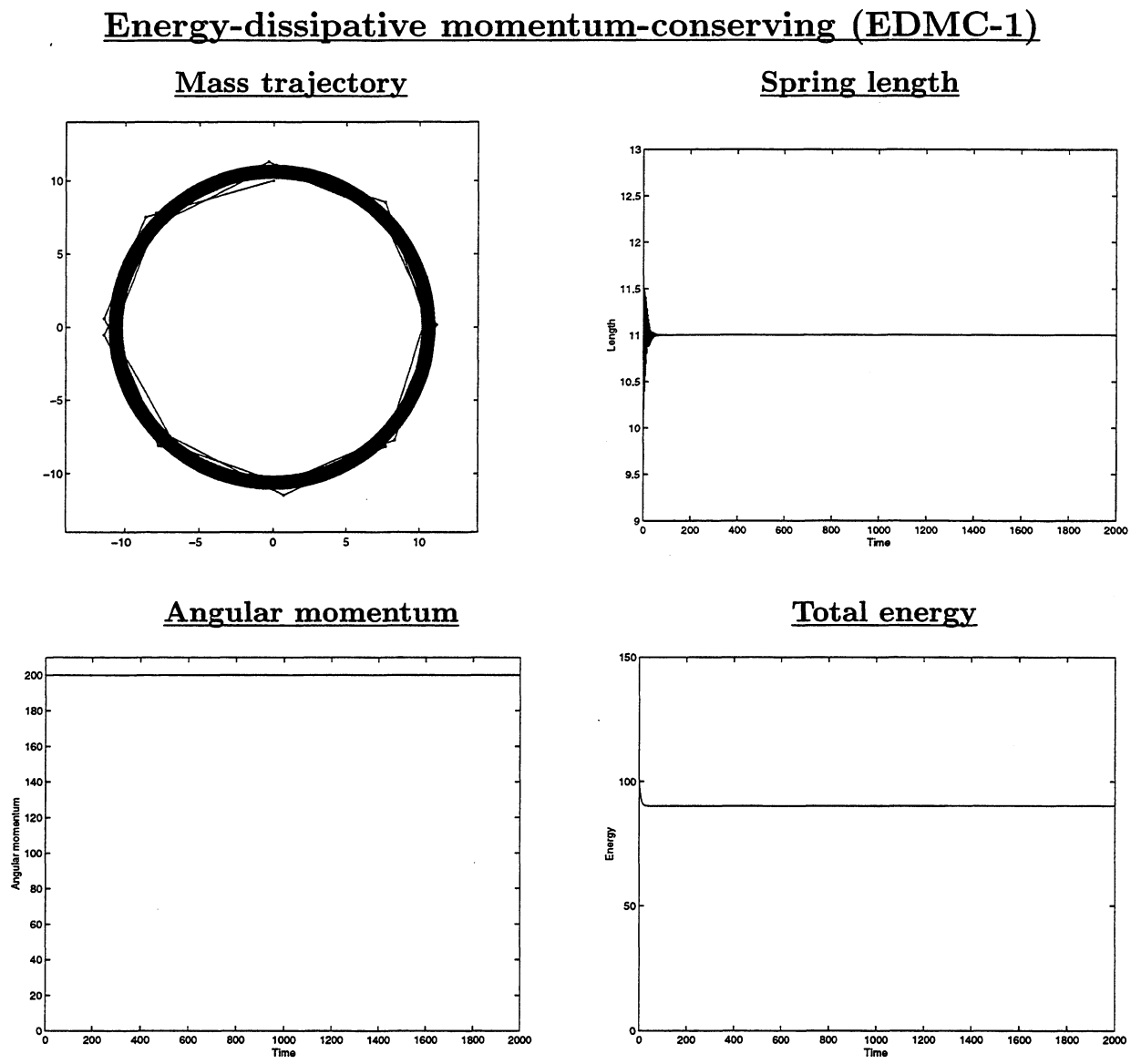

FIGURE 3.7. Nonlinear mass-spring system. Solution obtained with the (energy-dissipative, momentum-conserving) scheme.

Figure 3.7 shows the results obtained with the new energy-dissipating, momentum-conserving (EDMC-1) scheme. The conservation of the angular momentum $\mu = \mu_o$ at all times is verified. We can also observe the elimination of the high-frequency dissipation in the spring's length after an initial time period, maintaining the spring at an essentially constant length. The long-term solution corresponds to the relative equilibrium for the assumed angular momentum, confirming the analyses presented in Section 3.2.2. A monotonic dissipation of the total energy to the equilibrium value is also observed. The spring continues the equilibrium rigid rotation for ever, approximating closely the exact rigid limit solution (2.7). In fact, the approximation of this limit solution is second order in time, as

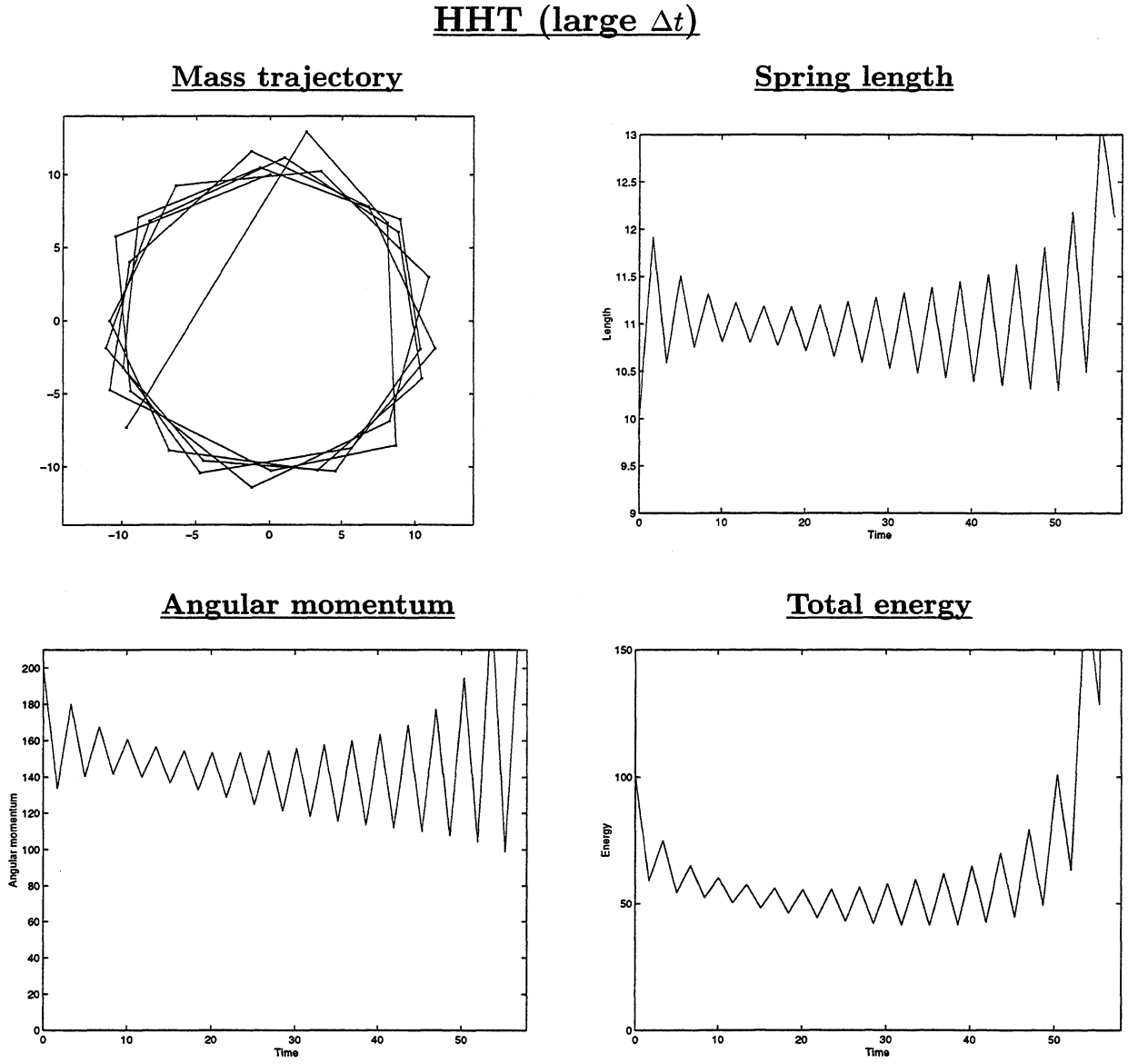

FIGURE 3.8. Nonlinear mass-spring system. Solution obtained with the HHT scheme with a larger time step ($\Delta t = 1.6775$).

discussed in Section 3.2.2. The improved long-term response of the newly proposed scheme in front of existing schemes is concluded.

To illustrate the lack of unconditional dissipativity in traditional "dissipative" time-stepping schemes, we include in Figure 3.8 the results obtained with the same HHT scheme considered before (i.e. with $\rho_\infty = 0.8$), but with a larger time step of $\Delta t = 1.6775$. We observe that, after an initial period of energy decay, the total energy starts increasing eventually, leading to non convergence of the numerical simulation at a time of $t \approx 58$. The lack of dissipativity for this scheme and time step becomes evident.

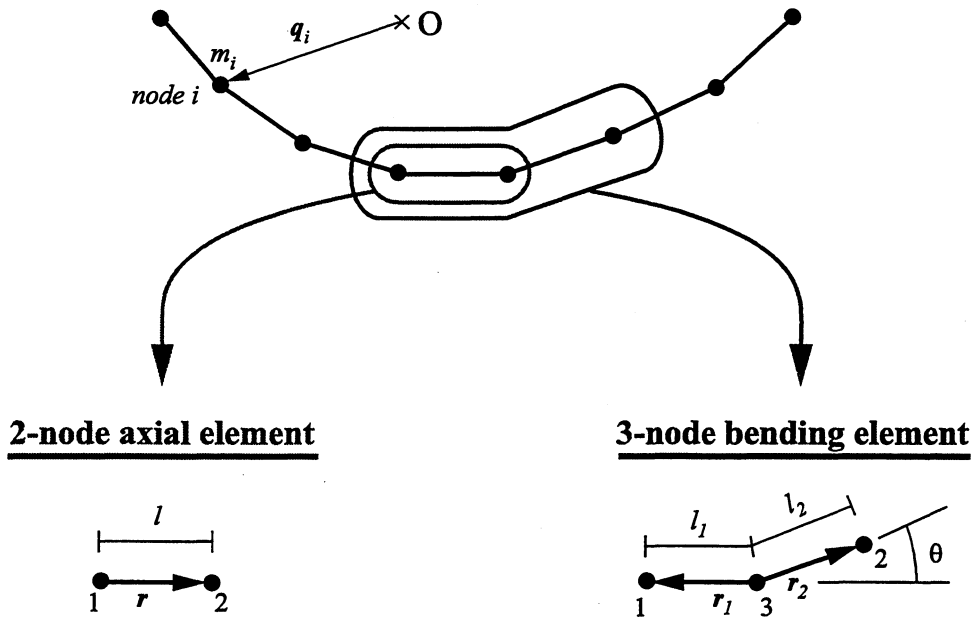

FIGURE 4.1. Model problem II: thin beams. Geometric definition of a simple model for the simulation of the axial and bending contributions of a thin beam.

4. Model Problem II: a Simplified Model of Thin Beams

We consider in this section a simple model of the bending of thin beams to illustrate an additional property of the previous ideas in the development of dissipative numerical scheme: namely, the flexibility of introducing a priori the numerical dissipation in the desired components of the problem. The numerical model of beam bending developed in this section considers the axial and bending contributions of the beam deformation through the simple consideration of axial and bending springs. We plan to present the formulation of similar schemes in the context of general geometrically exact theories of Cosserat rods in a forthcoming publication.

4.1. A simple model of beam bending

Consider a system of n_{point} point masses connected by axial and bending springs, modeling the corresponding components of the deformation of a thin beam. The usual assumption of neglecting the shear deformation is implied in the word "thin" (that is, of the Euler-Bernoulli type). We consider, for simplicity, the plane case, although the developments presented herein apply to general three-dimensional problems with the addition, if desired, of similar contributions modeling the torsion component of the beam or rod.

Figure 4.1 illustrates a typical configuration of the system of point masses m_i with corresponding position vector denoted by $\boldsymbol{q}_i$. Denoting the linear momentum of each mass

by $\boldsymbol{p}_i$, the governing equations read

$$\left.\begin{aligned} \dot{\boldsymbol{q}}_i &= m_i^{-1}\boldsymbol{p}_i \,, \\ \dot{\boldsymbol{p}}_i &= -\mathop{\mathbf{A}}_{e=1}^{n_{\text{elem}}} \boldsymbol{f}_i^{(e)}(\boldsymbol{q}) + \boldsymbol{f}_i^{ext} \,, \end{aligned}\right\} \tag{4.1}$$

(no sum in i implied) with $\boldsymbol{q} := \{\boldsymbol{q}_1, \boldsymbol{q}_2, \ldots, \boldsymbol{q}_{n_{point}}\}$, for a set of external forces $\boldsymbol{f}_i^{ext}$ and a system of internal forces $\boldsymbol{f}_i^{(e)}$ acting on mass m_i $(i = 1, n_{point})$, the latter composed by the assembly of different n_{elem} "elements" as described below. In particular, we consider the contribution of 2-node axial elements modeling the stiffness of the system to stretch axially, and of 3-node bending elements modeling the stiffness of the system to bend. To this purpose we present next the axial and bending elements depicted in Figure 4.1 separately.

i. *A 2-node axial element.* Every two masses m_i are assumed connected by a nonlinear spring characterized by a potential

$$V_{ax} = V_{ax}(l) \qquad \text{for} \quad l := \sqrt{\boldsymbol{r}\cdot\boldsymbol{r}} \tag{4.2}$$

for the vector $\boldsymbol{r} = \boldsymbol{q}_{e_2} - \boldsymbol{q}_{e_1}$ connecting nodes 1 and 2 of the axial element; see Figure 4.1. With this notation, the axial forces acting on each node are obtained through the corresponding derivative of the potential $V(l)$, thus leading to

$$\boldsymbol{f}_{ax}^{(e)} := \left\{ \begin{matrix} \boldsymbol{f}_{ax_{e_1}}^{(e)} \\ \boldsymbol{f}_{ax_{e_2}}^{(e)} \end{matrix} \right\} = \left\{ \begin{matrix} \partial_{q_{e_1}} V \\ \partial_{q_{e_2}} V \end{matrix} \right\} = \frac{1}{l}\partial_l V \left\{ \begin{matrix} -\boldsymbol{r} \\ \boldsymbol{r} \end{matrix} \right\} \tag{4.3}$$

as a simple calculation shows. The analogy with the developments of Section 2.1 is apparent.

ii. *A 3-node bending element.* In the spirit of the simplicity of the current model problem, we introduce torsional springs between any three different masses $\{\boldsymbol{q}_{e_1}, \boldsymbol{q}_{e_2}, \boldsymbol{q}_{e_3}\}$ to model the bending stiffness. Denoting by ϑ the angle between the relative vectors in such an element, we can write

$$\cos\vartheta = -\frac{\lambda}{\nu} \qquad \text{for} \quad \lambda = \boldsymbol{r}_1 \cdot \boldsymbol{r}_2 \quad \text{and} \quad \nu := l_1 l_2 \,, \tag{4.4}$$

with

$$\boldsymbol{r}_i := \boldsymbol{q}_{e_i} - \boldsymbol{q}_{e_3} \quad \text{and} \quad l_i = \sqrt{\boldsymbol{r}_i \cdot \boldsymbol{r}_i} \quad (i = 1, 2) \,, \tag{4.5}$$

following the notation of Figure 4.1. A bending potential

$$V_{bend} = \tilde{V}_{bend}(\vartheta) = \hat{V}_{bend}(\lambda, \nu) \tag{4.6}$$

is introduced. The simulations presented in Section 4.3 consider the particular potential

$$V_{bend} = \tfrac{1}{2}\, C_b\, \tan^2 \frac{\vartheta}{2} = \tfrac{1}{2}\, C_b\, \frac{\nu+\lambda}{\nu-\lambda}\,, \tag{4.7}$$

for a material constant C_b. The potential (4.7) penalizes the full overlapping of the element for $\vartheta \to \pm\pi$. The associated nodal forces are then obtained as

$$\begin{aligned} \boldsymbol{f}^{(e)}_{bend} := \left\{ \begin{array}{c} \boldsymbol{f}^{(e)}_{bend_{e_1}} \\ \boldsymbol{f}^{(e)}_{bend_{e_2}} \\ \boldsymbol{f}^{(e)}_{bend_{e_3}} \end{array} \right\} &= \left\{ \begin{array}{c} \partial_{q_{e_1}} V_{bend} \\ \partial_{q_{e_2}} V_{bend} \\ \partial_{q_{e_3}} V_{bend} \end{array} \right\} = \partial_\lambda \hat{V}_{bend} \left\{ \begin{array}{c} \boldsymbol{r}_2 \\ \boldsymbol{r}_1 \\ -\boldsymbol{r}_1 - \boldsymbol{r}_2 \end{array} \right\} \\ &+ \partial_\nu \hat{V}_{bend} \left[\frac{l_2}{l_1} \left\{ \begin{array}{c} \boldsymbol{r}_1 \\ 0 \\ -\boldsymbol{r}_1 \end{array} \right\} + \frac{l_1}{l_2} \left\{ \begin{array}{c} 0 \\ \boldsymbol{r}_2 \\ -\boldsymbol{r}_2 \end{array} \right\} \right], \end{aligned} \tag{4.8}$$

as a simple calculation shows.

Remark 4.1.

1. Equation $(4.1)_1$ assumes no additional contributions to the kinetic energy of the system but of the linear momenta $\boldsymbol{p}_i$; that is, the kinetic energy is given by

$$K(\boldsymbol{p}) = \sum_{i=1}^{n_{point}} \tfrac{1}{2} m_i^{-1} \|\boldsymbol{p}_i\|^2 \,. \tag{4.9}$$

   This assumption accounts for neglecting any contribution arising from a rotatory inertia. It is well-known that this lack of rotatory inertia introduces infinite phase velocities in the high-frequency range of the bending modes of an Euler-Bernoulli beam (see e.g. GRAFF [1975], page 181). For the problems considered in Section 4.3, typical in structural dynamics applications, this high-frequency content of the beam's response in bending is not manifested, allowing to simplify the forthcoming developments.

2. The system of equations (4.1) defines also a Hamiltonian system with the conservation property

$$H(\boldsymbol{q},\boldsymbol{p}) = K(\boldsymbol{p}) + \sum_e \left[V^{(e)}_{ax}(\boldsymbol{q}) + V^{(e)}_{bend}(\boldsymbol{q}) \right] = \; constant \,, \tag{4.10}$$

   for the case with no external loading $\boldsymbol{f}^{ext}_i = 0$ $(i = 1, n_{point})$, as a simple calculation shows. Similarly, for the case of no external loading and no impose displacements (i.e., no impose $\boldsymbol{q}$) straightforward manipulations show the conservation laws

$$\boldsymbol{l} := \sum_{i=1}^{n_{point}} \boldsymbol{p}_i = \; constant \qquad \text{and} \qquad \boldsymbol{\mu} := \sum_{i=1}^{n_{point}} \boldsymbol{p}_i \cdot \widehat{\mathbb{J}} \boldsymbol{q}_i = \; constant \,, \tag{4.11}$$

for the linear and angular momenta, respectively. □

4.2. An unconditionally dissipative time-stepping scheme

Conservative and dissipative approximations of the axial contributions (4.3) are obtained exactly in the same way as in (3.14) for the spring model problem considered in Section 3.2. In this way, the velocity equation is approximated in time by

$$\frac{\boldsymbol{q}_{i_{n+1}} - \boldsymbol{q}_{i_n}}{\Delta t} = m_i^{-1} \left(1 + \frac{1}{4}\,\chi_2\,\frac{\pi_{i_{n+1}} - \pi_{i_n}}{\pi_{i_{n+1}} + \pi_{i_n}}\right) \boldsymbol{p}_{i_{n+\frac{1}{2}}} \quad \text{for} \quad i = 1, n_{point}\,, \tag{4.12}$$

with $\pi_{i_n} := \|\boldsymbol{p}_{i_n}\|$ and $\pi_{i_{n+1}} := \|\boldsymbol{p}_{i_{n+1}}\|$. The discrete counterpart of the axial nodal forces contributions are obtained through the expression

$$\boldsymbol{f}_{ax}^{(e)} = \left\{ \begin{array}{c} \boldsymbol{f}_{ax_{e_1}}^{(e)} \\ \boldsymbol{f}_{ax_{e_2}}^{(e)} \end{array} \right\} = \frac{1}{l_{n+1} + l_n}\,\frac{V_{ax}(l_{n+1}) - V_{ax}(l_n) + \mathcal{D}_{V\,ax}}{l_{n+1} - l_n} \left\{ \begin{array}{c} -\boldsymbol{r} \\ \boldsymbol{r} \end{array} \right\}_{n+\frac{1}{2}}\,, \tag{4.13}$$

for a dissipation function $\mathcal{D}_{V\,ax}$ defined as in (3.8). The conservation/dissipation relation

$$\sum_{i=1}^{n_{point}} \boldsymbol{f}_{ax_i}^{(e)} \cdot \left(\boldsymbol{q}_{i_{n+1}} - \boldsymbol{q}_{i_n}\right) = V_{ax}^{(l_{n+1})} - V_{ax}^{(l_n} + \mathcal{D}_{V\,ax}\,, \tag{4.14}$$

follows easily, as it is for the relations

$$\sum_{i=1}^{n_{point}} \boldsymbol{f}_{ax_i}^{(e)} = 0 \qquad \text{and} \qquad \sum_{i=1}^{n_{point}} \boldsymbol{f}_{ax_i}^{(e)} \cdot \widehat{\mathbb{J}}\boldsymbol{q}_{i_{n+\frac{1}{2}}} = 0\,, \tag{4.15}$$

showing the momentum conservation properties of the scheme for the Neumann problem, after following arguments similar to the ones presented in Proposition 3.1; additional details are omitted.

The bending counterpart is constructed in terms of the two variables λ and ν introduced in (4.4) as

$$\begin{aligned} \boldsymbol{f}_{bend}^{(e)} = \left\{ \begin{array}{c} \boldsymbol{f}_{bend_{e_1}}^{(e)} \\ \boldsymbol{f}_{bend_{e_2}}^{(e)} \\ \boldsymbol{f}_{bend_{e_3}}^{(e)} \end{array} \right\} &= \frac{\frac{1}{2}\left(V_{bend}^{(1,1)} + V_{bend}^{(1,0)}\right) - \frac{1}{2}\left(V_{bend}^{(0,1)} + V_{bend}^{(0,0)}\right) + \mathcal{D}_{V\lambda}}{\lambda_{n+1} - \lambda_n} \left\{ \begin{array}{c} \boldsymbol{r}_2 \\ \boldsymbol{r}_1 \\ -\boldsymbol{r}_1 - \boldsymbol{r}_2 \end{array} \right\}_{n+\frac{1}{2}} \\ &+ \frac{\frac{1}{2}\left(V_{bend}^{(1,1)} + V_{bend}^{(0,1)}\right) - \frac{1}{2}\left(V_{bend}^{(1,0)} + V_{bend}^{(0,0)}\right) + \mathcal{D}_{V\nu}}{\nu_{n+1} - \nu_n} \\ &\left[\frac{\bar{l}_2}{\bar{l}_1} \left\{ \begin{array}{c} \boldsymbol{r}_1 \\ 0 \\ -\boldsymbol{r}_1 \end{array} \right\}_{n+\frac{1}{2}} + \frac{\bar{l}_1}{\bar{l}_2} \left\{ \begin{array}{c} 0 \\ \boldsymbol{r}_2 \\ -\boldsymbol{r}_2 \end{array} \right\}_{n+\frac{1}{2}} \right] \end{aligned} \tag{4.16}$$

where $\bar{l}_i = (l_{i_{n+1}} + l_{i_n})/2$, and, for example,

$$\mathcal{D}_{V\lambda} = \chi_\lambda \left[\frac{1}{4} \left(V_{bend}^{(1,1)} + V_{bend}^{(1,0)} + V_{bend}^{(0,1)} + V_{bend}^{(0,0)} \right) - \frac{1}{2} \left(V_{bend}^{(\frac{1}{2},1)} + V_{bend}^{(\frac{1}{2},0)} \right) \right] \tag{4.17}$$

for a parameter $\chi_\lambda \geq 0$ and similarly for $\mathcal{D}_{V\nu}$ for a parameter $\chi_\nu \geq 0$. The convexification presented in Remark 3.1.2 is used, if required. We have made use of the notation

$$\begin{aligned} &V_{bend}^{(1,1)} := V_{bend}(\lambda_{n+1}, \nu_{n+1}) \,, \quad V_{bend}^{(1,0)} := V_{bend}(\lambda_{n+1}, \nu_n) \,, \dots \\ &V_{bend}^{(\frac{1}{2},1)} := V_{bend}(\frac{\lambda_{n+1} + \lambda_n}{2}, \nu_{n+1}) \,, \dots \end{aligned} \tag{4.18}$$

in these last expressions. A simple calculation leads to the relation

$$\sum_{i=1}^{n_{point}} \boldsymbol{f}_{bend_i}^{(e)} \cdot \left(\boldsymbol{q}_{i_{n+1}} - \boldsymbol{q}_{i_n} \right) = V_{bend}^{(1,1)} - V_{bend}^{(0,0)} + \mathcal{D}_{V\lambda} + \mathcal{D}_{V\nu} \,, \tag{4.19}$$

showing the conservative/dissipative character of the proposed scheme. Similarly, the momentum conserving relations

$$\sum_{i=1}^{n_{point}} \boldsymbol{f}_{bend_i}^{(e)} = 0 \qquad \text{and} \qquad \sum_{i=1}^{n_{point}} \boldsymbol{f}_{bend_i}^{(e)} \cdot \widehat{\mathbb{J}} \boldsymbol{q}_{i_{n+\frac{1}{2}}} = 0 \,, \tag{4.20}$$

follows, as it is the conservation of the corresponding relative equilibria for the Neumann problem. The proof follows the arguments of Proposition 3.1; details are omitted.

The purpose for the consideration of this simple model problem is to illustrate the flexibility in the introduction of the numerical dissipation in the proposed time-stepping algorithms. As illustrated by the numerical examples presented in Section 4.3, the axial part of the deformation leads to a high-frequency response when compared to the bending contributions. Therefore, the introduction of the dissipation in the axial contributions (that is, $\mathcal{D}_{V\lambda} = \mathcal{D}_{V\nu} = 0$) leads to an efficient way to eliminate the problems associated to the high-frequency range. We refer to Section 4.3 for complete details of these observations.

4.3. Representative numerical simulations

We present in this section a numerical example to illustrate the performance of the different time-stepping algorithms considered in this work when applied to the simple model problem of thin beams developed in the previous section. The problem is illustrated in Figure 4.2. It consists of two rigid links connected to a thin beam modeled by three internal equal masses m_b, with two additional masses $m_a = 10 \cdot m_b$ located at the ends of the rigid links. The potential (2.3) is considered for the axial contributions whereas the

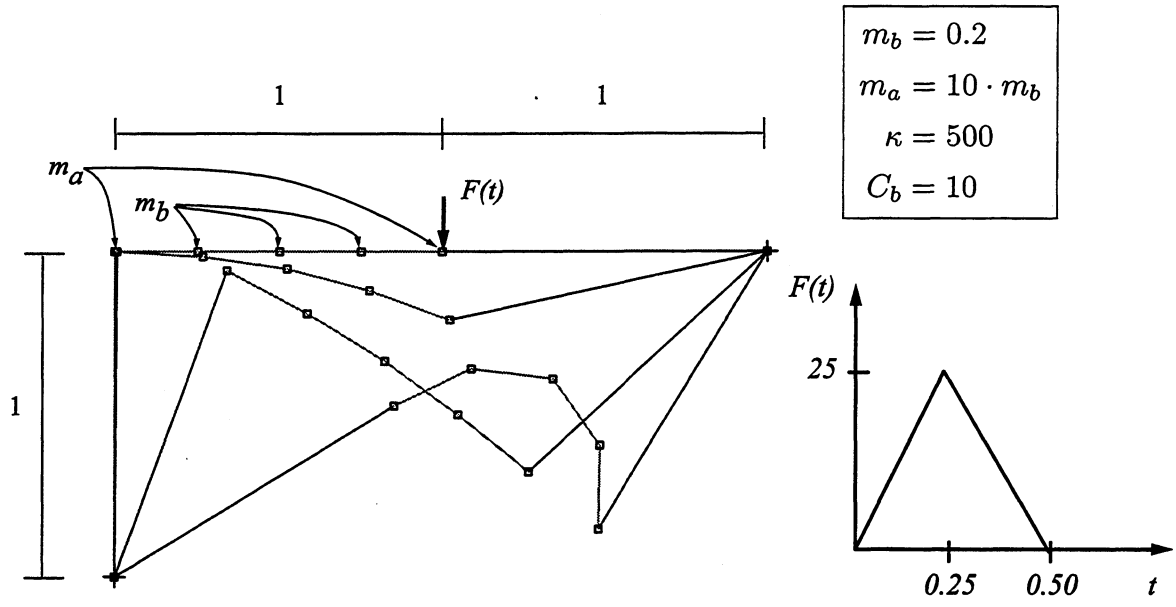

FIGURE 4.2. Thin beams: problem definition. A thin beam is attached to two rigid links in the configuration shown in the top position. A point force is applied downwards to the right end of the beam for an initial interval of $t = 0.50$. Different positions of the deformed configurations afterwards are shown in the figure as obtained by the EDMC-1 scheme.

bending potential (4.7) is considered for the bending contributions; the assumed stiffness parameters κ and C_b are included in Figure 4.2. The two connections between the beam and the two rigid links are pinned (i.e. no bending stiffness). An initial triangular force pulse

$$F(t) = \begin{cases} 100\, t\,, & 0 \leq t \leq 0.25\,, \\ 50 - 100\, t\,, & 0.25 \leq t \leq 0.50\,, \\ 0\,, & t \geq 0.50\,, \end{cases} \tag{4.21}$$

is applied as shown in this figure. The rigid character of the two links is imposed by a standard augmented Lagrangian scheme based again on the penalty potential (2.3).

After the application of the load (4.21) the system evolves such that, as shown in the numerical simulations presented below, the beam oscillates in the low bending modes with sudden axial forces appearing when the elements modeling the beam are aligned due to the sudden change of axial stiffness. Note also the large masses at the beam's ends. The high-frequency content of this sudden forces introduces significant difficulties for the time-stepping algorithms not exhibiting a high-frequency energy dissipation, an observation that can be traced back to CARDONA & GERARDIN [1988]. We also refer to BAUCHAU & THERON [1996] for a similar problem. The example presented herein has the advantage of

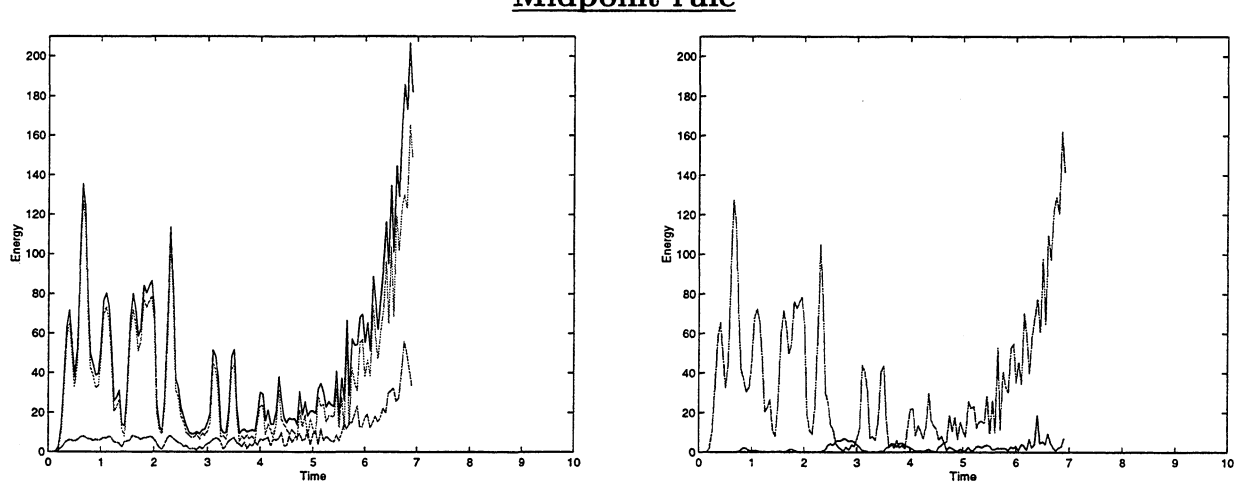

FIGURE 4.3. Thin beams. Solution obtained with the midpoint rule. Left column: Total energy (——) = kinetic (——) + potential (——) energies. Right column: axial (——) + bending (——) energies = potential energy.

exhibiting repeated aligned states thus building the high-frequency content in the solution.

Figures 4.3 and 4.4 depict the results for different time-stepping algorithms. Specifically, the energy evolution obtained by the midpoint rule, energy-momentum conserving and HHT schemes are presented. The left column in these figures shows the evolution of the kinetic and potential energies, and their sum, the total energy. The right column shows the evolution of the axial and bending potential energies, which add to the total potential energy shown in the left column. All the simulations are run with a constant time step $\Delta t = 0.05$.

Figure 4.3 includes the solution obtained with the midpoint rule. As depicted in this figure, the numerical simulation explodes after a relative short time interval. It is clear from this figure that the failure in this case is associated to an unbounded energy growth, and more specifically due to an unbounded growth of the axial energy. Figure 4.5 shows the evolution of the norm of the acceleration of the middle node of the beam. The uncontrollable growth of this quantity is evident.

The results for the energy-momentum conserving schemes are presented in Figure 4.4. The conservation of the total energy after the initial interval of application of the load is apparent in this case. The plot of the axial and bending energies illustrates clearly the oscillation of the beam between states of high energy content in its axial component. The simulation, however, stops for the given time step at one of these spikes in the axial at ($t \approx 4.2$). The Newton-Raphson scheme used to solve the incremental problem ceases to converge. Even though a reduction of the time step may possibly lead to converge, this response illustrates the difficulty in handling the incremental process by time-stepping

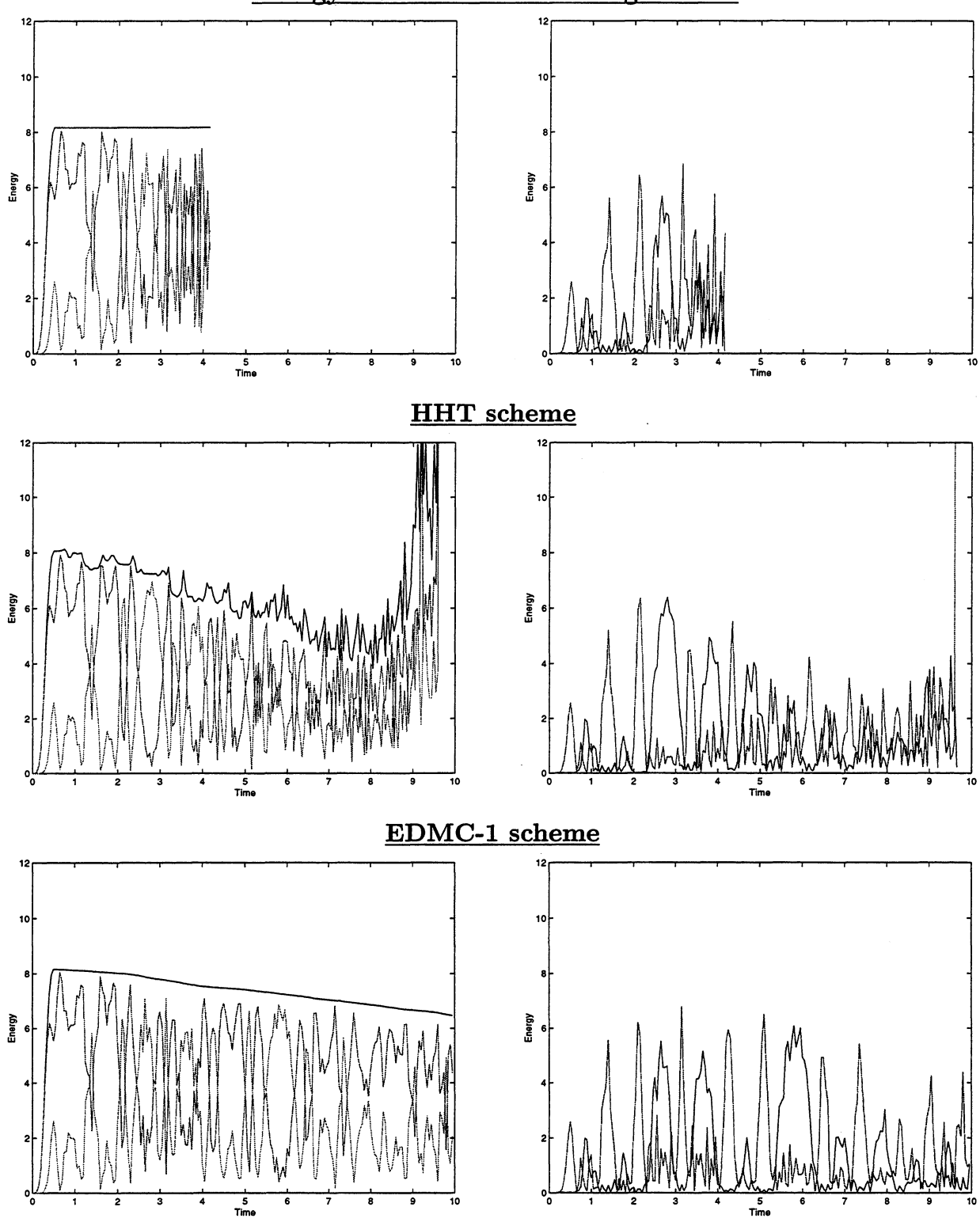

FIGURE 4.4. Thin beams. Comparison of different numerical schemes for a model problem. Left column: Total energy (——) = kinetic (——) + potential (——) energies. Right column: axial (——) + bending (——) energies = potential energy.

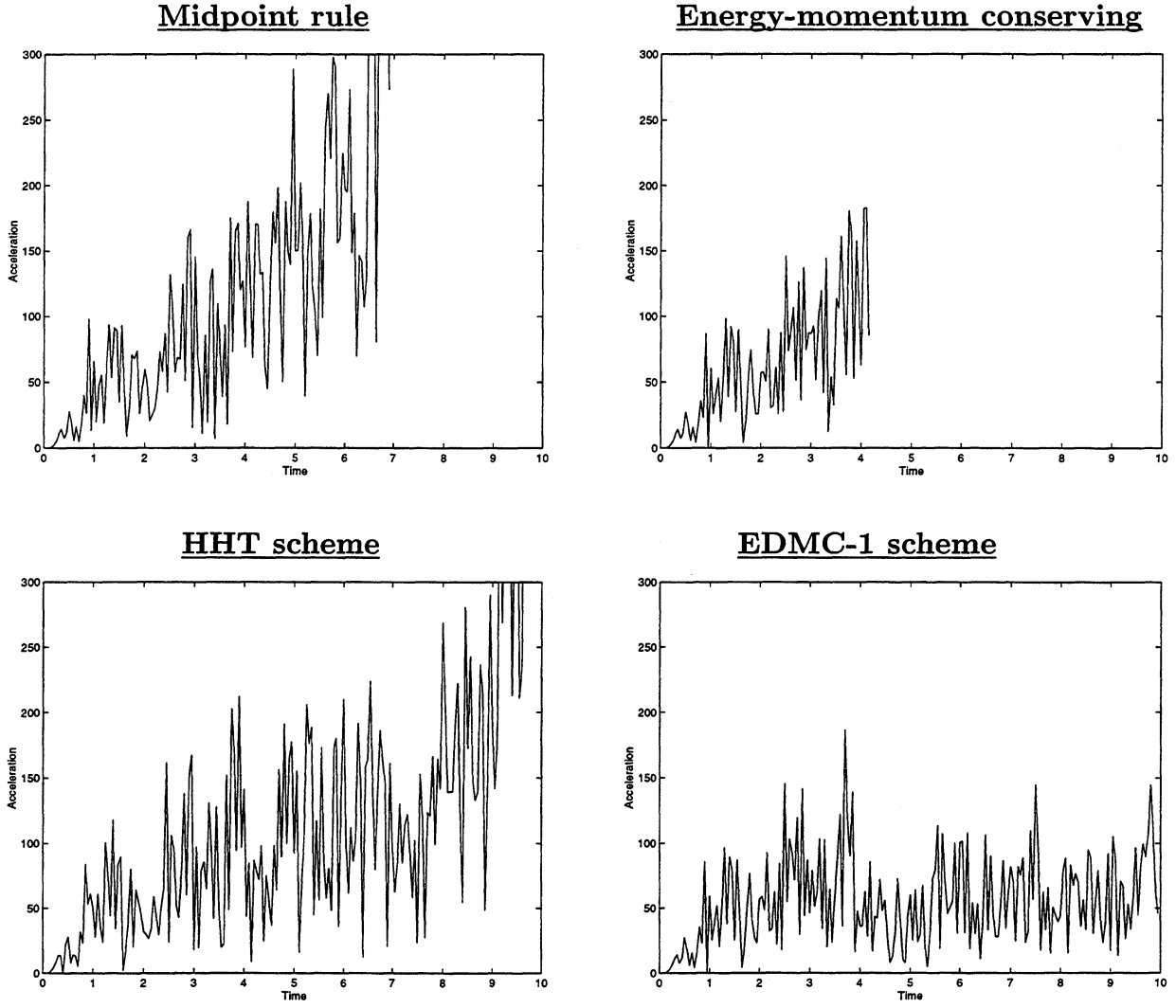

FIGURE 4.5. Thin beams. Evolution of the norm of the acceleration in the middle node of the beam obtained with different time-stepping schemes.

algorithms not exhibiting high frequency dissipation (in the current case, exhibiting a double unit root at infinite frequency), besides the possible consequences in the dynamic response of the algorithm in time. The solution obtained in the time step previous to this lack of convergence is shown in Figure 4.6.a. It clearly shows the aligned configuration of the beam, leading to the sudden increase in the axial stiffness as described above. Further proof of the dynamic character of the observed instability is given by the uncontrollable growth of the acceleration in the later stages of the simulation shown in Figure 4.5. The norm of the acceleration of the middle node in the beam is depicted versus time. This lack of control of the acceleration is characteristic in the performance of time-stepping algorithms not exhibiting dissipative properties in the high-frequency; see e.g. SIMO et al [1995].

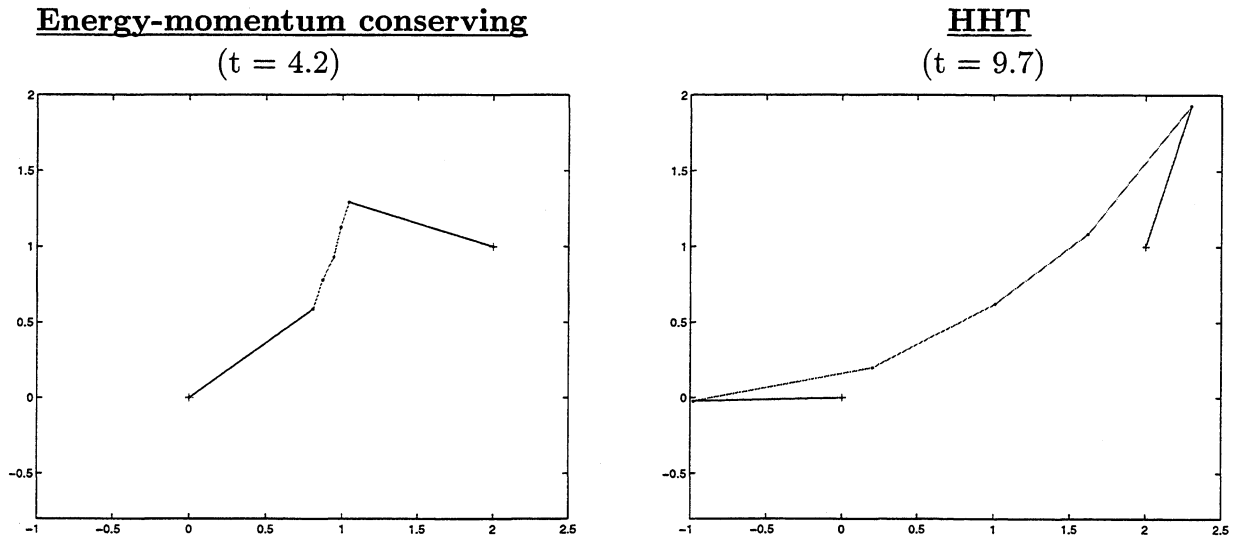

FIGURE 4.6. Thin beams. Last converged solutions obtained with the HHT and energy-momentum conserving schemes.

Figure 4.4 also shows the results for the HHT scheme. A large value of $\rho_\infty = 0.9$ for the spectral radius at infinity is considered. The resulting evolution of the total energy clearly depicts an overall energy decay (not monotonic) in the early stages of the simulation. However, this situation changes at a certain instant during the computation with an increase of the energy (even over the initial energy level), leading eventually to the stopping of the simulation for the considered time step. The lack of the unconditional dissipative properties of the scheme in the nonlinear range are evident, in contrast with its well-known stability in the linear range. The growth in the acceleration can also be observed in Figure 4.5, starting during the stages where an increase of the energy is observed. Figure 4.6.b shows the final converged solution before the stop of the calculation. The large content of axial energy is evident.

Figure 4.4 depicts also the solution obtained with the dissipative EDMC-1 scheme. A value of $\chi_1 = \chi_2 = 0.01$ is assumed for the axial terms, leading to the same spectral radius at infinity of $\rho_\infty = 0.9$ for these contributions as assumed previously for the HHT scheme. The monotonic decay of the total energy can be observed in this figure, passing the time steps where both the energy-momentum conserving and HHT schemes led to a lack of convergence. We have not observe any problem with the convergence in this simulation. We can also observe in Figure 4.4 the elimination of high-frequency in the evolution of the axial energy for this case when compared with the original energy-momentum conserving scheme at the stages right before the latter scheme failed to converge. The control of the evolution of the acceleration during these stages is also apparent in Figure 4.5. We conclude that the numerical scheme is able to handle better the sudden changes of axial stiffness, and its associated high-frequency content, thanks to this added numerical high-frequency dissipation.

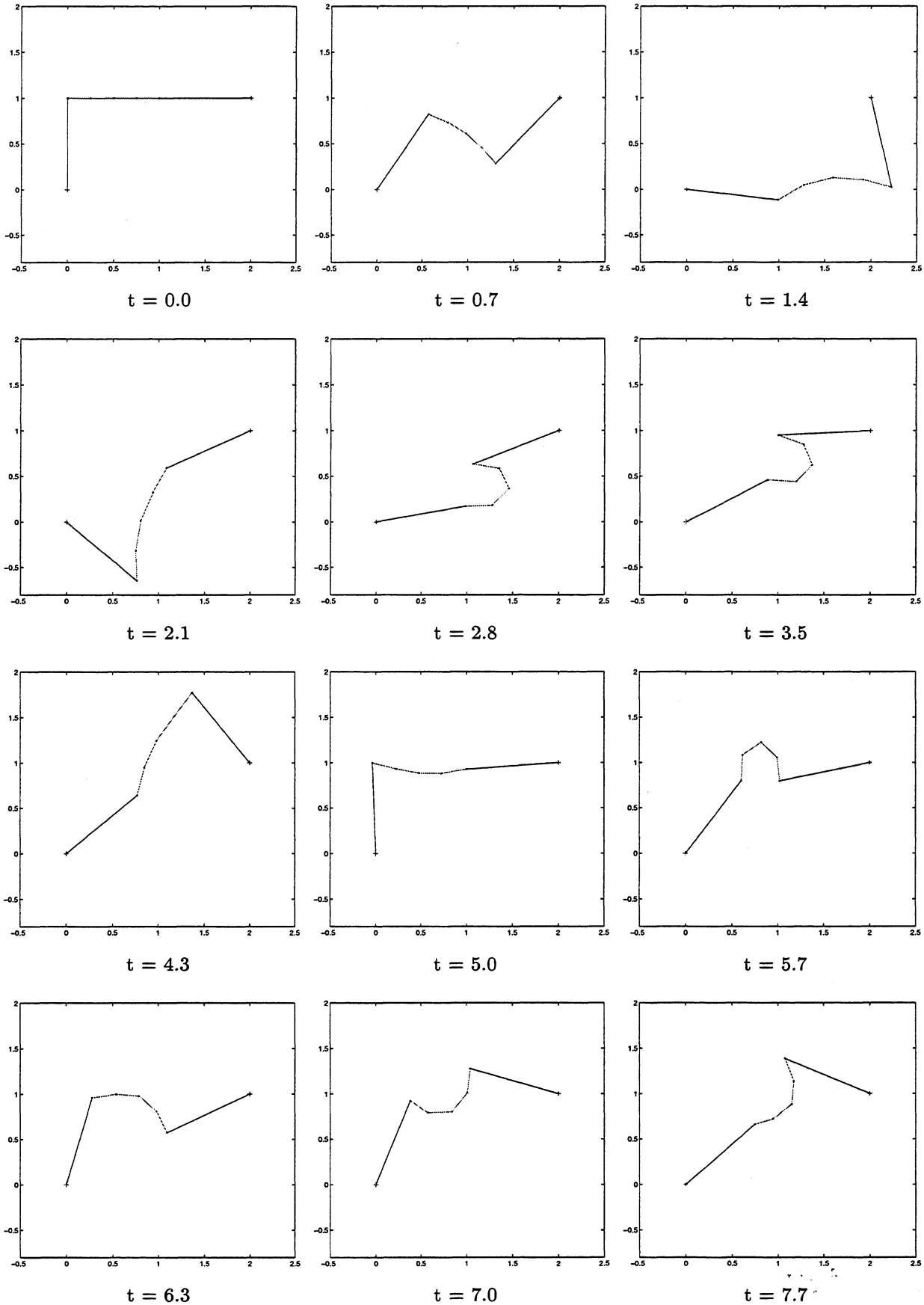

FIGURE 4.7. Thin beams. Configuration of the structure at different time. Solution obtained with the new EDMC-1 scheme.

5. Extensions to Nonlinear Elastodynamics

We present in this section the extension of the previous developments to the general case of nonlinear elastodynamics. To this purpose, we present in Section 5.1 a brief description of the governing equations and the dynamical properties of interest. After describing in Section 5.2 the ideas and analyses presented in the previous sections for the two considered model problems to the problem of interest in this section, we describe in Section 5.3 two representative numerical simulations illustrating the properties of the newly developed time-stepping schemes.

5.1. The governing equations

We denote by $\boldsymbol{\varphi} = \hat{\boldsymbol{\varphi}}(\boldsymbol{X}, t)$ the deformation of a solid body $\mathcal{B} \subset \mathbb{R}^{n_{\text{dim}}}$ ($n_{\text{dim}} = 1, 2$ or 3) with material particles $\boldsymbol{X} \in \mathcal{B}$, and by $\boldsymbol{p} = \hat{\boldsymbol{p}}(\boldsymbol{X}, t)$ the corresponding linear momentum density. The infinite-dimensional system of nonlinear elastodynamics can then be written as

$$\left.\begin{aligned} \dot{\boldsymbol{\varphi}} &= \rho_o^{-1}\, \boldsymbol{p}\,, \\ \int_{\mathcal{B}} \dot{\boldsymbol{p}} \cdot \delta\boldsymbol{\varphi}\; d\mathcal{B} + \int_{\mathcal{B}} \boldsymbol{S} : \boldsymbol{F}^T\, \text{GRAD}(\delta\boldsymbol{\varphi})\; d\mathcal{B} &= \int_{\mathcal{B}} \rho_o \boldsymbol{B} \cdot \delta\boldsymbol{\varphi}\; d\mathcal{B} + \int_{\mathcal{B}} \bar{\boldsymbol{T}} \cdot \delta\boldsymbol{\varphi}\; d\Gamma\,, \end{aligned}\right\} \tag{5.1}$$

for all admissible variations $\delta\boldsymbol{\varphi} \in \mathcal{V}$, that is, the space of variations satisfying homogeneous essential boundary conditions $\delta\boldsymbol{\varphi} = 0$ on $\partial_u\mathcal{B}$ (the part of the boundary with imposed deformations), as usual. The standard notation for the reference density of the solid $\rho_o > 0$, the deformation gradient $\boldsymbol{F} := \text{GRAD}\,\boldsymbol{\varphi}$, the second Piola-Kirchhoff stress tensor $\boldsymbol{S}$, the external body force $\boldsymbol{B}$, and imposed tractions $\bar{\boldsymbol{T}}$ on $\partial_T\mathcal{B}$ has been employed in (5.1). The case of interest corresponds to an hyperelastic solid characterized by a stored energy function $W = \hat{W}(\boldsymbol{C})$, with $\boldsymbol{C} := \boldsymbol{F}^T\boldsymbol{F}$ (by frame indifference), and the stress-strain relation

$$\boldsymbol{S} = 2\frac{\partial W}{\partial \boldsymbol{C}}\,. \tag{5.2}$$

Equation $(5.1)_2$ has been written in weak form given our interest to develop a finite element implementation of the resulting methods.

The equations (5.1) define an infinite dimensional Hamiltonian system, exhibiting in particular the classical law of conservation of energy

$$H(\boldsymbol{\varphi}, \boldsymbol{p}) = \int_{\mathcal{B}} \tfrac{1}{2}\, \rho_o^{-1}\, \|\boldsymbol{p}\|^2\; d\mathcal{B} + \int_{\mathcal{B}} W(\boldsymbol{C}(\boldsymbol{\varphi}))\; d\mathcal{B} = \textit{ constant}\,, \tag{5.3}$$

in the special case of a Neumann problem (that is, $\boldsymbol{B} = \bar{\boldsymbol{T}} = 0$ and $\partial_u\mathcal{B} = \emptyset$). Similarly in this case, the symmetry of the Hamiltonian (5.3) under rigid body motions, consisting

of rigid translations and rigid rotations ($G = \mathbb{R}^{n_{\rm dim}} \times SO(n_{\rm dim})$ in the notation of Section 2.2 above), leads to the conservation laws of the associated linear and angular momenta

$$\boldsymbol{l} := \int_{\mathcal{B}} \boldsymbol{p}\, d\mathcal{B} = \textit{ constant} \qquad \text{and} \qquad \boldsymbol{J} := \int_{\mathcal{B}} \boldsymbol{\varphi} \times \boldsymbol{p}\, d\mathcal{B} = \textit{ constant}\,, \tag{5.4}$$

for the cross product $\times$ of two vectors in $\mathbb{R}^3$ (or its corresponding embedding in lower dimensions, as employed in the previous sections; see Remark 2.1).

The presence of these symmetries lead to the existence of the associated relative equilibria characterized by the equilibrium deformation $\boldsymbol{\varphi}_e$ (up to a rigid body motion), for the equilibrium angular velocity $\boldsymbol{\Omega}_e$ and translational velocity $\boldsymbol{v}_e$. The equilibrium trajectories $\boldsymbol{\varphi}_{et}(\boldsymbol{X}, t)$ are generated by the infinitesimal rigid motion corresponding to $\boldsymbol{\Omega}_e$ and $\boldsymbol{v}_e$, that is, they are the solutions of the first order ordinary differential equation

$$\dot{\boldsymbol{\varphi}}_{et} = \boldsymbol{\Omega}_e \times \boldsymbol{\varphi}_{et} + \boldsymbol{v}_e \qquad \Big(\Longrightarrow \quad \boldsymbol{p}_{et} = \rho_o \left[\boldsymbol{\Omega}_e \times \boldsymbol{\varphi}_{et} + \boldsymbol{v}_e \right] \Big)\,, \tag{5.5}$$

with, say, $\boldsymbol{\varphi}_{et}(\boldsymbol{X}, 0) = \boldsymbol{\varphi}_e(\boldsymbol{X})\ \forall \boldsymbol{X} \in \mathcal{B}$. The integration of (5.5) leads to the solutions

$$\boldsymbol{\varphi}_{et}(\boldsymbol{X}, t) = \exp\left[t\hat{\boldsymbol{\Omega}}_e\right] \boldsymbol{\varphi}_e(\boldsymbol{X}) + \boldsymbol{u}(t) \qquad \text{for} \quad \boldsymbol{u}(t) := \left(\int_O^t \exp\left[\eta \hat{\boldsymbol{\Omega}}_e\right]\, d\eta \right) \boldsymbol{v}_e\,, \tag{5.6}$$

consisting of a rigid translation and a rigid rotation with constant axial vector $\boldsymbol{\Omega}_e$ (with $\hat{\boldsymbol{\Omega}}_e$ denoting the corresponding skew tensor). Carrying on the time integration in (5.6) leads to the alternative closed-form expression

$$\boldsymbol{u}(t) = \frac{1}{\|\boldsymbol{\Omega}_e\|^2} \left(1 - \exp\left[t\hat{\boldsymbol{\Omega}}_e\right] \right) \boldsymbol{\Omega}_e \times \boldsymbol{v}_e + \frac{t}{\|\boldsymbol{\Omega}_e\|^2} \left(\boldsymbol{\Omega}_e \cdot \boldsymbol{v}_e \right) \boldsymbol{\Omega}_e\,,$$

with the well-defined limit $\boldsymbol{u}_e(t) = \boldsymbol{v}_e t$ for $\|\boldsymbol{\Omega}_e\| \to 0$. Again, the above solutions fix the arbitrary superposed rigid body motion by assuming, without loss of generality, that $\boldsymbol{\varphi}_{et}(\boldsymbol{X}, 0) = \boldsymbol{\varphi}_e(\boldsymbol{X})$.

Inserting the expression (5.6) in (5.1), we obtain the weak equation

$$\int_{\mathcal{B}} \boldsymbol{S}(\boldsymbol{\varphi}_e) : \boldsymbol{F}_e^T\, \textsc{Grad}(\delta\boldsymbol{\varphi})\, d\mathcal{B} = \int_{\mathcal{B}} \rho_o \boldsymbol{\Omega}_e \times \left[\boldsymbol{\Omega}_e \times \boldsymbol{\varphi}_e + \boldsymbol{v}_e \right] \cdot \delta\boldsymbol{\varphi}\, d\mathcal{B}\,, \tag{5.7}$$

characterizing the relative equilibria. The weak equation $(5.7)_2$ is to be understood for all variations $\delta\boldsymbol{\varphi} \in \mathcal{V}/G_{\boldsymbol{l}_e, \boldsymbol{\mu}_e}$, that is, and following the notation introduced in Section 2.2, up to rigid body motions preserving the linear and angular momenta, $\boldsymbol{l}_e$ and $\boldsymbol{\mu}_e$ respectively. Using the relations (5.4) with (5.5), we obtain the following equilibrium relations for these momenta

$$\boldsymbol{l}_e = M \left[\boldsymbol{v}_e + \boldsymbol{\Omega}_e \times \boldsymbol{\varphi}_e^{(c)} \right] \qquad \text{and} \qquad \boldsymbol{\mu}_e = \mathcal{I}_e^{(c)} \boldsymbol{\Omega}_e + \boldsymbol{\varphi}_e^{(c)} \times \boldsymbol{l}_e\,. \tag{5.8}$$

with $\boldsymbol{\Omega}_e \times \boldsymbol{l}_e = 0$ and $\boldsymbol{\Omega}_e \times \mathcal{I}_e^{(c)} \boldsymbol{\Omega}_e = 0$ (i.e. $\boldsymbol{\Omega}_e$ is an eigenvector of the locked inertia $\mathcal{I}_e^{(c)}$), for the total mass $M = \int_{\mathcal{B}} \rho_o \, d\mathcal{B}$, the position of the center of mass $\boldsymbol{\varphi}_e^{(c)} := (\int_{\mathcal{B}} \rho_o \boldsymbol{\varphi}_e d\mathcal{B})/M$, and the locked inertia tensor at equilibrium

$$\mathcal{I}_e^{(c)} := \int_{\mathcal{B}} \rho_o \left[\|\boldsymbol{\varphi}_e\|^2 \mathbf{1} - \boldsymbol{\varphi}_e \otimes \boldsymbol{\varphi}_e \right] \, d\mathcal{B} - M \left[\|\boldsymbol{\varphi}_e^{(c)}\|^2 \mathbf{1} - \boldsymbol{\varphi}_e^{(c)} \otimes \boldsymbol{\varphi}_e^{(c)} \right] . \tag{5.9}$$

We refer to SIMO et al [1991] for complete details. In particular, all the arguments characterizing these solutions as the stationary points of the corresponding augmented Hamiltonian, exactly as for the simple model considered in Section 2, can be found in this reference. From a physical point of view, we can observe that $(5.7)_2$ can be understood as the equilibrium of the solid under the action of the centrifugal force associated to the rigid motion.

5.2. An energy decaying scheme

The developments presented in the previous sections for the two model problems considered then translate directly to the system (5.1) of nonlinear elastodynamics. In the context of the finite element method, the resulting scheme reads

$$\frac{\boldsymbol{x}_{n+1}^A - \boldsymbol{x}_n^A}{\Delta t} = \left(1 + \frac{1}{4} \chi_2 \, \frac{\|\boldsymbol{v}_{n+1}^A\| - \|\boldsymbol{v}_n^A\|}{\|\boldsymbol{v}_{n+1}^A\| + \|\boldsymbol{v}_n^A\|} \right) \boldsymbol{v}_{n+\frac{1}{2}}^A \qquad (A = 1, \ldots, n_{node}) , \tag{5.10}$$

$$\boldsymbol{M}_L \, \frac{\boldsymbol{v}_{n+1} - \boldsymbol{v}_n}{\Delta t} + \underbrace{\int_{\mathcal{B}} \boldsymbol{B}_{n+\frac{1}{2}}^T \boldsymbol{S} \, d\mathcal{B}}_{\boldsymbol{f}_{(int)}} - \boldsymbol{f}_{(ext)} = 0 , \tag{5.11}$$

for a typical spatial finite element discretization involving the nodal positions (and corresponding nodal displacements) $\boldsymbol{x}_n^A = \boldsymbol{\varphi}(\boldsymbol{X}^A, t_n) = \boldsymbol{X}^A + \boldsymbol{d}_n^A$ $(A = 1, n_{node})$, and nodal velocities $\boldsymbol{v} := \{\boldsymbol{v}^1, \ldots, \boldsymbol{v}^{n_{node}}\}$, and the linearized strain operator $\boldsymbol{B}_{n+\frac{1}{2}}$, defined by the relation

$$\boldsymbol{B}_{n+\frac{1}{2}} \delta \boldsymbol{d} := \boldsymbol{F}_{n+\frac{1}{2}}^T \, \text{GRAD}(\delta \boldsymbol{\varphi}) , \tag{5.12}$$

for an admissible variation $\delta \boldsymbol{\varphi}$ and its corresponding nodal values $\delta \boldsymbol{d}$. The stress $\boldsymbol{S}$ in (5.11) is given by the relation

$$\boldsymbol{S} = \boldsymbol{S}_{cons} + 2 \frac{\mathcal{D}_W}{\|\boldsymbol{C}_{n+1} - \boldsymbol{C}_n\|} \underbrace{\frac{\boldsymbol{C}_{n+1} - \boldsymbol{C}_n}{\|\boldsymbol{C}_{n+1} - \boldsymbol{C}_n\|}}_{:= \boldsymbol{N}} , \tag{5.13}$$

for the Euclidean norm of a rank-two tensor $\|\boldsymbol{C}\|^2 := C_{ij} C_{ij}$ and for a conserving approximation $\boldsymbol{S}_{cons}$ of the stress, that is, satisfying the relation

$$\boldsymbol{S}_{cons} : \tfrac{1}{2} (\boldsymbol{C}_{n+1} - \boldsymbol{C}_n) = W(\boldsymbol{C}_{n+1}) - W(\boldsymbol{C}_n) . \tag{5.14}$$

The simulations presented in Section 5.3 consider the particular expression

$$\boldsymbol{S}_{cons} = 2\frac{W(\boldsymbol{C}_{n+1}) - W(\boldsymbol{C}_n)}{\|\boldsymbol{C}_{n+1} - \boldsymbol{C}_n\|}\boldsymbol{N} + 2\left[\boldsymbol{I} - \boldsymbol{N}\otimes\boldsymbol{N}\right]\partial_{\boldsymbol{C}}W(\frac{\boldsymbol{C}_{n+1}+\boldsymbol{C}_n}{2})\,, \tag{5.15}$$

with the well-defined limit

$$\boldsymbol{S}_{cons} = 2\,\partial_{\boldsymbol{C}}W(\frac{\boldsymbol{C}_{n+1}+\boldsymbol{C}_n}{2}) \qquad \text{for} \quad \boldsymbol{C}_n = \boldsymbol{C}_{n+1}\,, \tag{5.16}$$

first proposed in SIMO & GONZALEZ [1996], where $\boldsymbol{N}$ has been defined in (5.13). The dissipation function $\mathcal{D}_W = \widehat{\mathcal{D}_W}(\boldsymbol{C}_n, \boldsymbol{C}_{n+1})$ is constructed using the ideas presented in Section 2 for model problem I. In particular, the consistency condition

$$\frac{\widehat{\mathcal{D}_W}(\boldsymbol{C}_n, \boldsymbol{C}_{n+1})}{\|\boldsymbol{C}_{n+1} - \boldsymbol{C}_n\|} \longrightarrow 0 \qquad \text{as} \quad \|\boldsymbol{C}_{n+1} - \boldsymbol{C}_n\| \longrightarrow 0\,, \tag{5.17}$$

is imposed. The simulations presented in Section 5.3 are based on the residual expression

$$\mathcal{D}_W := \chi_1\left[\tfrac{1}{2}\Big(W(\boldsymbol{C}_{n+1}) + W(\boldsymbol{C}_n)\Big) - W(\frac{\boldsymbol{C}_{n+1}+\boldsymbol{C}_n}{2})\right]\,, \tag{5.18}$$

for a scalar parameter χ_1, as in model problem I. Alternative expressions following the arguments in Remark 3.1.1 can also be considered. Finally, equation (5.11) makes use of a lumped mass matrix $\boldsymbol{M}_L$ (obtained, for example, by the traditional row sum). This consideration allows to arrive to a nodal form of the update equation $(5.11)_1$, thus simplifying considerably the final numerical implementation.

Remarks 5.1.

1. Formulations involving a consistent mass approximation in (5.11) are constructed as follows. Denote by N_A the finite element shape function of node $A = 1, \ldots, n_{node}$, so the consistent mass block corresponding to two typical nodes is given by

$$\boldsymbol{M}_{AB} = \int_{\mathcal{B}} \rho_o N_A\, N_B\, d\mathcal{B}\, \mathbf{1} \in \mathbb{R}^{n_{\text{dim}}\times n_{\text{dim}}} \quad (A, B = 1, \ldots, n_{node})\,. \tag{5.19}$$

   Equation $(5.11)_1$ is then replaced by the relation

$$\frac{\boldsymbol{x}^A_{n+1} - \boldsymbol{x}^A_n}{\Delta t} = \boldsymbol{v}^A_{n+\frac{1}{2}} + \boldsymbol{g}^A_{diss} \quad (A = 1, \ldots, n_{node})\,, \tag{5.20}$$

   where the nodal vectors $\boldsymbol{g}^A_{diss} \in \mathbb{R}^{n_{\text{dim}}}$ are the solution of the system of equations

$$\boldsymbol{M}_{AB}\boldsymbol{g}^B_{diss} = \frac{1}{4}\,\chi_2 \int_{\mathcal{B}} \rho_o N_A\, \frac{\|\boldsymbol{v}_{n+1}\| - \|\boldsymbol{v}_n\|}{\|\boldsymbol{v}_{n+1}\| + \|\boldsymbol{v}_n\|}\boldsymbol{v}_{n+\frac{1}{2}}\, d\mathcal{B}\,. \tag{5.21}$$

Calculations similar to the ones presented in Proposition 5.1 below show the very same conservation/dissipation properties for this consistent mass formulation, with $\mathcal{D}_K$ given in this case by

$$\mathcal{D}_K = \frac{1}{8}\,\chi_2 \int_{\mathcal{B}} \rho_o \left(\|\boldsymbol{v}_{n+1}\| - \|\boldsymbol{v}_n\|\right)^2 \, d\mathcal{B} \geq 0 \,, \tag{5.22}$$

and the linear and angular momenta given by the continuum relations (5.4). The resulting global character of the nodal displacement updates (5.20) by (5.21) leads to a much more involved implementation. Efficient iterative schemes can be devised; details are omitted. Nevertheless, the original lumped formulation (5.11) is preferred due to this added computational cost.

2. The expression resulting of (5.13) and (5.20) for the stress tensor $\boldsymbol{S}$ can be written as

$$\boldsymbol{S} = \hat{\boldsymbol{S}} + \left[2\frac{W(\boldsymbol{C}_{n+1}) - W(\boldsymbol{C}_n) + \mathcal{D}_W}{\|\boldsymbol{C}_{n+1} - \boldsymbol{C}_n\|} - \hat{\boldsymbol{S}} : \boldsymbol{N}\right] \boldsymbol{N} \,, \tag{5.23}$$

for $\hat{\boldsymbol{S}} := 2\partial_{\boldsymbol{C}} W((\boldsymbol{C}_{n+1} + \boldsymbol{C}_n)/2)$. We note, however, that any other expression of $\hat{\boldsymbol{S}}$ consistent with the continuum stress formula (5.2) can be used. The numerical properties described in Proposition 5.1 still hold for the resulting first order formula. □

The proposed numerical scheme exhibit the same properties as presented in Section 3 for the simple model problem of the nonlinear spring-mass system. We summarize these properties in the following proposition.

Proposition 5.1 *The numerical scheme (5.10)-(5.11) possesses the following conservation/dissipation properties for the Neumann problem of nonlinear elastodynamics (i.e.* $\boldsymbol{f}^{(ext)} = 0$ *and* $\partial_u \mathcal{B} = \emptyset$*):*

1. *The discrete linear and angular momenta are conserved. That is, given* $M_L = diag(m_A)$ $(A = 1, n_{node}$*, with* $m_A > 0)$ *with*

$$\boldsymbol{l}^h := \boldsymbol{M}_L \boldsymbol{v} = \sum_{A=1}^{n_{node}} m_A \boldsymbol{v}^A \qquad \text{and} \qquad \boldsymbol{J}^h := \sum_{A=1}^{n_{node}} m_A \, \boldsymbol{x}^A \times \boldsymbol{v}^A \,, \tag{5.24}$$

for the spatial nodal coordinates $\boldsymbol{x}^A := \boldsymbol{\varphi}(\boldsymbol{X}^A)$*, we have*

$$\boldsymbol{l}^h_{n+1} = \boldsymbol{l}^h_n \qquad \text{and} \qquad \boldsymbol{J}^h_{n+1} = \boldsymbol{J}^h_n \tag{5.25}$$

unconditionally in the time step Δt*.*

2. *The total energy*

$$H = \tfrac{1}{2}\boldsymbol{v}\cdot\boldsymbol{M}_L\boldsymbol{v} + \int_{\mathcal{B}} W(\boldsymbol{C})\; d\mathcal{B}\,, \tag{5.26}$$

satisfies the relation

$$H_{n+1} - H_n = -\left[\mathcal{D}_K + \mathcal{D}_V\right] \qquad \textit{for} \quad \mathcal{D}_V := \int_{\mathcal{B}} \mathcal{D}_W\; d\mathcal{B}\,, \tag{5.27}$$

with $\mathcal{D}_W$ *given by* (5.18) *and*

$$\mathcal{D}_K = \frac{1}{8}\,\chi_2 \sum_{A=1}^{n_{point}} m_A \left(\|\boldsymbol{v}^A_{n+1}\| - \|\boldsymbol{v}^A_n\|\right)^2 \geq 0\,, \tag{5.28}$$

for $\chi_2 \geq 0$. *Hence the scheme is unconditionally dissipative (i.e., the energy decays or is conserved for any time step* Δt*) iff* $\mathcal{D}_V \geq 0$. *This last inequality follows from the convexity of* $W(\boldsymbol{C})$*, or its convexification otherwise (see Remark* 3.1.*2).*

3. *The discrete dynamical system preserves the relative equilibria of the continuum system. That is, the discrete relative equilibria* $\boldsymbol{\varphi}_e$ *satisfy the finite element equation*

$$\sum_{A=1}^{n_{node}} m_A\; \boldsymbol{\Omega}_e \times \left(\boldsymbol{\Omega}_e \times \boldsymbol{\varphi}^A_e + \boldsymbol{v}_e\right) + \int_{\mathcal{B}} \boldsymbol{B}^T_e \boldsymbol{S}(\boldsymbol{\varphi}_e)\; d\mathcal{B} = 0\,, \tag{5.29}$$

the counterpart of (5.7)*, with the corresponding group motions* (5.6) *approximated by the discrete relations*

$$\left.\begin{aligned} \boldsymbol{x}^A_n &= \boldsymbol{\Lambda}_n \boldsymbol{\varphi}^A_e + \boldsymbol{u}_n\,, \\ \boldsymbol{v}^A_n &= \boldsymbol{\Lambda}_n \left[\boldsymbol{\Omega}_e \times \boldsymbol{\varphi}^A_e + \boldsymbol{v}_e\right] \end{aligned}\right\} \tag{5.30}$$

where $\boldsymbol{\varphi}^A_e = \boldsymbol{\varphi}_e(\boldsymbol{X}^A)$ *and the sequences* $\{\boldsymbol{\Lambda}_n\}_{n=0}^{\infty}$ *and* $\{\boldsymbol{u}_n\}_{n=0}^{\infty}$ *are defined for some initial value* $\boldsymbol{\Lambda}_o$ *and* $\boldsymbol{u}_o$ *(an arbitrary rigid body motion) by the relations*

$$\boldsymbol{\Lambda}_{n+1} = \boldsymbol{\Lambda}_n cay(\Delta t \hat{\boldsymbol{\Omega}}_e) \qquad \textit{and} \qquad \boldsymbol{u}_{n+1} = \boldsymbol{u}_n + \Delta t\; \boldsymbol{\Lambda}^*_n\; \boldsymbol{v}_e\,, \tag{5.31}$$

for $\boldsymbol{\Lambda}^*_n := \left(\boldsymbol{\Lambda}_n + \boldsymbol{\Lambda}_{n+1}\right)/2$ *and*

$$cay\left(\Delta t \hat{\Omega}_e\right) := \left[1 + \frac{\Delta t}{2}\hat{\Omega}_e\right]\left[1 - \frac{\Delta t}{2}\hat{\Omega}_e\right]^{-1} \quad \in SO(3)\,, \tag{5.32}$$

in the general three-dimensional case.

Proof: The proof follows arguments similar to the ones presented in Section 3.2.2 for the proof of Proposition 3.1. Briefly, we have:

i. *Conservation of linear momentum.* The evolution of the linear momentum for the Neumann problem of interest is given by

$$\begin{aligned}\left(\boldsymbol{l}^h_{n+1}-\boldsymbol{l}^h_n\right)\cdot\boldsymbol{a} &= \sum_{A=1}^{n_{node}} m_A\left(\boldsymbol{v}^A_{n+1}-\boldsymbol{v}^A_n\right)\cdot\boldsymbol{a} = \sum_{A=1}^{n_{node}} \boldsymbol{f}^A_{(int)}\cdot\boldsymbol{a} \\ &= \int_{\mathcal{B}} \boldsymbol{S}:\boldsymbol{F}^T_{n+\frac{1}{2}}\,\text{GRAD}(\boldsymbol{a})\,d\mathcal{B}=0 \qquad \forall\boldsymbol{a}\in\mathbb{R}^{n_{\text{dim}}}\end{aligned} \tag{5.33}$$

after noting that $\delta\boldsymbol{\varphi}=\boldsymbol{a}$ is an admissible variation ($\partial_u\mathcal{B}=\emptyset$). The relation $(5.25)_1$ follows.

ii. *Conservation of angular momentum.* The evolution of the angular momentum for the Neumann problem of interest is given by

$$\begin{aligned}\left(\boldsymbol{J}^h_{n+1}-\boldsymbol{J}^h_n\right)\cdot\boldsymbol{w} &= \sum_{A=1}^{n_{node}} m_A\left(\boldsymbol{x}^A_{n+\frac{1}{2}}\times\left(\boldsymbol{v}^A_{n+1}-\boldsymbol{v}^A_n\right)+\left(\boldsymbol{x}^A_{n+1}-\boldsymbol{x}^A_n\right)\times\boldsymbol{v}^A_{n+\frac{1}{2}}\right)\cdot\boldsymbol{w} = \\ &= \sum_{A=1}^{n_{node}}\left(\boldsymbol{x}^A_{n+\frac{1}{2}}\times\boldsymbol{f}^A_{(int)}\right)\cdot\boldsymbol{w} \\ &\quad+\sum_{A=1}^{n_{node}} m_A\left(1+\frac{1}{4}\,\chi_2\,\frac{\|\boldsymbol{v}^A_{n+1}\|-\|\boldsymbol{v}^A_n\|}{\|\boldsymbol{v}^A_{n+1}\|+\|\boldsymbol{v}^A_n\|}\right)\underbrace{\boldsymbol{v}^A_{n+\frac{1}{2}}\times\boldsymbol{v}^A_{n+\frac{1}{2}}}_{=0}\cdot\boldsymbol{w} \\ &= \sum_{A=1}^{n_{node}}\boldsymbol{f}^A_{(int)}\cdot\underbrace{\left(\boldsymbol{w}\times\boldsymbol{x}^A_{n+\frac{1}{2}}\right)}_{\widehat{\boldsymbol{W}}\boldsymbol{x}^A_{n+\frac{1}{2}}} = \int_{\mathcal{B}}\boldsymbol{S}:\boldsymbol{F}^T_{n+\frac{1}{2}}\underbrace{\text{GRAD}\left(\widehat{\boldsymbol{W}}\boldsymbol{\varphi}_{n+\frac{1}{2}}\right)}_{\widehat{\boldsymbol{W}}\boldsymbol{F}_{n+\frac{1}{2}}}\,d\mathcal{B} \\ &= \int_{\mathcal{B}}\underbrace{\boldsymbol{F}_{n+\frac{1}{2}}\boldsymbol{S}\boldsymbol{F}^T_{n+\frac{1}{2}}}_{symmetric}:\underbrace{\widehat{\boldsymbol{W}}}_{skew}\,d\mathcal{B}=0 \qquad \forall\boldsymbol{w}\in\mathbb{R}^{n_{\text{dim}}}\end{aligned} \tag{5.34}$$

for the skew-symmetric tensor $\widehat{\boldsymbol{W}}$ with axial vector $\boldsymbol{w}$. Note that $\delta\boldsymbol{\varphi}=\boldsymbol{W}\boldsymbol{x}^A_{n+\frac{1}{2}}$ is an admissible variation for the Neumann problem ($\partial_u\mathcal{B}=\emptyset$). The relation $(5.25)_2$ follows.

iii. *Energy evolution.* The evolution of the kinetic energy is given by

$$K^h_{n+1}-K^h_n = \sum_{A=1}^{n_{node}} m_A\left(\boldsymbol{v}^A_{n+1}-\boldsymbol{v}^A_n\right)\cdot\boldsymbol{v}^A_{n+\frac{1}{2}} = \sum_{A=1}^{n_{node}} m_A\left(\boldsymbol{v}^A_{n+1}-\boldsymbol{v}^A_n\right)\cdot\left(\boldsymbol{x}^A_{n+1}-\boldsymbol{x}^A_n\right)$$

$$\underbrace{-\sum_{A=1}^{n_{node}} \frac{1}{4}\,\chi_2\, m_A\, \frac{\|\boldsymbol{v}_{n+1}^A\| - \|\boldsymbol{v}_n^A\|}{\|\boldsymbol{v}_{n+1}^A\| + \|\boldsymbol{v}_n^A\|}\, \left(\boldsymbol{v}_{n+1}^A - \boldsymbol{v}_n^A\right) \cdot \boldsymbol{v}_{n+\frac{1}{2}}^A}_{\mathcal{D}_K}$$

$$= \sum_{A=1}^{n_{node}} \boldsymbol{f}_{(int)}^A \cdot \left(\boldsymbol{x}_{n+1}^A - \boldsymbol{x}_n^A\right) - \mathcal{D}_K \tag{5.35}$$

after using once again (5.10) and (5.11). The energy evolution equation (5.27) follows after noting the relation

$$\sum_{A=1}^{n_{node}} \boldsymbol{f}_{(int)}^A \cdot \left(\boldsymbol{x}_{n+1}^A - \boldsymbol{x}_n^A\right) = \int_{\mathcal{B}} \left(W_{n+1} - W_n - \mathcal{D}_W\right)\, d\mathcal{B} \tag{5.36}$$

after using (5.20).

iv. *Relative equilibria.* We first observe that the velocities $(5.30)_2$ are such that $\|\boldsymbol{v}_{n+1}^A\| = \|\boldsymbol{v}_n^A\|$ $(A = 1, n_{node})$, so $\mathcal{D}_K = 0$ Similarly, we have $\boldsymbol{C}_{n+1} = \boldsymbol{C}_n = \boldsymbol{C}_e$ for the deformations defined by the nodal displacements (5.29), thus leading to $\mathcal{D}_V = 0$ and the limit formula (5.16). The existence of the solutions (5.30) and (5.31) satisfying (5.29) can be verified by direct calculation after noting the relation

$$\boldsymbol{\Lambda}_{n+1} - \boldsymbol{\Lambda}_n = \frac{\Delta t}{2}\, (\boldsymbol{\Lambda}_n + \boldsymbol{\Lambda}_{n+1})\, \hat{\Omega}_e\,, \tag{5.37}$$

for the rotations $(5.31)_1$. □

5.3. Representative numerical simulations

We illustrate in this section the previous theoretical developments with two representative examples, in plane strain and three-dimensional settings, respectively. Figure 5.1 depicts the geometric definition of the problems under consideration, consisting of a circular cylinder and two panel arms, a configuration in satellite type structures. In both cases, we consider a Neo-Hookean stored energy function

$$W(\boldsymbol{C}) = \frac{\lambda}{2} \log^2 J + \tfrac{1}{2}\, \mu(I_1 - 3) - \mu \log J \tag{5.38}$$

for $J = \sqrt{\det \boldsymbol{C}}$ and $I_1 = \operatorname{tr} \boldsymbol{C}$. The parameters $\lambda = 3,000$, $\mu = 750$ and density $\rho_o = 8.93$ are assumed for the cylinder, and $\lambda = 100$, $\mu = 25$ and $\rho_o = 0.5$ for the arms.

In both the plane and three-dimensional cases, the solids have free boundaries and no external body or surface loads are applied. The motion is started by imposing an initial velocity at each node corresponding to a rotation around an axis passing through the

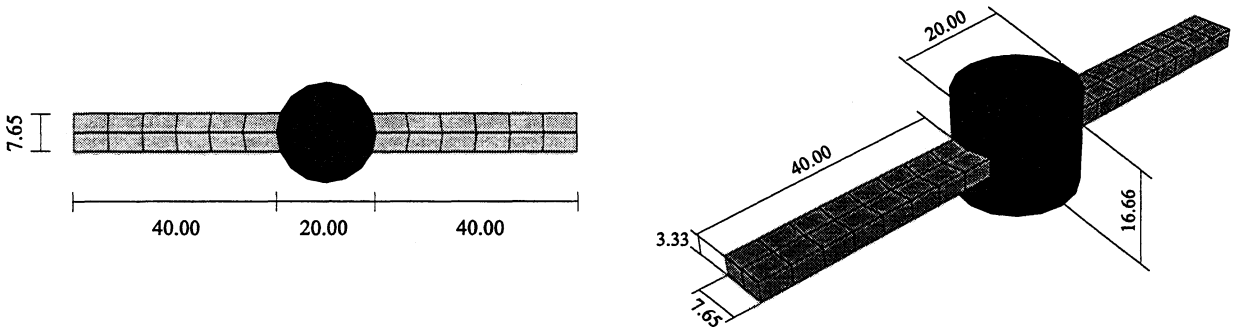

Plane strain problem **Three-dimensional problem**

FIGURE 5.1. Nonlinear elastodynamics. Geometric definition of the solids considered in the plane strain and three-dimensional problems, respectively.

center of symmetry. That is, the initial nodal velocities are perpendicular to the vector joining the nodal point to the center, with a magnitude proportional to the radius and the initial angular velocity Ω_o. For the plane strain case, this rotation is plane. The initial nodal displacements vanish. These initial conditions lead to a deformation and rotation (tumbling in the general three-dimensional case), with the center of the solid being at rest at all instances by symmetry.

Figures 5.2 and 5.3 depict the solution obtained by the new EDMC-1 scheme for the plane strain case with $\Omega_o = 0.28112$. The dissipation parameters of $\chi_1 = \chi_2 = 0.1$ have been chosen, wit a constant time step of $\Delta t = 0.3$. The initial stages of the simulation are shown in Figure 5.2, where we can clearly observe the bending and axial modes of the more flexible arms in the initial motion. Figure 5.3 shows later stages of the same simulation. We can observe the effective elimination of these high-frequency modes, with the solution consisting essentially of a rigid rotation locked at an equilibrium position. This response confirms fully the analyses presented in the previous sections for the proposed algorithms. Indeed, Figure 5.4 includes the evolution of the angular momentum (one component in this plane problem) and the total energy. The conservation of the former at the initial value of $\mu = 1.2974 \cdot 10^5$ is verified, with the total energy depicting also a monotonic dissipation to the asymptotic value of $H_\infty = 1.5272 \cdot 10^4$.

For comparison, we also run this same plane strain problem with the HHT scheme ($\alpha = 0.9$), with the same constant time step of $\Delta t = 0.3$. Figure 5.5 shows the evolution of the angular momentum and total energy for this case. We observe that the energy dissipation is not monotonic, and that the angular momentum is not conserved. In fact, the angular momentum decreases (observe the decreasing trend in the end of the assumed simulation time, as well), leading to a slow down of the overall rotation of the solid corresponding

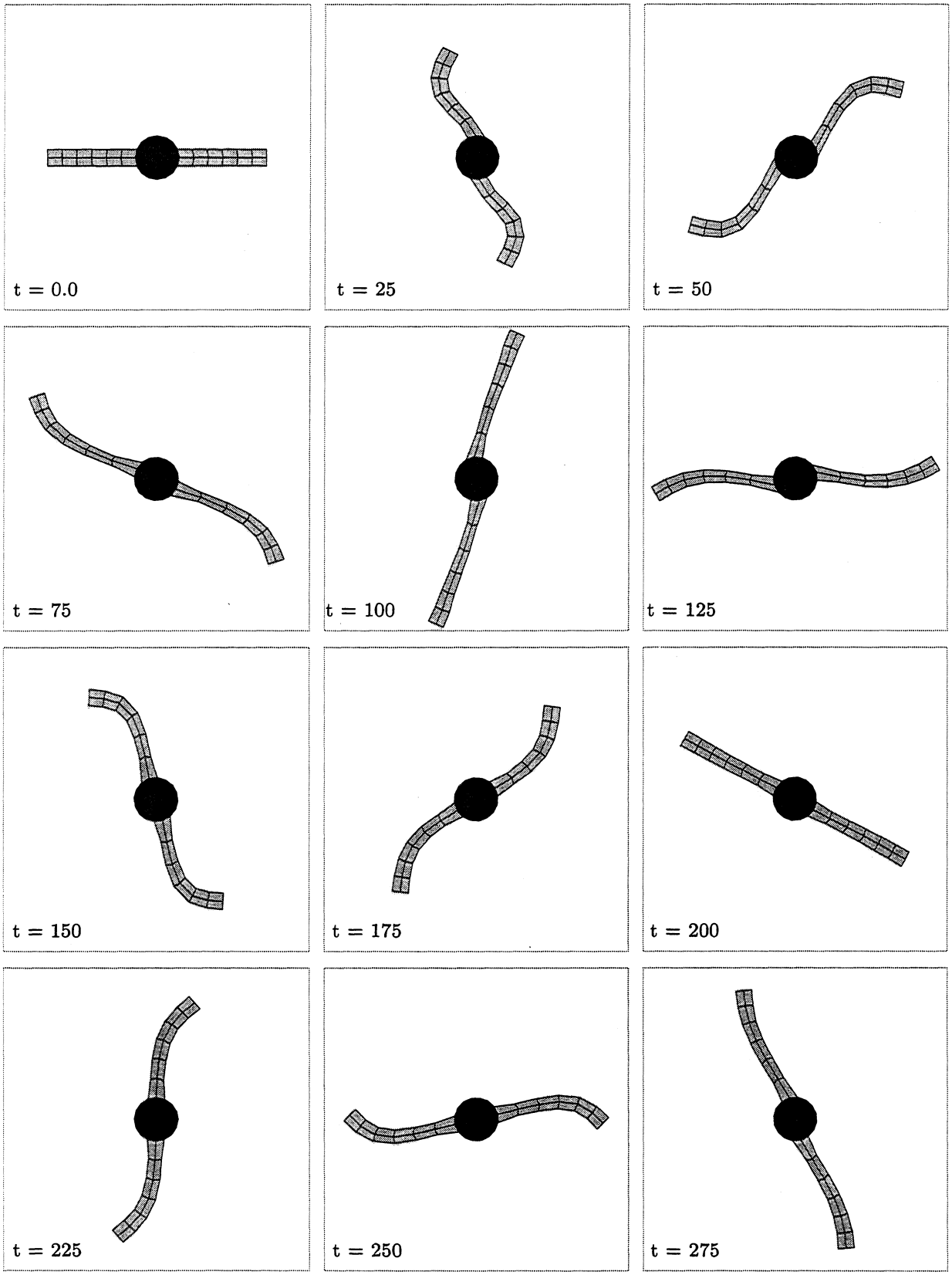

FIGURE 5.2. Plane strain simulation. Short-term solution obtained with the new energy-dissipative momentum-conserving (EDMC-1) time-stepping scheme.

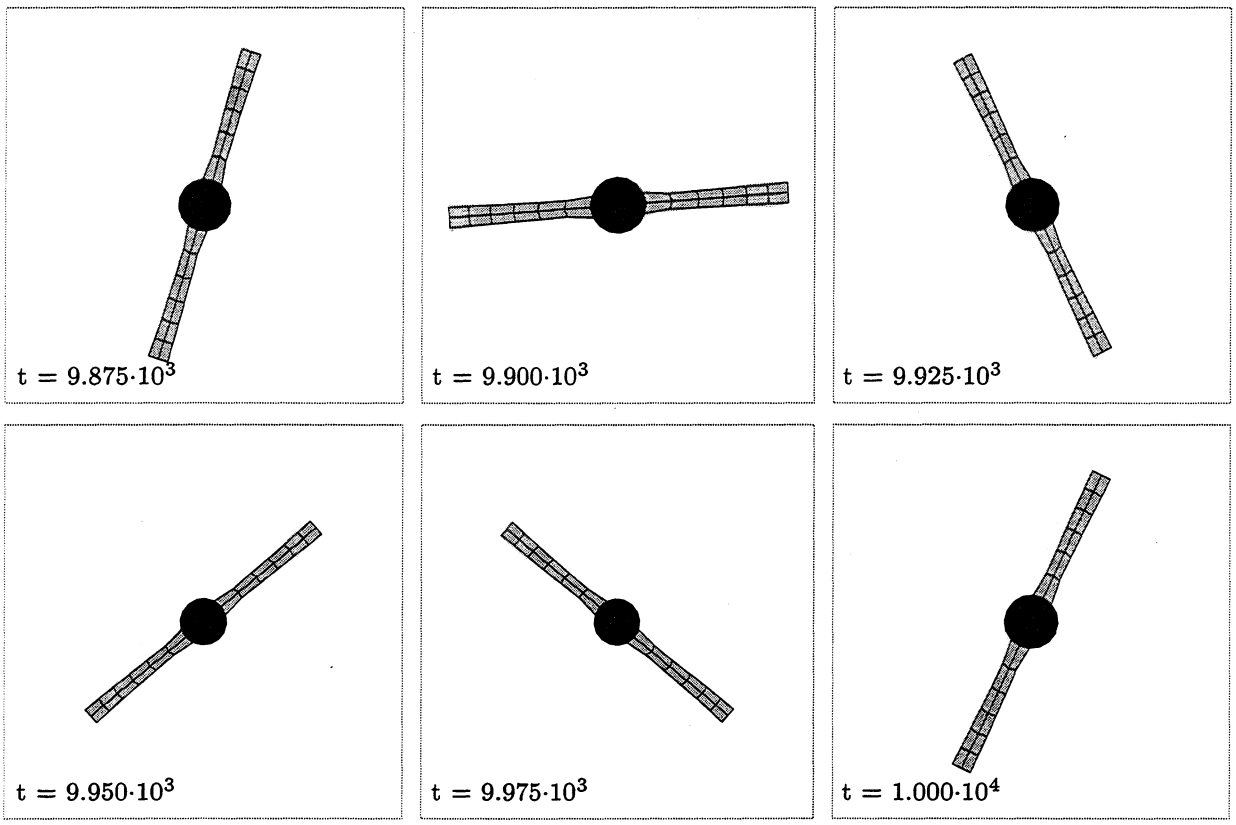

FIGURE 5.3. Plane strain simulation. Long-term solution obtained with the new energy-dissipative, momentum-conserving (EDMC-1) time-stepping scheme.

to the group motions of these problems. The deficient dissipative properties of the HHT scheme obtained in the analyses and numerical simulation of the model problems considered previously are then also observed in this more general setting of nonlinear elastodynamics.

To illustrate more clearly the conservation of the relative equilibria by the new EDMC-1 scheme, we obtain the deformation φ_e corresponding to the relative equilibrium by solving the weak equation (5.7) with a prescribed angular velocity Ω_e at equilibrium (and $v_e = 0$). The corresponding angular momentum μ_e at equilibrium is given by (5.4) and has the value $\mu_e = 1.2974 \cdot 10^5$ assumed in the previous simulations started away from equilibrium. Due to the symmetry in this problem, the imposed essential boundary conditions when solving (5.7) consist of fixing the central node of the cylinder, and constraining the rotation around it. Figure 5.6 shows the resulting deformed configuration of the solid.

Once the exact solution φ_e at equilibrium is obtained, we repeat the dynamic simulations with the initial nodal displacements corresponding to $\varphi_o = \varphi_e$ and the initial nodal velocities corresponding to $v_o = \Omega_e e_3 \times \varphi_e$, with e_3 being the unit vector perpendicular to the plane of the problem (φ_e is measured from the center of the solid). As before, no degrees of freedom are restrained in the dynamic simulations. Therefore, the exact solution

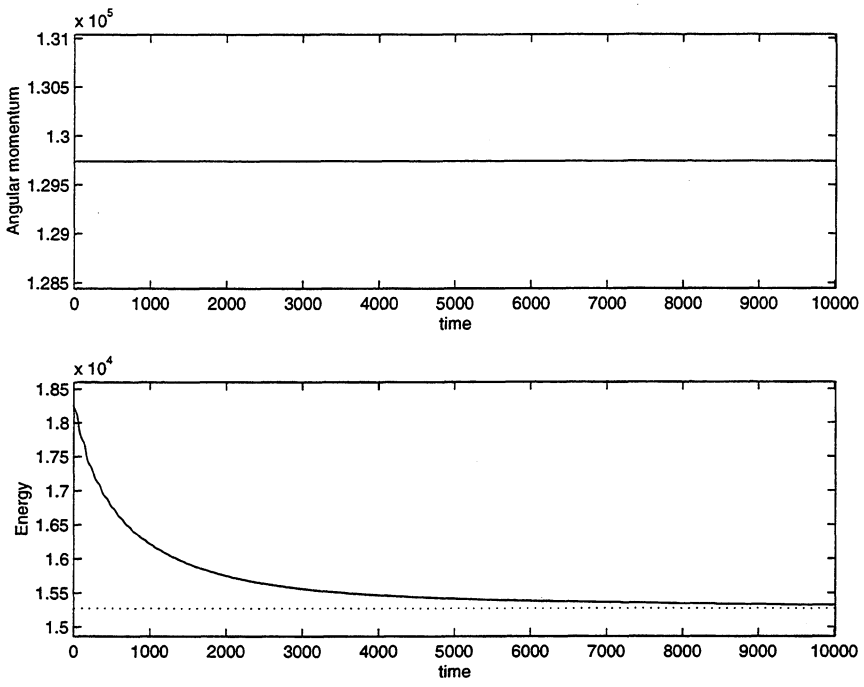

FIGURE 5.4. Plane strain simulation. Evolution of the angular momentum and total energy in time along the numerical solution presented in Figures 5.2 and 5.3 obtained with the EDMC-1 scheme ($\chi_1 = \chi_2 = 0.1$). Constant time step of $\Delta t = 0.3$.

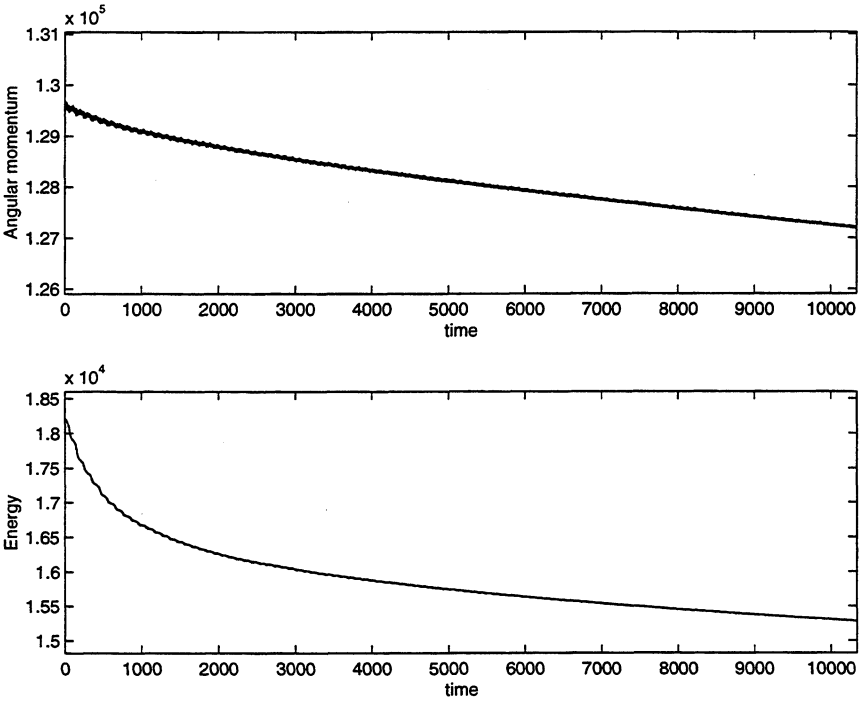

FIGURE 5.5. Plane strain simulation. Evolution of the angular momentum and total energy in time for the HHT method ($\alpha = 0.9$). Constant time step of $\Delta t = 0.3$.

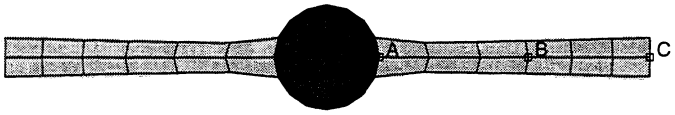

FIGURE 5.6. Deformed configuration corresponding to the relative equilibrium. Points A, B, and C are marked on the horizontal symmetry axis. These are the points whose trajectories are depicted in the following plots.

for these initial conditions should be a uniform rotation about the center of symmetry of the solid.

Figures 5.7 and 5.8 depict the evolution of the angular momentum and total energy obtained with the the EDMC-1 ($\chi_1 = \chi_2 = 0.1$) and HHT ($\alpha = 0.9$) schemes. Figure 5.9 depicts the relative errors of the radial distance to the center, that is,

$$\varepsilon^I = \frac{r^I(t) - r^I(0)}{r^I(0)} \,, \tag{5.39}$$

for the nodes A, B, and C (see Figure 5.6). The conservation of the energy and the angular momentum, and the error measures ε^I give a complete idea of how close a motion is to a relative equilibrium.

From the plots in Figures 5.7 and 5.9, we can clearly observe that the motion obtained with the EDMC-1 scheme is a rigid rotation about the center of symmetry of the solid, with constant energy and angular momentum. Notice also that the values of the angular momentum and the energy during the motion are $\mu_e = 1.2974 \cdot 10^5$ and $H_e = 1.5272 \cdot 10^4$ respectively. These values correspond to the constant angular momentum μ and the asymptotic value of the total energy H_∞ in the original numerical simulations starting from general initial conditions. The deformed configurations at the later stages of the simulation depicted in Figure 5.3 are also to be compared with the equilibrium configuration of Figure 5.6. These results confirm the conservation by the EDMC-1 scheme of the relative equilibria, and the dissipation to these (non-static) equilibria in the general case, shown in the analyses and numerical simulations for the model problems considered previously.

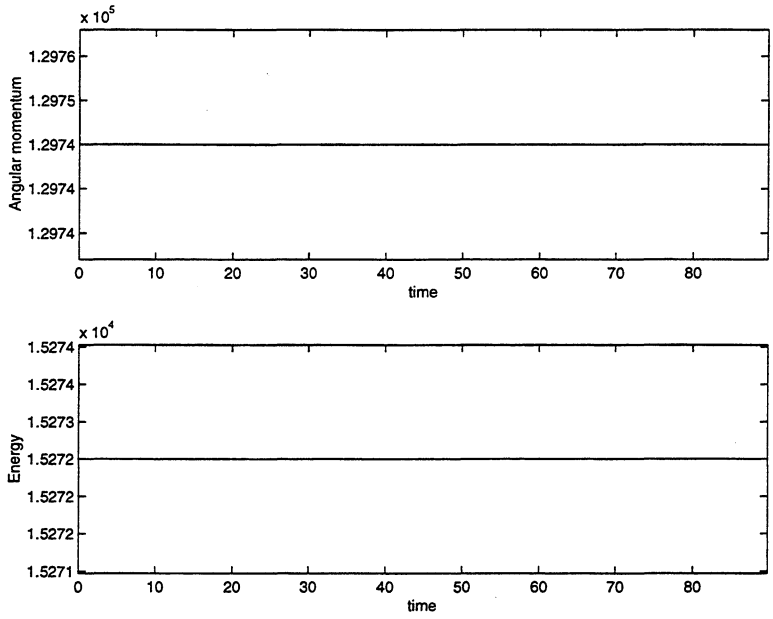

FIGURE 5.7. Plane strain problem. Energy and angular momentum with initial conditions corresponding to a relative equilibrium. EDMC-1 method with $\chi_1 = \chi_2 = 0.1$. 300 time steps of size $\Delta t = 0.3$

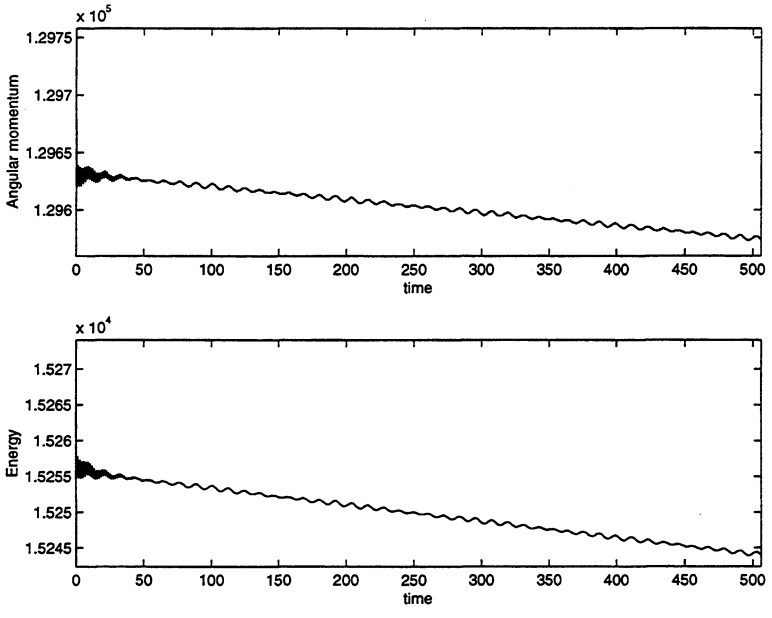

FIGURE 5.8. Plane strain problem. Energy and angular momentum with initial conditions corresponding to a relative equilibrium. HHT method, $\alpha = 0.9$. Time steps of size $\Delta t = 0.3$, final time $T_f = 500$. Both the energy and the angular momentum decrease in the simulation, so the relative equilibrium can not be conserved.

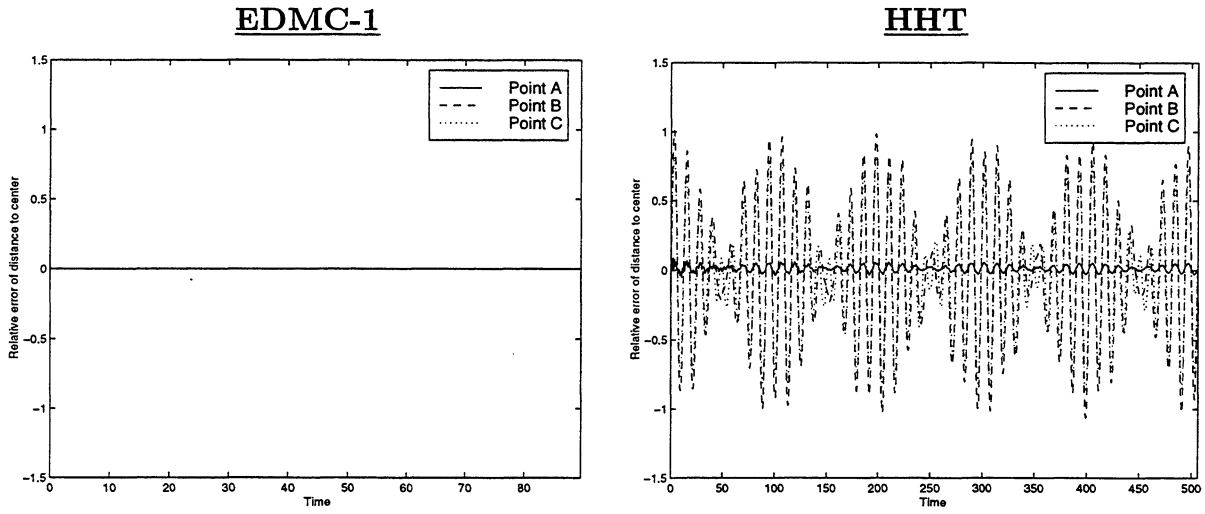

FIGURE 5.9. Relative error in distance to center of the solid of nodes A, B and C. Left: EDMC-1 scheme ($\chi_1 = \chi_2 = 0.1$). Right: HHT scheme ($\alpha = 0.9$). Constant time step $\Delta t = 0.3$.

This situation is to be contrasted with the solutions obtained with the HHT scheme. As shown in Figure 5.8 the angular momentum and total energy of the solid are both dissipated even though the initial conditions correspond to the exact relative equilibrium. The appearance of internal modes of vibration for this case is clear in the evolution of the radial relative errors presented in Figure 5.9.

To conclude we present in Figures 5.10 and 5.11 the results obtained with the EDMC-1 scheme for a similar problem but in general three dimensions. As in the previous plane case, the initial conditions are given by zero nodal displacements and the nodal velocities of a rigid rotation. The initial axis of rotation is $(1, 1, 1)$ in a Cartesian coordinate system with origin at the center of cylinder, and two orthogonal directions along the axis of the cylinder and the middle line of one of the panels, respectively. The initial angular velocity is $\Omega_o = 0.2$. These initial conditions do not correspond to a relative equilibrium and lead to a general motion consisting of a tumbling rotation and internal vibration modes of the solid. In particular, the deformed configurations of Figure 5.10 clearly show the bending, torsional and axial oscillations of the solid arms. Figure 5.11 shows the solution at a much later time for the same numerical simulation. The progressive elimination of these modes can be observed, without requiring the elimination of the overall rotation of the solid. Figure 5.12 depicts the evolution of the three Cartesian components of the angular momentum and the total energy of the solid in time. The conservation of the angular momentum and the monotonic decay of the energy to the relative equilibria is verified. The additional fact that these dissipative properties are totally controllable, as shown by the analyses presented above, make the proposed time-stepping schemes very interesting for problems involving this type of free motions.

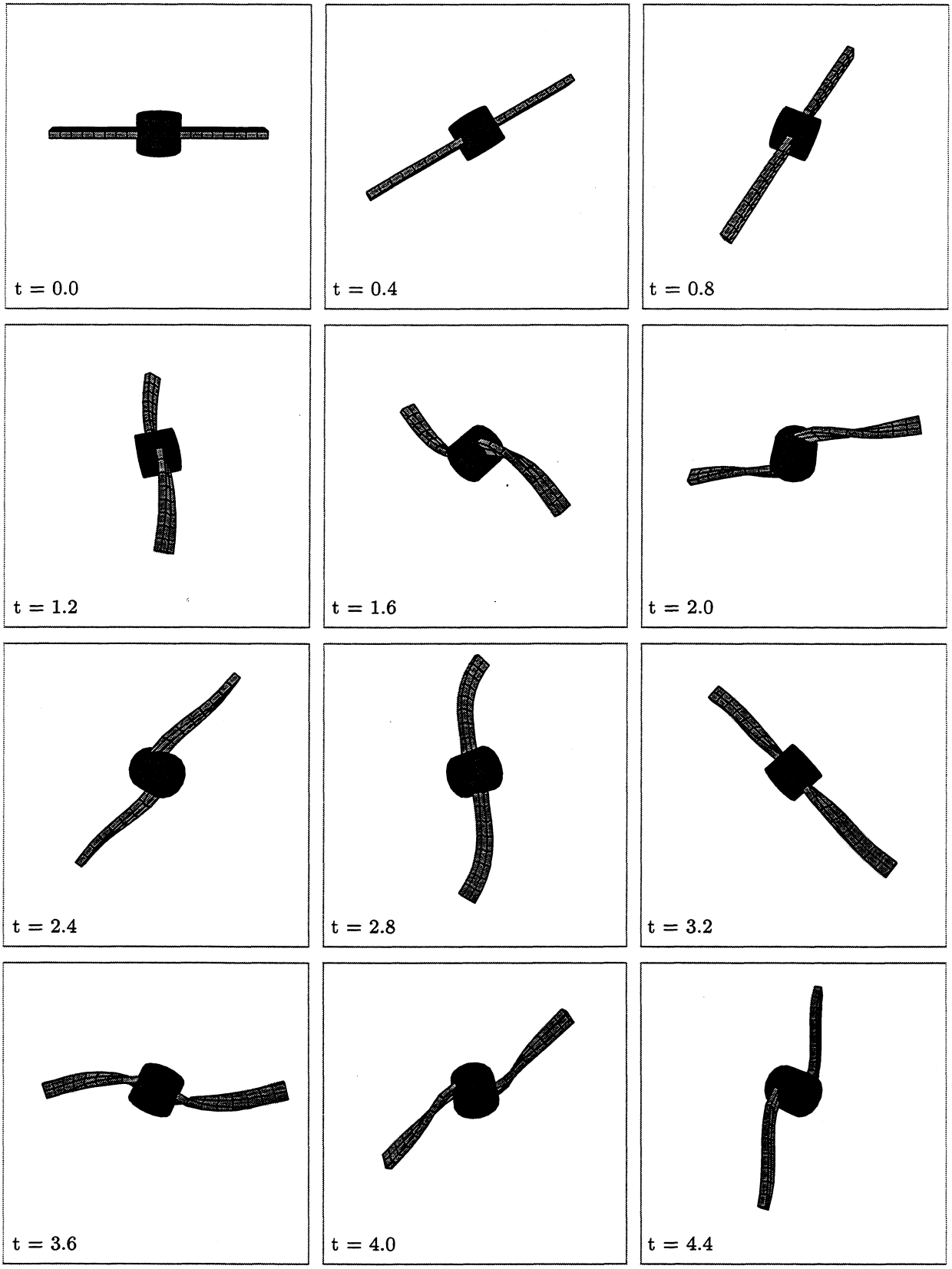

FIGURE 5.10. Three-dimensional problem. Solution obtained with the new energy-dissipative, momentum-conserving (EDMC-1) time-stepping scheme.

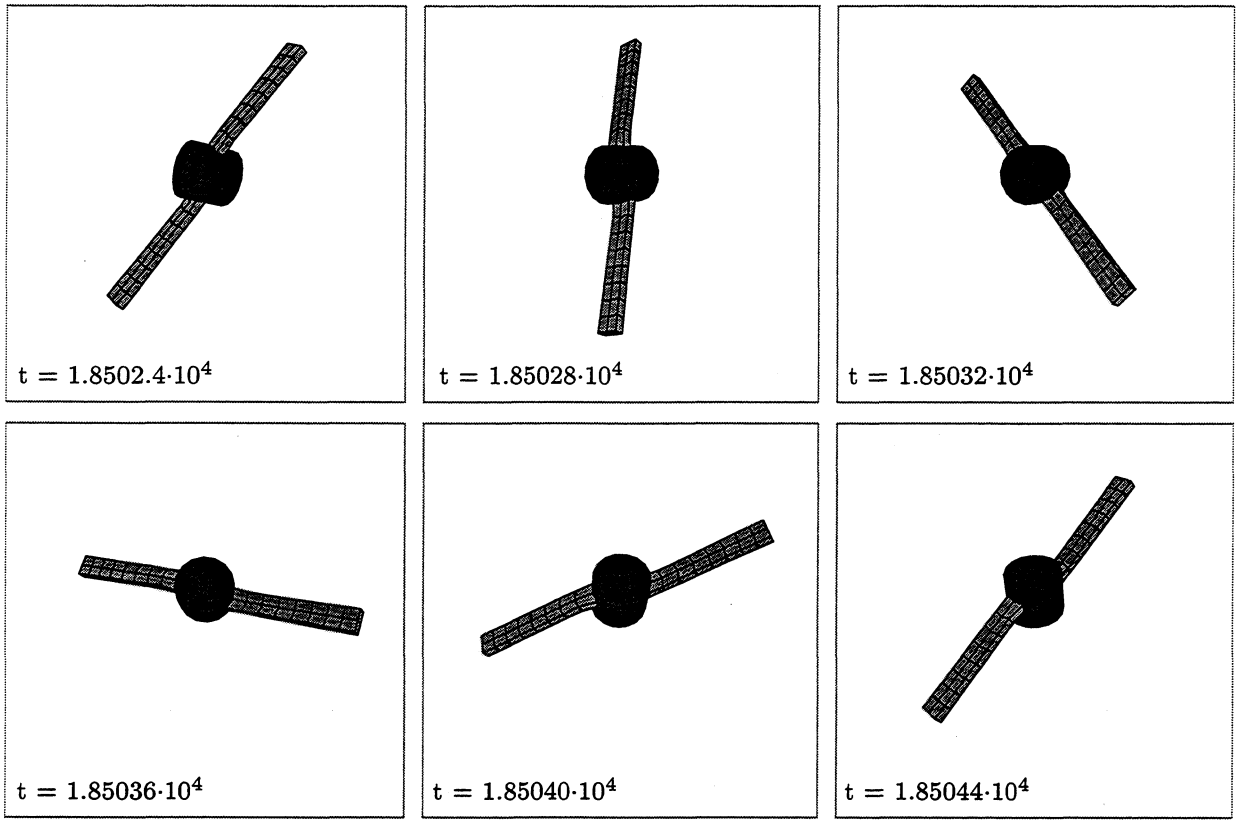

FIGURE 5.11. Three-dimensional problem. Long-term solution obtained with the new energy-dissipative, momentum-conserving (EDMC-1) time-stepping scheme.

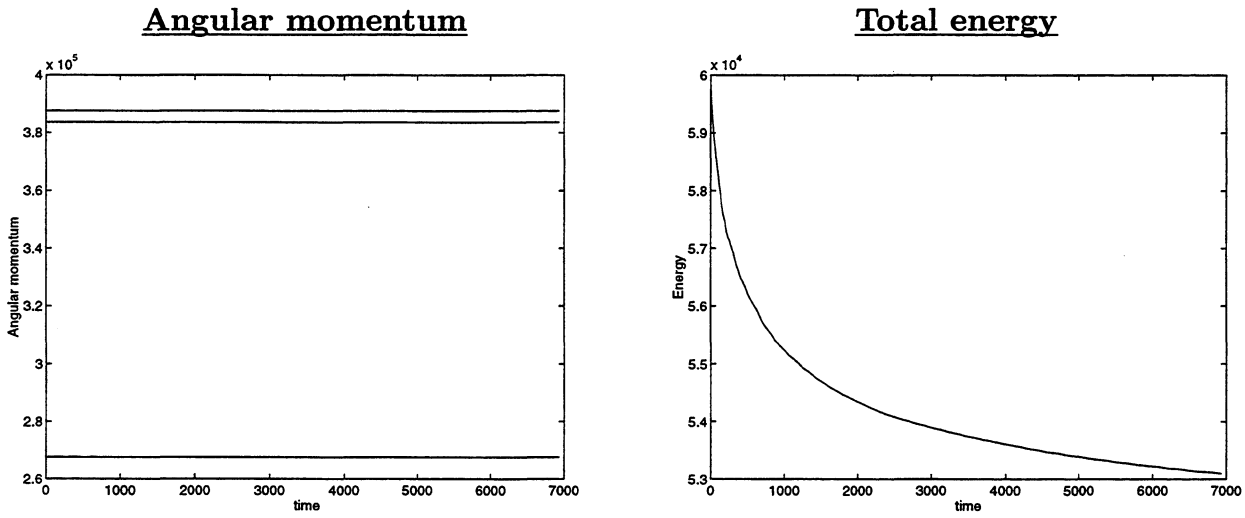

FIGURE 5.12. Three-dimensional problem. Evolution of the total energy and the three Cartesian components of the angular momentum obtained with the EDMC-1 scheme.

6. Concluding Remarks

We have presented in this paper the formulation of time-stepping algorithms that exhibit numerical dissipation in the high-frequency range in the general context of nonlinear dynamics. In particular, we have presented analyses of existing and new methods for two simple model problems and the fully nonlinear case of three-dimensional nonlinear elastodynamics. Several representative numerical simulations have been presented illustrating the performance of the new schemes as related to the presented analyses.

As a final conclusion, we emphasize once more the importance not only of having rigorously proven the dissipative properties in the high-frequency range for general nonlinear problems, but also the need for the numerical schemes to preserve the relative equilibria of the exact system. The lack of numerical dissipation in the group motions of systems with symmetry is of the key importance for the simulation of elastic systems in free motions. The results presented in this first part of this work show a simple way of introducing this dissipation, in a fully controlled manner. Even though, the resulting algorithms are only first order accurate in time (but leading to a second order approximation of the group motions), we believe that obtaining a correct qualitative picture of the exact dynamics for a fixed time step, as obtained with the proposed schemes, is even a more important property, especially after noting the qualitatively distorted picture of the phase space obtained with more traditional numerical schemes, including high order schemes. Extensions leading to higher order methods that exhibit the aforementioned conservation properties for general problems of nonlinear elastodynamics (general potentials) and a controllable numerical dissipation can be obtained by preserving the structure of the numerical algorithms presented herein, but with high-order expressions of the dissipative contributions. These ideas are the focus of the forthcoming second part of this work.

Acknowledgments: Financial support for this research was provided by the AFOSR under contract no. F49620-97-1-0196 with UC Berkeley. This support is gratefully acknowledged.

References

ABRAHAM, R. & MARSDEN, J.E. [1978] *Foundations of Mechanics,* 2^{nd} edition, Addison-Wesley, New York.

ARMERO, F. & PETOCZ, E. [1996] "Formulation and Analysis of Conserving Algorithms for Fricitonless Dynamic Contact/Impact Problems," *Computer Methods of Applied Mechanics and Engineering,* **158**, 269-300.

ARMERO, F. & PETOCZ, E. [1997] "A New Dissipative Time-Stepping Algorithm for Frictional Contact Problems: Formulation and Analysis," *Computer Methods of Applied Mechanics and Engineering,* in press.

ARNOLD, V.I.; KOZLOV, V.V. & NEISHTADT, A.I. [1988] "Mathematical Aspects of Classical and Celestial Mechanics," in *Dynamical Systems III,* edited by V.I. Arnold, Springer-Verlag, Berlin.

BATHE [1986] *Finite Element Procedures for Solids and Structures: Nonlinear Analysis,* MIT Center for Advanced Engineering Studies, report no.73-2200, Cambridge (see also a summary in BATHE [1996] *Finite Element Procedures,* Prentice Hall, New York, page 827).

BAUCHAU, O.A. & THERON, N.J. [1996] "Energy Decaying Scheme for Non-linear Beam Models," *Comp. Meth. Appl. Mech. Engr.,* **134**, 37-56.

BAYLISS, A. & ISAACSON, E. [1975] "How to Make Your Algorithm Conservative," *American Mathematical Society,* A594-A595.

BOTASSO, C. & BORRI, M. [1998] "Integrating Rotations," *Comp. Meth. Appl. Mech. Engr.,* **164**, 307-331.

CARDONA, A. & GERARDIN, M. [1988] "A Beam Finite Element Non-Linear Theory with Finite Rotations," *Int. J. Num. Meth. Engr.,* **26**, 2403-2438.

CRISFIELD, M.A.; GALVANETTO, U. & JELENIC, G. [1997] "Dynamics of 3-D Co-Rotational Beams," *Computational Mechanics,* **20**, 507-519.

CRISFIELD, M. & SHI, J. [1994] "A Co-Rotational Element/Time-Integration Strategy for Non-Linear Dynamics," *Int. J. Num. Meth. Eng.,* **37**, 1897-1913.

DACOROGNA, B. [1989] *Direct Methods in the Calculus of Variations,* Springer-Verlag, New York.

GONZALEZ, O. & SIMO, J.C. [1996] "On the Stability of Symplectic and Energy-Momentum Algorithms for Nonlinear Hamiltonian Systems with Symmetry," *Comp. Meth. Appl. Mech. Eng.,* **134**, p 197-222.

GONZALEZ, O. & J.C. SIMO [1995] "Exact Energy-Momentum Conserving Algorithms for General Models in Nonlinear Elasticity," *Comp. Meth Appl. Mech. Eng.*, to appear.

GRAFF, K.F. [1975] *Wave Motion in Elastic Solids,* Dover Publications, New York.

HILBER, H.M. [1976] "Analysis and Design of Numerical Integration Methods in Structural Dynamics", Ph.D. Thesis, U.C. Berkeley.

HILBER, H.M; HUGHES, T.J.R.; TAYLOR, R.L. [1977] "Improved numerical dissipation for time integration algorithms in structural dynamics", *Earthquake engineering and Structural Dynamics* **5**, 283-292.

HIRSCH, M.W. & SMALE, S. [1974] *Differential Equations, Dynamical Systems, and Linear Algebra,* Academic Press, New York.

HUGHES, T.J.R.; CAUGHEY, T.K. AND LIU, W.K. [1978] "Finite Element Methods for Nonlinear Elastodynamics that Conserve Energy," *Journal of Applied Mechanics,* **45**, 366-370.

HUGHES, T.J.R. [1987] *The Finite Element Method,* Prentice-Hall,

HUGHES, T.J.R. [1983] "Analysis of transient algorithms with particular reference to stability behaviour," *Computational methods for transient analysis, Ed. T. Belytschko, T.J.R. Hughes, North-Holland*

KUHL, D. & CRISFIELD, M.A. [1997] "Energy Conserving and Decaying Algorithms in Non-Linear Structural Dynamics", submitted to *Int. J. Num. Meth. Eng.*

KUHL, D. & RAMM, E. [1996] "Constraint Energy Momentum Algorithm and its Application to Non-Linear Dynamics of Shells," *Computer Methods of Applied Mechanics and Engineering,* **136**, 293-315.

LABUDDE, R.A. & GREENSPAN, D. [1976] "Energy and Momentum Conserving Methods of Arbitrary Order for the Numerical Integration of Equations of Motion," *Numerisch Mathematik,* Part I **25** 323-346, Part II **26** 1-16.

MARSDEN, J.E. [1992] *Lectures on Mechanics,* London Mathematical Society Lecture Note Series, **174**, Cambridge University Press.

MARSDEN, J.E. & RATIU, T.S. [1994] *Introduction to Mechanics and Symmetry,* Springer-Verlag, New York.

ROMERO, I. & ARMERO, F. [1999] "Discrete Relative Equilibria of Time-Stepping Algorithms for a Model Problem of Nonlinear Dynamics," Report UCB/SEMM no. 99-03.

SIMO, J.C. & GONZALEZ, O. [1994] "Recent Results on the Numerical Integration of Infinite-Dimensional Hamiltonian Systems," in *Recent Developments in Finite Element Analysis,* ed. by T.J.R. Hughes, O. Oñate, and O.C. Zienkiewicz, CIMNE, Barcelona.

SIMO, J.C.; LEWIS, D.R. & MARSDEN, J.E. [1991] "Stability of Relative Equilibria I: The Reduced Energy Momentum Method," *Arch. Rat. Mech. Anal.*, **86**, 213-231.

SIMO, J.C.; POSBERGH, T.A. & MARSDEN, J.E. [1991] "Stability of Relative Equilibria. Part II: Application to Nonlinear Elasticity," *Arch. Rat. Mech. Anal.*, **115**, 61-100.

SIMO, J.C. & TARNOW, N. [1992] "The Discrete Energy–Momentum Method. Conserving Algorithms for Nonlinear Elastodynamics," *ZAMP*, **43**, 757-793.

SIMO, J.C.; TARNOW, N. & DOBLARE, M. [1995] "Nonlinear Dynamics of Three-Dimensional Rods: Exact Energy and Momentum Conserving Algorithms," *Int. J. Num. Meth. Eng.*, **38**, 1431-1473.

WOOD, W.L. [1990] *Practical Time-Stepping Schemes*, Clarendon Press, Oxford.

Appendix I. Characterization of discrete relative equilibria

Relative equilibria of Hamiltonian systems with symmetries correspond to the trajectories generated by the action of an one-parameter subgroup of the symmetry group, the so-called group motions. For the spring-mass model problem of interest herein, these equilibria have been characterized in Section 2.2 as the rigid rotation of the spring, with a constant angular velocity Ω_e and constant stretch of the spring l_e related by equation (2.22). The goal of this appendix is to characterize the corresponding solutions of the discrete dynamical systems generated by typical time-stepping algorithms. We summarize only the main ideas involved in the analysis and refer to ROMERO & ARMERO [1999] for complete details of the derivations involved.

More specifically, we investigate the existence of discrete solutions of the form

$$\boldsymbol{q}_{e_{n+1}} = \boldsymbol{\Lambda}\boldsymbol{q}_{e_n} \qquad \text{and} \qquad \boldsymbol{p}_{e_{n+1}} = \boldsymbol{\Lambda}\boldsymbol{p}_{e_n} \ , \tag{I.1}$$

for a rotation $\boldsymbol{\Lambda} \in G = SO(2)$, constant for all time increments $[t_n, t_{n+1}]$ $n = 0, 1, 2, \ldots$. A constant time step $\Delta t = t_{n+1} - t_n$ for all n is assumed. Denoting $\boldsymbol{q}_e \equiv \boldsymbol{q}_{e_o}$ and $\boldsymbol{p}_e \equiv \boldsymbol{p}_{e_o}$ (note that relative equilibria are defined up to a rotation), we conclude that for the assumed solution

$$\boldsymbol{q}_{e_n} = \boldsymbol{\Lambda}^n \boldsymbol{q}_e \quad \text{and} \quad \boldsymbol{p}_{e_n} = \boldsymbol{\Lambda}^n \boldsymbol{p}_e \qquad \Longrightarrow \qquad \begin{cases} \|\boldsymbol{q}_{e_n}\| = \|\boldsymbol{q}_e\| =: l_e \ , \\ \|\boldsymbol{p}_{e_n}\| = \|\boldsymbol{p}_e\| \ , \end{cases} \ , \tag{I.2}$$

for all $n = 0, 1, \ldots$ If ϑ denotes the angle between the $\boldsymbol{q}_n$ and $\boldsymbol{q}_{n+1}$ vectors, we can write

$$\boldsymbol{\Lambda} = \begin{pmatrix} \cos\vartheta & -\sin\vartheta \\ \sin\vartheta & \cos\vartheta \end{pmatrix} \ , \tag{I.3}$$

in a Cartesian basis $\{\boldsymbol{e}_1, \boldsymbol{e}_2\}$. Without loss of generality, we consider

$$\boldsymbol{q}_e = l_e \ \boldsymbol{e}_1 \ . \tag{I.4}$$

The solution (I.1) defines the relative equilibria of the discrete dynamical system defined by numerical scheme, generated by the constant rotation $\boldsymbol{\Lambda} \in SO(2)$ (or alternatively by $\vartheta \in \mathbb{R}$ as defined in (I.3)).

I.1. The generalized α-method

We consider first the generalized α-method defined by equations (3.2). In this case, the generalized midpoint vector $\boldsymbol{q}_{n+\alpha} = (1-\alpha)\boldsymbol{q}_n + \alpha\boldsymbol{q}_{n+1}$ can be written as

$$\boldsymbol{q}_{n+\alpha} = \boldsymbol{G}\boldsymbol{q}_{n+1} = \boldsymbol{G}\boldsymbol{\Lambda}\boldsymbol{q}_n \qquad \text{with} \quad \boldsymbol{G} := (1-\alpha)\boldsymbol{\Lambda}^T + \alpha\boldsymbol{1} \ , \tag{I.5}$$

and similarly for the generalized midpoint momenta $\boldsymbol{p}_{n+\alpha}$. We note that the matrix $\boldsymbol{G}$ is not a rotation, except for $\alpha = 0$ or 1, and that it commutes with $\boldsymbol{\Lambda}$ that is, $\boldsymbol{G\Lambda} = \boldsymbol{\Lambda G}$, as it can be easily verified from the definition $(I.5)_2$ Introducing the definition

$$\nu = \frac{\Delta t^2}{m} \frac{\hat{V}'(\|\boldsymbol{q}_{e_{n+\alpha}}\|)}{\|\boldsymbol{q}_{e_{n+\alpha}}\|} = \frac{\Delta t^2}{m} \frac{\hat{V}'(\|\boldsymbol{G}\boldsymbol{q}_e\|)}{\|\boldsymbol{G}\boldsymbol{q}_e\|} , \tag{I.6}$$

the evaluation of equations (3.2) leads, after some algebraic manipulations, to the relation

$$\boxed{\boldsymbol{p}_e = m/\Delta t \left[\boldsymbol{\Lambda} - \mathbf{1} + \nu(\tfrac{1}{2} - \beta)\boldsymbol{G} + \nu\beta\boldsymbol{\Lambda G}\right] \boldsymbol{q}_e ,} \tag{I.7}$$

for the linear momenta $\boldsymbol{p}_e$ at equilibrium and, after using (I.4), the equation

$$\boxed{\left[\kappa_2\boldsymbol{\Lambda}^2 + \kappa_1\boldsymbol{\Lambda} + \kappa_T\boldsymbol{\Lambda}^T + \kappa_0\mathbf{1}\right] \boldsymbol{e}_1 = \mathbf{0} ,} \tag{I.8}$$

where we have introduced the notation

$$\boxed{\begin{aligned} \kappa_0 &= 1 + \nu(\tfrac{1}{2} - 2\beta + 3\alpha\beta + \gamma - 2\alpha\gamma) , \\ \kappa_1 &= -2 + \nu(-3\alpha\beta + \beta + \frac{\alpha}{2} + \alpha\gamma) , \\ \kappa_2 &= 1 + \alpha\beta\nu , \\ \kappa_T &= \nu\left[(\beta - \tfrac{1}{2})(1 - \alpha) + (1 - \gamma)(1 - \alpha)\right] . \end{aligned}} \tag{I.9}$$

Relative equilibria will then exist if equation (I.8) has a solution defining ϑ and $l_e = \|\boldsymbol{q}_e\|$ through (I.6).

Remarks I.1.

1. The combination $\boldsymbol{\Lambda} = \mathbf{1}$, $\nu = 0$ is a solution for every combination (α, β, γ). This situation corresponds to the trivial solution with the mass at rest $\vartheta = 0$ and $l_e = l_o$ (the stress-free length of the spring). Any consistent time-stepping algorithm possesses this solution trivially.

2. Equation (I.8) can be interpreted as the sum of four vectors $\boldsymbol{e}_1, \boldsymbol{\Lambda e}_1, \boldsymbol{\Lambda}^2\boldsymbol{e}_1, \boldsymbol{\Lambda}^T\boldsymbol{e}_1$ each one scaled by a factor $\kappa_0, \kappa_1, \kappa_2, \kappa_T$ respectively. □

We analyze next the solutions of equation (I.8) for the different time-stepping algorithms identified in Section 3.

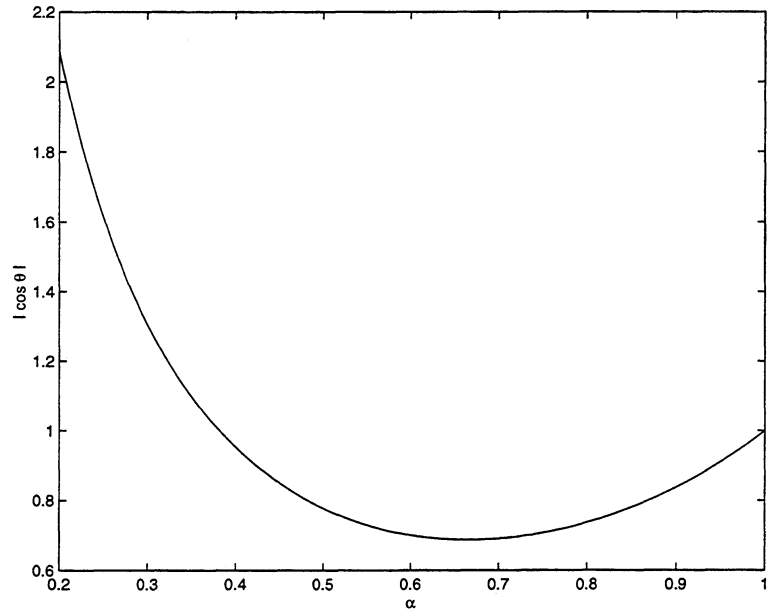

FIGURE I.1. HHT method. $\max_\nu |\cos\vartheta|$ for $0.2 \leq \alpha \leq 1$. If $|\cos\vartheta| \leq 1$, we must restrict α to $0.35 \leq \alpha \leq 1$

Algo.1. *The HHT-α method.* The Hilber-Hughes-Taylor α-method (see HILBER et al [1977]] corresponds to equations (3.2) with parameters

$$(\alpha, \beta, \gamma) = \left(\alpha, \frac{(2-\alpha)^2}{4}, \frac{(3-2\alpha)}{2}\right), \quad 0.7 \leq \alpha \leq 1, \tag{I.10}$$

The values of the parameters κ_i are given in this case

$$\begin{aligned} \kappa_0 &= 1 + \frac{\nu}{4}\alpha(3\alpha^2 - 6\alpha + 4), \\ \kappa_1 &= -2 + \frac{\nu}{4}(-3\alpha^3 + 9\alpha^2 - 8\alpha + 4), \\ \kappa_2 &= 1 + \frac{\nu}{4}\alpha(2-\alpha)^2, \\ \kappa_T &= \frac{\nu}{4}\alpha^2(1-\alpha). \end{aligned} \tag{I.11}$$

The introduction of these parameters in (I.8) with $\boldsymbol{\Lambda}$ given by (I.3) leads to the system of equations

$$\begin{cases} \kappa_2 \cos(2\vartheta) + (\kappa_1 + \kappa_T)\cos\vartheta + \kappa_0, = 0 \\ \kappa_2 \sin(2\vartheta) + (\kappa_1 - \kappa_T)\sin\vartheta \quad = 0 \end{cases} \quad \Longrightarrow \quad \cos\vartheta = \frac{\kappa_T - \kappa_1}{2\kappa_2} \quad (\text{for } \vartheta \neq 0), \tag{I.12}$$

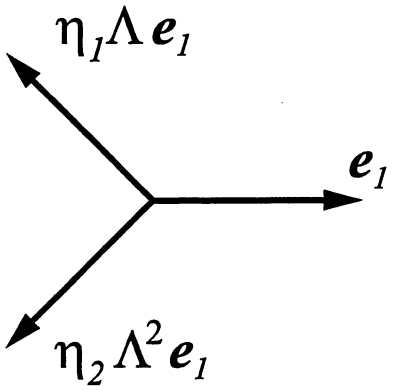

FIGURE I.2. Sketch of relation (I.15). The sum of these three vectors must vanish for the algorithm to have a discrete relative equilibria.

Figure I.1 depicts this last relation, showing the maximum $\cos\vartheta$ as a function of α. For a given α this maximum is attained as $\nu \to \infty$. Furthermore, to have $\left|\frac{\kappa_T - \kappa_1}{2\kappa_2}\right| \leq 1$ for any value of ν, we must restrict $\alpha > 0.35$. Note that the HHT only considers $\alpha > 0.7$. Introducing (I.11) in $(\text{I.12})_1$ we obtain

$$\kappa_T(\kappa_T - \kappa_1) + \kappa_2(\kappa_0 - \kappa_2) = 0 \Leftrightarrow \frac{1}{4}(\alpha - 1)\alpha^2\nu^2 = 0 \,, \tag{I.13}$$

This equation is satisfied in three cases: $\nu = 0$ (the trivial static equilibrium), $\alpha = 1$ and $\alpha = 0$. The case $\alpha = 1$ corresponds to the trapezoidal rule and is analyzed below. The case $\alpha = 0$ is beyond the restriction (I.10) We conclude that *there is no dissipative HHT scheme possessing a discrete relative equilibrium.*

Algo.2. *A "dissipative" Newmark scheme.* Newmark's method is recovered from the general expression (3.2) with $\alpha = 1$ and $0 \leq \beta, \gamma \leq 1$. The particular combination

$$\tfrac{1}{2} < \gamma \leq 1 \,, \quad \beta = (\gamma + \tfrac{1}{2})^2/4 \,, \tag{I.14}$$

defines a one-parameter family of first-order algorithms that are unconditionally stable and exhibit numerical dissipation in the high frequencies, for *linear problems.* With the consideration of $\alpha = 1$ in (I.9), equation (I.8) reduces to

$$\left[\eta_2 \boldsymbol{\Lambda}^2 + \eta_1 \boldsymbol{\Lambda} + \mathbf{1}\right] \boldsymbol{e}_1 = \mathbf{0} \,, \tag{I.15}$$

with

$$\eta_1 = \frac{-2 + \nu(\frac{1}{2} + \gamma - 2\beta)}{1 + \nu(\beta - \gamma + \frac{1}{2})} \qquad \text{and} \qquad \eta_2 = \frac{(1 + \beta\nu)}{1 + \nu(\beta - \gamma + \frac{1}{2})} \,. \tag{I.16}$$

We note that $1+\nu(\beta-\gamma+\frac{1}{2})$ is always positive if $\beta=(\gamma+\frac{1}{2})^2/4$, $\frac{1}{2}<\gamma\leq 1$. Figure I.2 depicts the relation (I.15). It becomes clear from this figure that a necessary condition for (I.15) to have solution is that $\eta_2=1$. Defining $\epsilon=\gamma-\frac{1}{2}>0$, we have

$$\eta_2=\frac{1+\beta\nu}{1+\beta\nu-\nu\epsilon}>1\,, \tag{I.17}$$

so $\eta_2>1$ strictly for every $\nu>0$. This implies that (I.15) does not have a solution and hence, *this dissipative family of Newmark's method do not exhibit relative equilibria in the problem under consideration.*

Algo.3. *The trapezoidal rule.* The consideration of the parameter values $(\alpha,\beta,\gamma)=(1,\frac{1}{4},\frac{1}{2})$ reduces equation (I.15) to the system of equations

$$\begin{cases}\cos 2\vartheta+\eta\cos\vartheta=-1\,,\\ \sin 2\vartheta+\eta\sin\vartheta=0\,,\end{cases} \tag{I.18}$$

in terms of the incremental angle ϑ and $\eta=(\nu/2-2)/(1+\nu/4)$. Equations (I.18) have the nontrivial solution $\eta=-2\cos\vartheta$. This implies that *the trapezoidal rule admits discrete relative equilibria in the problem under consideration.* The corresponding $\boldsymbol{p}_e$ is recovered from (I.7) by the relation

$$\boldsymbol{p}_e=\frac{m}{\Delta t}\sqrt{\nu}\,\widehat{\mathbb{J}}\,\boldsymbol{q}_e\,, \tag{I.19}$$

where $\widehat{\mathbb{J}}$ has been defined in (2.16).

It is interesting to observe that *the trapezoidal exhibits the same relative equilibria as the exact continuum problem.* This statement is shown by observing first that the energy is conserved along the solution (I.1) by (I.2). Similarly, the angular momentum at the relative equilibrium is given by

$$\mu_e=\boldsymbol{p}_e\cdot\widehat{\mathbb{J}}\boldsymbol{q}_e=\frac{m}{\Delta t}\sqrt{\nu}\,l_e^2\,, \tag{I.20}$$

after using (I.7), and is conserved. Noting that $\boldsymbol{G}=\mathbf{1}$ in this case, the definition (I.6) leads to

$$\nu\Big|_{trap}=\frac{\Delta t^2}{m}\frac{\hat{V}'(l_e)}{l_e}\,, \tag{I.21}$$

so (I.20) leads to the equation in l_e

$$V'_{\mu_e}(l_e):=V'(l_e)-\frac{\mu_e^2}{m\,l_e^3}=0\,, \tag{I.22}$$

that is, exactly the same equation $(2.22)_3$ as for the continuum system. We conclude that the discrete relative equilibria of the trapezoidal rule are the exact ones, with the energy

and angular momentum conserved along then. It is important to point out that this scheme does not conserve energy nor the momentum from general initial conditions. Interesting enough the algorithm still inherits the exact relative equilibria.

Algo.4. *The midpoint rule.* A similar calculation for the midpoint rule parameters $(\alpha, \beta, \gamma) = (\frac{1}{2}, \frac{1}{2}, 1)$ shows that exactly the same system of equation (I.18) as in the trapezoidal rule is obtained. We conclude then that the midpoint rule also exhibits discrete relative equilibria, characterized also by the expressions (I.19) and (I.20). The nature of these relative equilibria is completely different when compared with their counterpart of the trapezoidal rule (that is, the exact ones). The difference stems from the expression

$$\nu\Big|_{midp} = \frac{\Delta t^2}{m} \frac{\hat{V}'(\|\boldsymbol{G}\boldsymbol{q}_e\|)}{\|\boldsymbol{G}\boldsymbol{q}_e\|} \quad \Longrightarrow \quad V'(\|\boldsymbol{G}\boldsymbol{q}_e\|) = \frac{\mu_e^2}{m\, l_e^4} \|\boldsymbol{G}\boldsymbol{q}_e\| \,, \tag{I.23}$$

characterizing the relative equilibria of the midpoint rule. The relations (I.23) are to be contrasted with (I.21) and the exact equation (I.22). Noting that

$$\|\boldsymbol{G}\boldsymbol{q}_e\| = \frac{l_e}{\sqrt{2}} \sqrt{1 + \cos\vartheta} \,, \tag{I.24}$$

and that ϑ depends of the time step Δt, we conclude that the relative equilibria of the midpoint rule depend on the time step. The same conclusion, together with relation (I.23), was obtained for this case in GONZALEZ & SIMO [1996] after a complex reduction of the discrete dynamical system defined by the numerical algorithm to the reduced space of axial oscillations of the spring/mass system.

Remark I.2. For the newly proposed EDMC-1 scheme (3.14), we note that for the solution (I.1) under investigation $\mathcal{D}_V = \mathcal{D}_K = 0$, given (I.2). The scheme reduces then to the energy-momentum scheme (3.5) along this solution, leading to a second order, energy-momentum conserving approximation. In addition, we obtain exactly the same equations (I.18)-(I.21) of the trapezoidal rule, as a straightforward calculation shows following the same arguments of the previous section. Note that the expression (3.6) applies in this case, given (I.2). We conclude that the proposed EDMC-1 scheme inherits the same relative equilibria of the continuum system. As shown in Proposition 3.1, the corresponding group motions are given by the Cayley transform (3.23) approximating the exponential map (2.20). □